

ИНСТИТУТ ЗА ФИЗИКУ

ПРИМЉЕНО:			
Рад.јед.	б р о ј	Арх.шифра	Прилог
0801 -	1363 / 1		

Naučnom већу Instituta za Fiziku

Predmet: Molba za pokretanja postupka za reizbor u zvanje naučni saradnik

Molim Naučno веће Instituta za Fiziku u Beogradu da u skladu sa Pravilnikom o postupku i načinu vrednovanja i kvantitativnom iskazivanju naučno-istraživačkih rezultata pokrene postupak za moj reizbor u zvanje naučni saradnik.

U prilogu dostavljam:

1. Mišljenje rukovodioca laboratorije sa predlogom članova komisije za izbor u zvanje,
2. Stručnu biografiju,
3. Pregled naučne aktivnosti,
4. Elemente za kvalitativnu analizu naučnog doprinosa,
5. Elemente za kvantitativnu analizu naučnog doprinosa,
6. Spisak objavljenih radova i njihove kopije,
7. Potvrdu o citiranosti radova,
8. Rešenje o prethodnom izboru u zvanje.

Beograd 30.07.2024.

dr Andrej Bunjac



ИНСТИТУТ ЗА ФИЗИКУ

ПРИМЉЕНО: 30-07-2024			
Рад.јед.	б р о ј	Арх.шифра	Прилог
0801	1363	2	

Naučnom veću Instituta za fiziku

Mišljenje rukovodioca laboratorije o reizboru dr Andreja Bunjca u zvanje naučni saradnik

Dr Andrej Bunjac je zaposlen na Institutu za fiziku u Beogradu u Laboratoriji za atomske sudarne procese. Njegov istraživački rad u periodu nakon prethodnog izbora odvijao se u oblasti interakcije jakog laserskog zračenja sa atomskim sistemima primenom različitih teorijskih i numeričkih metoda. S obzirom da ispunjava sve predviđene uslove u skladu sa Pravilnikom o postupku, načinu vrednovanja i kvantitativnom iskazivanju naučnoistraživačkih rezultata istraživača MNPTR, saglasan sam sa pokretanjem postupka reizbora u zvanje naučni saradnik i molim Naučno veće Instituta za fiziku da pokrene postupak za reizbor dr Andreja Bunjca u navedeno zvanje.

Predlažem sledeće članove komisije:

1. dr Nenad Simonović, naučni savetnik, Institut za fiziku
2. dr Duška Popović, naučni savetnik, Institut za fiziku
3. prof. dr Goran Poparić, redovni profesor, Fizički fakultet.

Beograd, 30. 07. 2024.

Rukovodilac laboratorije

N. Simonović

Dr Nenad Simonović

Буњац Б. Андреј

Curriculum vitae



Контакт:

E-mail: bunjac@ipb.ac.rs

Лични подаци:

Датум рођења: 03. 12. 1988.

Место рођења: Београд – Савски Венац

Образовање:

2011 – Дипломирао основне студије физике на Физичком факултету у Београду, студијска група: *"Теоријска и експериментална физика"*.

2012 – Дипломирао мастер студије на Физичком факултету у Београду са дипломским радом под називом: *"Модерна теорија поларизације диелектрика"*.

2012 – Уписао докторске студије физике (група *"Квантна, математичка и нанофизика"*) под менторством Др Татјане Вуковић.

2014 – Променио смер докторских студија на *"Физика атома и молекула"* под менторством Др Ненада Симоновића.

2018 – Одбранио докторску дисертацију под називом *"Израчунавање насељености атомских стања, угаоне расподеле и енергијског спектра фотоелектрона код атомских система у јаким ласерским пољима применом временски зависних метода"* под менторством Др Ненада Симоновића.

Професионална ангажованост:

- Новембар 2012 – Новембар 2014: запослен на пројекту *"Карбоснке и неорганске наноструктуре ниске димензионалности"* под руководством Др Милана Дамњановића.
- У летњем семестру 2013/2014 држао експерименталне вежбе из предмета Физика 1 на факултету за физичку хемију.
- Новембар 2014 – сада: запослен на пројекту *"Физика судара и фотопроцеса у атомским, (био)молекулским и нанодимензионим системима"* под руководством Др Братислава Маринковића.
- Септембар 2014 – 2017: изводи наставу математике у *Brook Hill International School* у Београду.
- 2017 – 2021: изводи наставу математике у *International School Savremena* у Београду.
- Члан организационог комитета конференције *"COST XLIC WG2 Expert meeting on biomolecules, 27th – 30th April 2015, Fruška Gora"*.
- 2018 – 2022: Учествовао у COST акцији CA17126 под називом *"Towards understanding and modelling intense electronic excitation (TUMIEE)"*

- 2019 – 2023: Учествовао у COST акцији CA18222 под називом “*Attosecond Chemistry (AttoChem)*”
- 2020 – 2023: Сарадња са лабораторијом “*JPL*” у изради рачунарских кодова за решавање Лапласове једначине на не-униформној мрежи као и пропацију наелектрисане честице кроз тако израчунато поље.
- 2021 – 2024: Учешће на пројекту FRAP OPM у сарадњи са немачким институтом “*Leibniz Institute for Photonic Technologies*” под руководством Др. Зорана Грујића.

Преглед научне активности кандидата

Истраживачка област којом се кандидат бавио пре и након последњег избора у звање је интеракција јаких поља са атомским системима. У истраживањима су кориштени теоријски и нумерички методи који се углавном односе на решавање временски зависне Шредингерове једначине и анализу добијених резултата.

Истраживана је пре свега интеракција атомских система са јаким ласерским зрачењем која доводи до процеса мултифотонске и тунелне јонизације, што је била и тема докторске дисертације кандидата (*Израчунавање насељености атомских стања, угаоне расподеле и енергијског спектра фотоелектрона код атомских система у јаким ласерским пољима применом временски зависних метода*) коју је одбранио 2018. године под менторством др Ненада Симоновића. Кандидат је до сада објавио седам радова у међународним часописима, три пре последњег избора у звање и четири након тога. Поред тога коаутор је на великом броју публикација које се односе на саопштења на међународним и домаћим конференцијама.

I. Научна активност до претходног избора у звање научни сарадник

У периоду до претходног избора у звање научни сарадник кандидат је проучавао интеракцију атома алкалних метала, као што су атоми натријума и литијума, са јаким ласерским пољем који су изабрани због могућности рачунања у једноелектронској слици (због изузетно захтевних нумеричких процедура). На овим системима испитивани су ефекти јонизације у различитим режимима спољашњег електромагнетног поља, а рачунате су вероватноће јонизације, угаоне расподеле и енергијски спектар фотоелектрона, као и насељености побуђених стања након примењеног ласерског пулса, а све у циљу испитивања ефеката попут резонантно појачане мултифотонске јонизације (REMPI), јонизације преко прага (ATI), као и рачунања динамичког Штарковог помака. Резултати су објављени у 3 рада у међународним часописима и приказани као 5 саопштења на међународним конференцијама. Такође су били и садржај једног предавања по позиву на међународној конференцији.

1. Рачунање стопе јонизације атома натријума у режиму тунелирања у квазистатичкој апроксимацији

Кандидат је испрограмио нумеричку процедуру за рачунање стопа јонизације и енергија везаних стања код алкалних метала у ласерском пољу велике таласне дужине (око 14 μm) користећи моделни Хелманов потенцијал за опис система. При овако великим таласним дужинама могуће је користити квазистатичку апроксимацију. Кандидат је испитао домен важења квазистатичке апроксимације користећи симулацију реалног пулса за поређење. Показано је да се ова апроксимација може користити у домену у ком је Келдишев параметар $\gamma = \frac{\omega\sqrt{2I_p}}{F}$ мањи од 0.2. Резултати симулација су у добром слагању са објављеним резултатима на сличним системима. Сви добијени резултати приказани су на једној међународној конференцији и објављени у једном раду:

A. Bunjac, D. B. Popović, and N. S. Simonović,

“Wave-packet analysis of strong-field ionization of sodium in the quasistatic regime”,

Eur. Phys. J. D: At. Mol. Clusters & Opt. Phys. **70**(5), 116 (2016). [6 pp]

Topical Issue: Advances in Positron and Electron Scattering, P. Limao -Vieira, G. Garcia,

E. Krishnakumar, J. Sullivan, H. Tanuma and Z. Petrovic (Guest editors)

[DOI: 10.1140/epjd/e2016-60738-0](https://doi.org/10.1140/epjd/e2016-60738-0)

<http://link.springer.com/article/10.1140%2Fepjd%2Fe2016-60738-0>

ISSN: 1434-6060

(Категорија M23)

2. Рачунање угаоних расподела и енергијског спектра фотоелектрона атома натријума и литијума у јаким ласерским пољима.

У оквиру мултифотонског режима нумерички је испитан атом натријума изложен кратким ласерским пулсевима у широком опсегу фреквенција и интензитета поља. Кандидат је опет испрограмирао нумеричку процедуру за еволуцију таласне функције помоћу решавања временски зависне Шредингерове једначине. Као резултат ове симулације дају вероватноће насељености атомских стања и показују услове при којима се одвија резонантно попуњавање. Интерполацијом добијених резултата предложен је метод за рачунање динамичког Штарковог помака под условом резонантности, као и метод за рачунање енергијског спектра фотоелектрона који репродукује профиле добијене услед резонантно појачане мултифотонске јонизације. Добијени резултати упоређени су недавно објављеним експерименталним подацима и дају добро слагање. Поред тога, рачунате су угаоне расподеле фотоелектрона атома натријума и литијума третираних интензивним ласерским пулсевима у трајању неколико десетина фемтосекунди. Из добијених профила импулсном простору израчунати су енергијски спектри који су упоређени са недавно објављеним експерименталним резултатима и дају добро слагање. Ови резултати објављени су у 2 рада:

A. Bunjac, D. B. Popović and N. S. Simonović,

“Resonant dynamic Stark shift as a tool in strong-field quantum control: calculation and application for selective multiphoton ionization of sodium”,

Phys. Chem. Chem. Phys. **19**, 19829-19836 (2017). [on-line 07.07.2017]

<https://doi.org/10.1039/C7CP02146A>

From themed collection XUV/X-ray light and fast ions for ultrafast chemistry

ISSN: 1463-9076

(Категорија M21)

A. Bunjac, D. B. Popović and N. S. Simonović,

“Calculations of photoelectron momentum distributions and energy spectra at strong-field multiphoton ionization of sodium”,

Eur. Phys. J D **71**(8), 208 (2017). [6pp, online 8 Aug.2017]

[doi: 10.1140/epjd/e2017-80276-5](https://doi.org/10.1140/epjd/e2017-80276-5)

Contribution to the Topical Issue: “Physics of Ionized Gases (SPIG 2016)”, Edited by G. Poparic,

B. Obradovic, D. Maric and A. Milosavljevic.

ISSN: 1434-6060

(Категорија M23)

II. Научна активност након претходног избора

У периоду након претходног избора у звање кандидат је наставио са 1) проучавањем интеракцију атома натријума са јаким ласерским пољем. Поред тога отворене су две нове теме: 2) Хиперфино цепање и време живота најнижег нивоа позитронијума у јаком електричном пољу и 3) утицај Рабијеве динамике на енергијски спектар фотоелектрона насталих при резонантној двофотонској јонизацији атома јаким ласерским импулсима. Резултати су објављени у 3 рада у међународним часописима и приказани већем броју саопштења на међународним конференцијама.

1. Селективна вишефотонска јонизација натријума фемтосекундним ласерским импулсима: анализа парцијалних таласа

У оквиру ове теме проучавана је вишефотонска јонизација натријума фемтосекундним ласерским пулсевима таласне дужине 800 нм у опсегу ласерских пикова интензитета који припадају домену јонизације преко баријере. Расподела импулса фотоелектрона и енергетски спектри одређени су нумерички решавањем временски зависне Шредингерове једначине за три вредности интензитета ласера из овог домена. Положаји пикова који се односе на Фриманове резонанције у израчунатим спектрима слажу се са позицијама пикова у експериментално одређеним спектрима. Анализирајући ове пикове методом парцијалних таласа откривено је да је сваки пик суперпозиција доприноса фотоелектрона произведених резонантно појачаном вишефотонском јонизацијом преко различитих међустања. Показано је да је при одговарајућим интензитетима ласера могућа селективна јонизација, која се одвија претежно кроз једно међустање. Добијени резултати приказани су на више међународних и домаћих научних скупова и објављени у једном раду:

A. Bunjac, D. B. Popović, and N. S. Simonović,

“On the selective multiphoton ionization of sodium by femtosecond laser pulses: A partial-wave analysis”,

Phys. Lett. A **394**, 127197 (2021). [6 pp]

<https://doi.org/10.1016/j.physleta.2021.127197>

(Категорија M22)

2. Хиперфино цепање и време живота најнижег нивоа позитронијума у јаком електричном пољу

Ова тема се бави додатном нестабилношћу позитронијума, који већ има коначан животни век услед анихилације, сада због могућности јонизације изазване електричним пољем. Прорачуни стопе јонизације коришћењем нумеричких метода показују да, у поређењу са анихилацијом, она постаје доминантна у опсегу јачине поља који припада режиму јонизације преко баријере (ОВИ). С друге стране, хиперфино цепање најнижег нивоа позитронијума опада у домену тунелирања, узимајући на почетку ОВИ-домена вредност која је око 20% нижа од вредности без поља. Како се јачина поља даље повећава, ово цепање варира прилично споро, али овде долази до додатног цепања нивоа триплета, чија је брзина упоредива са овом варијацијом. Коначно, показано је да су најнижи нивои енергије и стопе јонизације за атом водоника и позитронијум, одређени унутар грубе структуре, повезани са

скалирајућим трансформацијама. Добијени резултати приказани су на више међународних и домаћих научних скупова и објављени у једном раду:

M. Z. Milošević, A. Bunjac, D. B. Popović and N. S. Simonović

"Hyperfine splitting and lifetime of the positronium lowest level in a strong electric field"

J. Phys. B: At. Mol. Opt. Phys. **54**, 035001 (2021)

<https://doi.org/10.1088/1361-6455/abce96>

(Категорија M22)

3. Утицај Рабијеве динамике на енергијски спектар фотоелектрона насталих при резонантној двофотонској јонизацији атома јаким ласерским импулсима

У овој теми проучавани су ефекти Рабијеве динамике на енергијски спектар фотоелектрона, насталих при резонантној двофотонској јонизацији атома водоника јаким ласерским пулсевима, у које спадају асиметрија Аутлер-Таунсових дублета у спектрима и појава интерференционих образаца између пикова дублета. Под Рабијевом динамиком се подразумевају Рабијеве осцилације електронске популације између основног и побуђеног $2p$ стања атома водоника, изазване интензивним кратким ласерским пулсевима који резонантно спрежу два стања. Исти ласерско зрачење доводи до накнадне фотојонизације из побуђеног стања.

Спектри су рачунати применом методе временски зависних амплитуда коришћењем два приступа различитог нивоа апроксимације. Први приступ подразумева решавање комплетног скупа једначина за амплитуде, који поред амплитуда спрегнутих ($1s$, $2p$) и стања континуума, укључује и амплитуде других дискретних (мање значајних) стања. Други приступ је модел на три нивоа који укључује само амплитуде два спрегнута стања и стања континуума. Упоредивањем спектра добијених коришћењем ова два приступа потврђујено је да се померање Аутлер-Таунсових дублета, које постоји само у спектрима добијеним решавањем комплетног скупа једначина, може приписати динамичком Штарковом помаку, што је последица спреге са осталим стањима. Коначно, утврђено је да је асиметрија интензитета компонената Аутлер-Таунсових дублета, која се појављује у спектрима добијеним коришћењем оба нумеричка приступа, првенствено последица смањења вероватноће прелаза између $2p$ и стања континуума са повећањем енергије фотоелектрона.

Утврђено је да, за Гаусове, полугаусове и правоугаоне пулсаве, које карактерише иста пулсна површина, коначне популације имају исте вредности и да се спектри састоје од сличних образаца који имају исти број пикова и приближно исто раздвајање између Аутлер-Таунсових пикова. Додатна анализа преко „обучених стања“ показала је да је механизам формирања структура са вишеструким пиковима током процеса фотојонизације исти без обзира на облик пулса. Ове чињенице оповргавају хипотезу предложену у ранијим студијама са Гаусовим пулсом, да се образац вишеструких пикова појављује услед динамичке интерференције фотоелектрона емитованих са временским кашњењем на растућој и опадајућој страни пулса, пошто хипотеза није применљива ни на полу-Гаусов пулс који нема растући део ни на правоугаони пулс чији је интензитет константан. Ови резултати објављени су у 2 рада:

A. Bunjac, D. B. Popović and N. S. Simonović

"Analysis of the asymmetry of Autler–Townes doublets in the energy spectra of photoelectrons produced at two-photon ionization of atoms by strong laser pulses", *Eur. Phys. J. D* **76**, 249 (2022)

<https://doi.org/10.1140/epjd/s10053-022-00572-7>

(Категорија M23)

N. S. Simonović, D. B. Popović and A. Bunjac

"Manifestations of Rabi Dynamics in the Photoelectron Energy Spectra at Resonant Two-Photon Ionization of Atom by Intense Short Laser Pulses"

Atoms **11** (2), 20 (2023)

<https://doi.org/10.3390/atoms11020020>

Елементи за квалитативну оцену научног доприноса

1. Квалитет научних резултата

i. Значај научних резултата

Кандидат Андреј Буњац је учествовао у изради 4 научна рада а од тога на 2 као први аутор дао кључни допринос. Од тога су два објављена у истакнутим међународним часописима категорије M22, један у међународном часопису категорије M23, а један у међународном часопису који још увек нема категоризацију. Такође имао је 8 саопштења на међународним конференцијама као и 10 саопштења на скуповима од националног значаја. Поменути радови су:

N. S. Simonović, D. B. Popović and A. Bunjac,
"Manifestations of Rabi Dynamics in the Photoelectron Energy Spectra at Resonant Two-Photon Ionization of Atom by Intense Short Laser Pulses"
Atoms 11 (2), 20 (2023)
<https://doi.org/10.3390/atoms11020020>

A. Bunjac, D. B. Popović and N. S. Simonović,
"Analysis of the asymmetry of Autler–Townes doublets in the energy spectra of photoelectrons produced at two-photon ionization of atoms by strong laser pulses",
Eur. Phys. J. D 76, 249 (2022)
<https://doi.org/10.1140/epjd/s10053-022-00572-7>

A. Bunjac, D. B. Popović and N. S. Simonović,
"On the selective multiphoton ionization of sodium by femtosecond laser pulses: A partial-wave analysis",
Phys. Lett. A 394, 127197 (2021)
<https://doi.org/10.1016/j.physleta.2021.127197>

M. Z. Milošević, A. Bunjac, D. B. Popović and N. S. Simonović,
"Hyperfine splitting and lifetime of the positronium lowest level in a strong electric field",
J. Phys. B: At. Mol. Opt. Phys. 54, 035001 (2021)
<https://doi.org/10.1088/1361-6455/abce96>

ii. Параметри квалитета часописа

Кандидат Андреј Буњац је укупно објавио 4 научна рада у међународним часописима (од којих се вреднују само 3) и то:

1 рад у истакнутом међународном часопису *Physics Letters A*

(M22, импакт фактор = 2.285, 2021 снп = 0.917)

1 рад у истакнутом међународном часопису “*Journal of Physics B: Atomic, Molecular and Optical Physics*”

(M22, импакт фактор = 1.778, 2021 снп = 0.713)

1 рад у међународном часопису “*Atoms*”

(нема категорију, импакт фактор = 1,8, 2023 снп = 0.761)

1 рад у међународном часопису “*The European Physical Journal D*”

(M23, импакт фактор = 1,3, 2022 снп = 0.604)

	ИФ	М	СНИП
Укупно	7.163	13	2.995
Усредњено по чланку	1.791	4.33	0.749
Усредњено по аутору	2.2395	3.92	0.939

iii. Подаци о цитираности

Према бази *Web of Science* радови Андреја Буњца цитирани 33 пута (29 изузимајући аутоцитате). Према бази *Google Scholar* цитирани су 48 пута.

2. Нормирање броја коауторских радова, патената и техничких решења

Сви радови Андреја Буњца имају 3-4 аутора те се признају са пуним бројем поена јер су резултати рачунати нумерички. Укупан број поена које је кандидат остварио је 21 што је више од захтеваног минимума (16) за избор у звање научни сарадник.

3. Учешће у пројектима, потпројектима и пројектним задацима

Кандидат је учествовао на *COST* акцији *CA18222 "Attosecond Chemistry"* од 2019 до 2023 године као и на *COST* акцији *CA17126 "Towards understanding and modelling intense electronic excitation"* од 2018 до 2022 уз неколицину саопштења на конференцијама као и објављених радова унутар наведених акција. Кандидат је такође учествовао на пројекту *FRAP OPM* у сарадњи са немачким институтом “*Leibniz Institute for Photonic Technologies*” под руководством Др. Зорана Грујића. Коначно, кандидат је учествовао у сарадњи са лабораторијом “*JPL*” у изради рачунарских кодова за решавање Лапласове једначине на не-униформној мрежи као и пропагацију наелектрисане честице кроз тако израчунато поље.

4. Утицај научних резултата

Списак радова и цитата дат је у прилогу.

5. Конкретан допринос кандидата у реализацији радова у научним центрима у земљи и иностранству

Кандидат је све своје научне активности реализовао у Институту за Физику Београд. Значајно је допринео сваком раду у ком је учествовао. Његов допринос је пре свега у креирању нумеричких кодова за опис интеракције валентних електрона са јаким ласерским пољима и реализацији нумеричких прорачуна, а затим и у анализи истих, као и у писању радова. Поред тога кандидат је допринео у изради кода за пропагацију наелектрисаних честица кроз нумерички задато електрично поље.

Елементи за квантитативну оцену научног доприноса

Радови објављени у научним часописима од међународног значаја, научна критика; уређивање часописа (M20):

	број	вредност	укупно
M22	2	5	10
M23	1	3	3

Зборници са међународних научних скупова (M30):

	број	вредност	укупно
M33	4	1	4
M34	4	0.5	2

Предавања по позиву на skupovima nacionalnog značaja (M60):

	број	вредност	укупно
M64	10	0.2	2

Поређење са захтеваним критеријума од министарства науке:

Научни сарадник	Поени који треба да припадају следећим категоријама	Неопходно	Остварено
Обавезни (1)	M10+M20+M31+M32+M33+M41+M42	10	19
Обавезни (2)	M11+M12+M21+M22+M23	6	13
Укупно	Све категорије	16	21

Списак објављених радова кандидата

RADOVI U MEĐUNARODNIM ČASOPISIMA

N. S. Simonović, D. B. Popović and A. Bunjac

"Manifestations of Rabi Dynamics in the Photoelectron Energy Spectra at Resonant Two-Photon Ionization of Atom by Intense Short Laser Pulses"

Atoms 11 (2), 20 (2023)

<https://doi.org/10.3390/atoms11020020>

(нема М категорију)

A. Bunjac, D. B. Popović and N. S. Simonović

"Analysis of the asymmetry of Autler–Townes doublets in the energy spectra of photoelectrons produced at two-photon ionization of atoms by strong laser pulses"

Eur. Phys. J. D 76, 249 (2022)

<https://doi.org/10.1140/epjd/s10053-022-00572-7>

(M23=3)

A. Bunjac, D. B. Popović and N. S. Simonović

"On the selective multiphoton ionization of sodium by femtosecond laser pulses: A partial-wave analysis"

Phys. Lett. A 394, 127197 (2021)

<https://doi.org/10.1016/j.physleta.2021.127197>

(M22=5)

M. Z. Milošević, A. Bunjac, D. B. Popović and N. S. Simonović

"Hyperfine splitting and lifetime of the positronium lowest level in a strong electric field"

J. Phys. B: At. Mol. Opt. Phys. 54, 035001 (2021)

<https://doi.org/10.1088/1361-6455/abce96>

(M22=5)

PUBLIKACUJE SA NAUČNIH SKUPOVA

Duška B. Popović, Andrej Bunjac, Nenad S. Simonović,

“A dressed states analysis of Autler-Townes patterns in the PES at resonant two-photon ionization of hydrogen by short laser pulses”,

Proc. 17th Photonics Workshop, March 10-14, 2024, Kopaonik, Book of Abstracts, Eds. D. Lukić, M. Lekić, Z. Grujić (Institute of Physics Belgrade, Belgrade, 2024), Progress Report, p.18.

ISBN 978-86-82441-62-5

<http://www.photonicsworkshop.ipb.ac.rs/17/index.php>

(M64=0,2)

Nenad Simonović, Duška Popović, Andrej Bunjac,

“Analysis of Autler-Townes patterns in photoelectron energy spectra at resonant two-photon ionization of atom by laser pulses of different shapes”,

Meeting COST Action Attochem (CA18222), September 18-20. 2023, Szeged, Hungary, Book of Abstracts, Organizer F. Martin, Poster Session P-20, p.57.

BoA_attochem2023_CA18222

<https://attochem.elte.hu>

(M34=0,5)

Andrej B. Bunjac, Zoran D. Grujić, M. M. Ćurčić, Theo Scholtes, Jonas Hinkel,

“Analysis of the dynamic RF projection phase in True Scalar Cs Magnetometers”,

Proc. 16th Photonics Workshop, March 12-15, 2023, Kopaonik, Book of Abstracts, Eds. D. Lukić, M. Lekić, Z. Grujić (Institute of Physics Belgrade, Belgrade, 2023), Progress Report, p.65.

ISBN 978-86-82441-59-5

<http://www.photonicsworkshop.ipb.ac.rs/16/index.php>

(M64=0,2)

Nenad S. Simonović, Duška B. Popović, Andrej Bunjac,

“Analysis of the photoelectron energy spectra at resonant two-photon ionization of hydrogen atom by intense short laser pulses”,

Proc. 16th Photonics Workshop, March 12-15, 2023, Kopaonik, Book of Abstracts, Eds. D. Lukić, M. Lekić, Z. Grujić (Institute of Physics Belgrade, Belgrade, 2023), Progress Report, p.33.

ISBN 978-86-82441-59-5

<http://www.photonicsworkshop.ipb.ac.rs/16/index.php>

(M64=0,2)

N. S. Simonović, D. B. Popović and A. Bunjac,

“Interference effects in the sequential two-photon ionization of hydrogen by short laser pulses”,

The 3rd Annual Workshop of the AttoChem COST action CA18222, October 18th - 21st, 2022, Prague, Czech Republic, Book of Abstracts, Organizers: Tomáš Slanina and Zdeněk Mašín, Poster P43, p.86.

AttoChem-2022-Book-of-Abstracts-v2.pdf

<https://attochem-prague.troja.mff.cuni.cz/>

(M34=0,5)

N. S. Simonović, D. B. Popović and A. Bunjac,

“Photoelectron Energy Spectra in Sequential Two-Photon Ionization of Hydrogen by Gaussian and Half-Gaussian Laser Pulses”,

Proc. 31st Summer School and Int. Symp. on Ionized Gases (SPIG2022), September 5 – 9, 2022, Belgrade, Serbia, Contributed papers & abstracts of invited lectures, topical invited lectures and progress reports, Editors Dragana Ilić, Vladimir Srećković, Bratislav Obradović and Jovan Cvetić (University of Belgrade, School of Electrical Engineering; University of Belgrade, Faculty of Physics; Serbian Academy of Sciences and Arts, Belgrade, 2022) Contributed Papers, pp.53-56.

ISBN 978-86-82296-02-7

Publ. Astron. Obs. Belgrade No. 102 (2022), 53 – 56.

ISSN 0373-3742

SPIG2022-Book-Online.pdf

<http://spig2022.ipb.ac.rs/>

(M33=1)

Marija M. Ćurčić, Andrej Bunjac, Saša Topić, Jonas Hinkel, Theo Scholtes, Zoran D. Grujić,

“All-optical Cs magnetometer based on free alignment precession”,

Proc. 15th Photonics Workshop, March 13-16, 2022, Kopaonik, Book of Abstracts, Eds. D. Lukić, M. Lekić, Z. Grujić (Institute of Physics Belgrade, Belgrade, 2022), Progress Report, p.65

Book of Abstracts

ISBN 978-86-82441-55-7

www.photonicsworkshop.ipb.ac.rs/15/

(M64=0,2)

Zoran D. Grujić, Andrej Bunjac, Saša Topić, Marija M. Ćurčić, Jonas Hinkel, Theo Scholtes,

“Why do we need accurate magnetometers and how to realize them”,

Proc. 15th Photonics Workshop, March 13-16, 2022, Kopaonik, Book of Abstracts, Eds. D. Lukić, M. Lekić, Z. Grujić (Institute of Physics Belgrade, Belgrade, 2022), Progress Report, p.63

Book of Abstracts

ISBN 978-86-82441-55-7

www.photonicsworkshop.ipb.ac.rs/15/

(M64=0,2)

Andrej B. Bunjac, Zoran D. Grujić, S. Topić, Theo Scholtes, Jonas Hinkel

“DC Transverse Magnetic Field Scan in True Scalar Cs Magnetometers”,

Proc. 15th Photonics Workshop, March 13-16, 2022, Kopaonik, Book of Abstracts, Eds. D. Lukić, M. Lekić, Z. Grujić (Institute of Physics Belgrade, Belgrade, 2022), Contributed Paper, p.62

Book of Abstracts

ISBN 978-86-82441-55-7

www.photonicsworkshop.ipb.ac.rs/15/

(M64=0,2)

Andrej Bunjac, Duška B. Popović and Nenad S. Simonović,

“Dynamic interference of photoelectrons in two-photon ionization of hydrogen by intense short laser pulses”,

Proc. 15th Photonics Workshop, March 13-16, 2022, Kopaonik, Book of Abstracts, Eds. D. Lukić, M. Lekić, Z. Grujić (Institute of Physics Belgrade, Belgrade, 2022), Progress Report, p.56

Book of Abstracts

ISBN 978-86-82441-55-7

www.photonicsworkshop.ipb.ac.rs/15/

(M64=0,2)

A. Bunjac, D. B. Popović and N. S. Simonović,

“Dynamic interference of photoelectrons at multiphoton ionization of atoms by short laser pulses”,

Proc. VIII International School and Conference on Photonics - PHOTONICA2021 & HEMMAGINERO workshop, 23 - 27 August 2021, Belgrade, Serbia, Book of abstracts, Eds: Mihailo Rabasović, Marina Lekić and Aleksandar Krmpot, (Institute of Physics Belgrade, Belgrade, Serbia) Abstract: 9. Laser - material interaction, p.152.

ISBN 978-86-82441-53-3

<http://www.photonica.ac.rs/docs/Book%20of%20abstracts%202021.pdf>

(M34=0,5)

Andrej Bunjac, Duška B. Popović, Nenad S. Simonović,

“Partial-wave analysis of the resonantly enhanced multiphoton ionization of sodium by femtosecond laser pulses”

Proc. 14th Photonics Workshop, March 14-17, 2021, Kopaonik, Book of Abstracts, Eds. D. Lukić, M. Lekić, Z. Grujić (Institute of Physics Belgrade, Belgrade, 2021) Oral presentation, p.21

Book of Abstracts

ISBN 978-86-82441-52-6

<http://www.photonicsworkshop.ipb.ac.rs/14/index.php>

(M64=0,2)

Andrej Bunjac, Duška B. Popovic, Nenad S. Simonovic,

“Partial-wave analysis of multiphoton ionization of sodium by short laser pulses in over-the-barrier regime”,

Proc. 1st Annual Workshop for the Cost Action CA18222 (AttoChemistry), September 9-11, 2020, Organized on-line, Book of Abstracts, Editor: Katalin Nagy-Póra, Poster Contribution P-34, page 81.

<http://atom.ubbcluj.ro/katalin/abstractbook.pdf>

(M34=0,5)

M. Z. Milošević, A. Bunjac, D. B. Popović and N. S. Simonović,

“Hyperfine Splitting of the Lowest State Energy of Positronium in Strong Electric Field”,

Proc. 30th Summer School and International Symposium on the Physics of Ionized Gases (SPIG2020), August 24 – 28, 2020, Šabac, Serbia, Contributed Papers & Abstracts Of Invited Lectures, Topical Invited Lectures and Progress Reports, Editors: Luka Č. Popović, Duško Borka, Dragana Ilić and Vladimir Srećković, (Faculty of Mathematics - Dept. of Astronomy, Astronomical Observatory of Belgrade, Institute of Physics - University of Belgrade, Belgrade, 2020) Contributed Paper, pp.51-54.

Publ. Astron. Obs. Belgrade No. 99, 51-54 (2020).

<http://spig2020.ipb.ac.rs/Spig2020-Book-Online.pdf>

ISSN: 0373-3742

ISBN 978-86-80019-94-9

(M33=1)

A. Bunjac, D. B. Popović and N. S. Simonović,

“Selective Multiphoton Ionization of Sodium by Femtosecond Laser Pulses”,

Proc. 30th Summer School and International Symposium on the Physics of Ionized Gases (SPIG2020), August 24 – 28, 2020, Šabac, Serbia, Contributed Papers & Abstracts Of Invited Lectures, Topical Invited Lectures and Progress Reports, Editors: Luka Č. Popović, Duško Borka, Dragana Ilić and Vladimir Srećković, (Faculty of Mathematics - Dept. of Astronomy, Astronomical Observatory of Belgrade, Institute of Physics - University of Belgrade, Belgrade, 2020) Contributed Paper, pp.35-38.

Publ. Astron. Obs. Belgrade No. 99, 35-38 (2020).

<http://spig2020.ipb.ac.rs/Spig2020-Book-Online.pdf>

ISSN: 0373-3742

ISBN 978-86-80019-94-9

(M33=1)

Andrej Bunjac, Duška B. Popović, Nenad S. Simonović,

“Multiphoton ionization of sodium by intense femtosecond laser pulses in the near IR domain”,

Proc. 13th Photonics Workshop, Kopaonik, 8-12 March 2020, Book of Abstracts, Eds. D. Lukić, M. Lekic, D Grujic (Institute of Physics Belgrade, Belgrade, 2020) Progress Report, Oral presentation, p.33.

Konferencija Trinaesta radionica fotonike (2019), Kopaonik 8-12.03.2020, Zbornik apstrakata, Urednici: D. Lukić, M. Lekic, D Grujic (Institut za fiziku Beograd, 2020) Usmeno izlaganje, str.33.

ISBN: 978-86-82441-50-2

<http://www.photonicsworkshop.ipb.ac.rs/13/index.php>

(M64=0,2)

A. Bunjac, D. B. Popović and N. S. Simonović,

“Dynamic Stark shift and multiphoton ionization of sodium by femtosecond laser pulses”,

Proc. PHOTONICA2019 - The Seventh International School and Conference on Photonics, 26 August – 30 August 2019, Belgrade, Serbia & Machine Learning with Photonics Symposium (ML-Photonica 2019) & ESUO Regional Workshop & COST action CA16221, Book of Abstracts, (Abstracts of Tutorial, Keynote, Invited Lectures, Progress Reports and Contributed Papers) Eds: Milica Matijević, Marko Krstić and Petra Beličev (Vinča Institute of Nuclear Sciences, Belgrade, 2019), Progress Report, print:p.29; on-line:p.33.

http://www.photonica.ac.rs/docs/PHOTONICA2019-Book_of_abstracts.pdf

ISBN 978-86-7306-153-5

(M64=0,2)

A. Bunjac, D. B. Popović and N. S. Simonović,

“Strong Field Multiphoton Ionization of Lithium”,

Proc. 29th Summer School and Int. Symp. on the Physics of Ionized Gases (SPIG2018), Aug. 28 - Sep. 1, 2018, Belgrade, Serbia, Contributed Papers & Abstracts of Invited Lectures, Topical Invited Lectures, Progress Reports and Workshop Lectures Editors: Goran Poparić, Bratislav Obradović, Duško Borka and Milan Rajković (Vinča Institute of Nuclear Sciences and Serbian Academy of Sciences and Arts, Belgrade, 2018). Contributed Paper, pp.15-18.

ISBN 978-86-7306-146-7

<http://www.spig2018.ipb.ac.rs/SPIG2018-book-online.pdf>

(M33=1)

PAPER

Hyperfine splitting and lifetime of the positronium lowest level in a strong electric field

To cite this article: M Z Milošević *et al* 2021 *J. Phys. B: At. Mol. Opt. Phys.* **54** 035001

View the [article online](#) for updates and enhancements.



IOP | ebooks™

Bringing together innovative digital publishing with leading authors from the global scientific community.

Start exploring the collection—download the first chapter of every title for free.

Hyperfine splitting and lifetime of the positronium lowest level in a strong electric field

M Z Milošević, A Bunjac, D B Popović and N S Simonović* 

Institute of Physics, University of Belgrade, Pregrevica 118, 11080 Belgrade, Serbia

E-mail: simonovic@ipb.ac.rs

Received 25 August 2020, revised 4 November 2020

Accepted for publication 27 November 2020

Published 18 January 2021



Abstract

When placed in an external electric field, positronium, which already has a finite lifetime due to annihilation, becomes additionally unstable due to field-induced ionization. Calculations of the ionization rate using *ab initio* methods show that, compared to annihilation, it becomes dominant in the range of field strengths belonging to over-the-barrier ionization (OBI) regime. On the other hand, the hyperfine splitting of the positronium lowest level decreases in the tunnelling domain, taking at the beginning of the OBI domain a value that is about 20% lower than the field-free value. As the field strength increases further, this splitting varies rather slowly, but here an additional splitting of triplet levels occurs, whose rate is comparable to this variation. Finally, it is demonstrated that the lowest energy levels and ionization rates for the hydrogen atom and positronium, determined within the gross structure, are related to scaling transformations.

Keywords: positronium, hyperfine splitting, electric field, ionization

(Some figures may appear in colour only in the online journal)

1. Introduction

In contrast to ordinary hydrogen-like atoms (H, He⁺, Li⁺⁺, etc), positronium (Ps) is an unstable system due to a non-negligible probability for annihilation of the electron-positron (e^-e^+) pair which constitutes this exotic atom [1]. The lifetimes of the singlet (1^1S_0) and triplet (1^3S_1) components of the ground-state of positronium, the so-called para-positronium (p-Ps) and ortho-positronium (o-Ps), are 125 ps and 142 ns, respectively [2]. The ground state energy of positronium is about half of that of hydrogen ($E \approx -6.8$ eV), but its hyperfine splitting (HFS), $E_{o-Ps} - E_{p-Ps} = 0.845$ meV [3], when compared to that for hydrogen, is more than three orders of magnitude larger. This splitting is a consequence of two spin-dependent interactions: (i) the spin-spin coupling (the interaction of individual magnetic momenta of e^- and e^+) and (ii) ‘the annihilation force’ (the possibility of virtual annihilation and re-creation of the e^-e^+ pair) [4].

When positronium is placed in an electric field another kind of instability arises—the field induced decay of e^-e^+ pair, i.e. the ionization of positronium by the electric, namely, the external electric field distorts the Coulomb potential of the pair, forming a potential (Stark) barrier through which the system can decay by tunnelling. The limiting case of this process when the barrier is suppressed below the energy of the atomic state, which takes place at very strong fields, is usually referred to as over-the-barrier ionization (OBI). Since the ionization rate increases with the field strength, at sufficiently strong fields the related lifetime may be much shorter than the lifetimes of p-Ps and o-Ps, leading to a reduction of the annihilation events. In a recent study it has been shown how the annihilation dynamics of the excited positronium can be controlled using parallel electric and magnetic fields [5, 6].

Tunnel ionization as well as the Stark shift of the energy levels of hydrogen-like atoms is successfully described analytically in the case of weak fields [7]. An improved formula [8] was recently used to determine the tunnelling rates for the field ionization of Rydberg positronium [9]. At stronger fields,

* Author to whom any correspondence should be addressed.

however, particularly in the OBI domain, accurate values for energies and ionization rates can be obtained only by applying *ab initio* (numerical) methods. In this paper we study the lowest state energy and the ionization rate of positronium in the range of field strengths from zero to a value deep in the OBI domain, using two different numerical methods: the Wave-Packet Propagation (WPP) method and the complex-rotation (CR) method. These methods were previously successfully used in studies of ordinary atoms and ions in strong fields [10–12].

Research into HFS of energy levels of the field-free positronium and under the influence of magnetic field began immediately after its discovery [13]. This research, as well as the research of fine and ultrafine structure of the positronium spectrum, has continued until today, resulting in a huge number of publications. One of the goals of studying this purely leptonic system was to test the precision of quantum electrodynamics. Existing measurements for a number of level transitions, like $1^3S_1-1^1S_0$ (ground-state HFS) [3, 14], $2^3S_1-1^3S_1$ [15, 16] and $2^3S_1-2^{2S+1}P_J$ [17–19], were generally in agreement with theoretical predictions (see [20, 21] and references therein). However, a recently reported discrepancy in measuring the fine structure of the $n = 2$ state with theoretical predictions [22] opens up new questions that require further research. On the other hand, research on effects of the electric field on the hyperfine structure of positronium spectrum is present in the literature to a much lesser extent (see reference [6] as a recent example). A reason may be the fact that HFS of energy levels of positronium is not strongly affected by an external electric field. A weak dependence of HFS on the electric field occurs due to the change of form of the positronium lowest state wave function when the field increases. The results which we present here are a contribution in this direction.

The paper is organized in the following way. In the next section we introduce the model and define the ionization regimes (tunnelling and OBI). Approximate formulae for the lowest state energy and ionization rate are given in section 3. Numerical methods are briefly described in the same section. The results for positronium, obtained using different methods, are presented and compared in section 4. In section 5 it is shown how the energies and ionization rates for positronium and hydrogen can be related using scaling properties of the Coulomb systems. A summary and discussion are given in section 6.

2. The model

2.1. Interaction with the electric field

The Hamiltonian describing the relative motion of a two-particle system consisting of one electron ($q_1 = -1$, $m_1 = 1$) and another particle of the opposite charge ($q_2 = +1$) and mass m_2 , placed in the external electric field of strength F , reads (in atomic units)

$$H_0 = -\frac{1}{2\mu}\nabla^2 - \frac{1}{r} - Fz, \quad (1)$$

where r is the inter-particle distance, z is its component in the field direction and $\mu = m_1m_2/(m_1 + m_2)$ is the reduced mass.

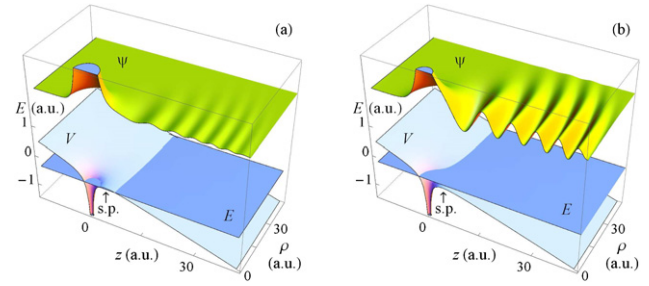


Figure 1. Potential $V = -1/r - Fz$, where $r = (\rho^2 + z^2)^{1/2}$ and $\rho = (x^2 + y^2)^{1/2}$ (bottom, light blue), the lowest energy level E (bottom, dark blue) and the real part of wave function ψ (top, green) corresponding to the lowest resonant state at the field strength $F = 0.05$ a.u. ($\approx 2.571 \times 10^{10}$ V m $^{-1}$) for: (a) hydrogen ($\mu = 1$, $E = -0.5061$ a.u.) and (b) positronium ($\mu = 1/2$, $E = -0.2846$ a.u.). The vertical arrow shows the position of the saddle point of the potential barrier. Note that at this field strength the ionization of hydrogen realizes by tunnelling, while in the case of positronium it is OBI.

For the hydrogen atom this mass is $\mu = 1$ (in the approximation of infinitely heavy nucleus), whereas for positronium it takes the value $\mu = 1/2$. Since the spin–orbit and spin–spin coupling, as well as other higher order terms, are neglected in Hamiltonian (1), it describes the so-called gross structure of the system. At the end of section 4 it will be shown that it is sufficient to use this method when considering the ionization rates.

When $F \neq 0$, the Coulomb potential $-1/r$ and the external field form the potential barrier (see figure 1) with the saddle point of height $V_{sp} = -2\sqrt{F}$ located at $\mathbf{r}_{sp} = (0, 0, 1/\sqrt{F})$. Since the potential energy outside the barrier asymptotically tends to $-\infty$, the system can decay by tunnelling at any energy E . Therefore, all bound states of the field-free atom become resonant (autoionizing) states when $F \neq 0$.

As it was already mentioned in the introduction, two ionization regimes can be distinguished: (i) the tunnel ionization (tunnelling) regime, when $E < V_{sp}$ (see figure 1(a)), and (ii) the OBI regime, when $E > V_{sp}$ (see figure 1(b)). Here we consider the ionization from the lowest state which in the limit $F \rightarrow 0$ approaches the ground state of the field-free atom. The value of the field strength which separates the ionization regimes F^* is the root of the equation

$$E(F^*) = V_{sp}(F^*) \equiv -2\sqrt{F^*}. \quad (2)$$

Thus, the tunnelling and OBI take place for: (i) $F < F^*$ and (ii) $F > F^*$, respectively.

2.2. The spin–spin coupling and the annihilation interaction

The interactions which lead to the energy splitting between the o-Ps and p-Ps ground states—the spin–spin coupling and the annihilation interaction—are described by two additional terms in the Hamiltonian which take the forms [23]

$$V_{ss} = \frac{\alpha^2}{4} \left[\frac{3(\vec{\sigma}_1 \cdot \mathbf{r})(\vec{\sigma}_2 \cdot \mathbf{r})}{r^5} - \frac{\vec{\sigma}_1 \cdot \vec{\sigma}_2}{r^3} + \frac{8\pi}{3} \vec{\sigma}_1 \cdot \vec{\sigma}_2 \delta(\mathbf{r}) \right], \quad (3)$$

$$V_{\text{ann}} = \frac{\pi\alpha^2}{2}(3 + \vec{\sigma}_1 \cdot \vec{\sigma}_2)\delta(\mathbf{r}). \quad (4)$$

Here $\mathbf{r} = \mathbf{r}_1 - \mathbf{r}_2$ is the relative radius vector of e^-e^+ pair, $\vec{\sigma}_{1,2}$ are the Pauli matrices describing the spin of these two particles and $\alpha = 1/137.036$ is the fine-structure constant. In analogy with ordinary atoms, this energy splitting is called the HFS, although for positronium it is of the same order of magnitude as the fine structure corrections.

Assuming that the spin–spin coupling and the annihilation interaction are not directly affected by the external electric field, the Hamiltonian for positronium in this field, which takes

into account the HFS, reads

$$H = H_0 + V_{\text{ss}} + V_{\text{ann}} = H_0 + V_{\text{hfs}}. \quad (5)$$

Using relations $\vec{\sigma}_1 \cdot \vec{\sigma}_2 = 2\mathbf{S}^2 - 3$ and $(\vec{\sigma}_1 \cdot \mathbf{r})(\vec{\sigma}_2 \cdot \mathbf{r}) = 2(\mathbf{S} \cdot \mathbf{r})^2 - r^2$, where $\mathbf{S} = (\vec{\sigma}_1 + \vec{\sigma}_2)/2$ is the total spin, and writing $\mathbf{r} = r\mathbf{e}_r$, the HFS term becomes

$$V_{\text{hfs}} = \frac{\alpha^2}{2r^3} [3(\mathbf{S} \cdot \mathbf{e}_r)^2 - \mathbf{S}^2] + \pi\alpha^2 \left(\frac{7}{3}\mathbf{S}^2 - 2 \right) \delta(\mathbf{r}). \quad (6)$$

The matrix which represents the operator $(\mathbf{S} \cdot \mathbf{e}_r)^2$ in the basis of singlet/triplet spin states $\{|S, M_S\rangle | S = 0, 1; M_S = -S, \dots, S\}$ has a quasi-diagonal form

$$(\mathbf{S} \cdot \mathbf{e}_r)^2 = \begin{pmatrix} 0 & 0 & 0 & 0 \\ 0 & \frac{1}{4}(\cos 2\vartheta + 3) & -\frac{\sin 2\vartheta e^{i\varphi}}{2\sqrt{2}} & \frac{1}{2}\sin^2\vartheta e^{2i\varphi} \\ 0 & -\frac{\sin 2\vartheta e^{-i\varphi}}{2\sqrt{2}} & \sin^2\vartheta & \frac{\sin 2\vartheta e^{i\varphi}}{2\sqrt{2}} \\ 0 & \frac{1}{2}\sin^2\vartheta e^{-2i\varphi} & \frac{\sin 2\vartheta e^{-i\varphi}}{2\sqrt{2}} & \frac{1}{4}(\cos 2\vartheta + 3) \end{pmatrix}, \quad (7)$$

while the corresponding matrix of the operator \mathbf{S}^2 is diagonal

$$(\mathbf{S}^2)_{SM_S, S'M'_S} = S(S+1)\delta_{SS'}\delta_{M_S M'_S}. \quad (8)$$

Thus, the HFS terms do not couple the singlet ($S = 0$) and the triplet ($S = 1$) states, but V_{ss} couples the triplet states with different values of M_S .

Since the first diagonal element ($SM_S = S'M'_S = 00$) of matrices (7) and (8) is zero, in the singlet case the spin-dependent terms in equation (6) vanish and V_{hfs} reduces to

$$V_{\text{hfs}}^{(S=0)} = -2\pi\alpha^2\delta(\mathbf{r}). \quad (9)$$

For the triplet case the spin-dependent terms in V_{hfs} are different from zero. Assuming, however, that their contribution is much smaller than the contribution of the term with delta-function, we neglect the M_S -coupling and characterize the lowest state by a definite value of quantum number M_S . In this approximation we only keep the diagonal matrix elements $[(\mathbf{S} \cdot \mathbf{e}_r)^2]_{1M_S, 1M_S}$ and $(\mathbf{S}^2)_{1M_S, 1M_S} = 2$ in the HFS term and apply the expression

$$V_{\text{hfs}}^{(S=1)} = \frac{\alpha^2}{2r^3} [3[(\mathbf{S} \cdot \mathbf{e}_r)^2]_{1M_S, 1M_S} - 2] + \frac{8}{3}\pi\alpha^2\delta(\mathbf{r}). \quad (10)$$

3. Methods

3.1. Approximate formulae

The lowest energy level E of the system described by Hamiltonian (1) can be written as the sum of the ground state

energy of the field-free atom ($-\mu/2$) and the Stark shift ΔE of this level at the field strength F . For weak fields ($F \ll F^*$) the later can be approximated by the quadratic term $-\alpha_p F^2/2$, where $\alpha_p = 9/(2\mu^3)$ is the polarizability of the ground state. Therefore

$$E = -\frac{\mu}{2} - \frac{9F^2}{4\mu^3}. \quad (11)$$

In the same range of field strengths, the ionization (tunnelling) rate w is given by the Landau formula [7]

$$w = \frac{4\mu^3}{F} \exp\left(-\frac{2\mu^2}{3F}\right). \quad (12)$$

Functions $E(F)$ and $w(F)$ are shown in figures 2(a) and (b), respectively, for $\mu = 1$ (H, dashed line) and $\mu = 1/2$ (Ps, full line).

3.2. The wave-packet propagation method

In this method the resonance position and width are determined from the time-evolution of the system. If $\psi(\mathbf{r}, 0)$ is the initial wave function (wave packet), the wave function $\psi(\mathbf{r}, t)$ at an arbitrary time t can be determined by numerically integrating the time dependent Schrödinger equation. For this purpose here a variant of the second-order-difference scheme [24] was used. The energy spectrum is obtained from the autocorrelation function $c(t) = \langle \psi(0) | \psi(t) \rangle$ by calculating its power spectrum (the square of the absolute value of its Fourier transform). The resonances are related to (approximate) Lorentzian profiles in the power spectrum containing the information about their positions (E) and widths (Γ). In order to calculate these parameters for the lowest state, the initial

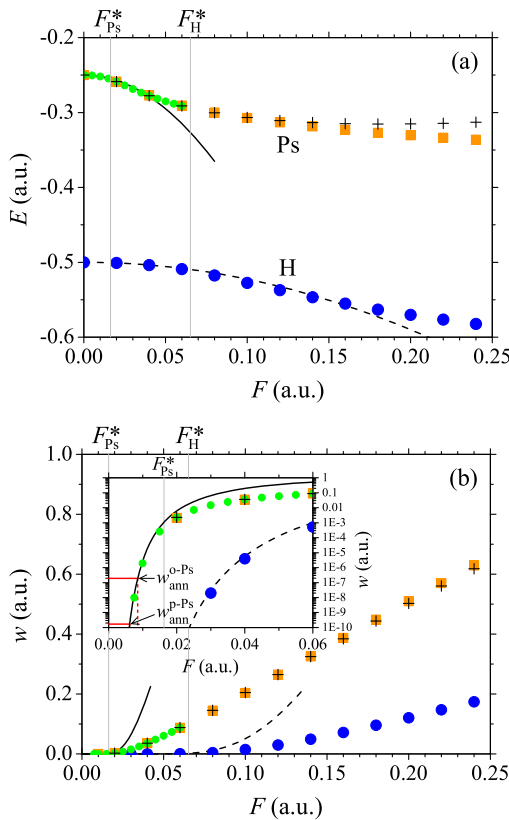


Figure 2. (a) The ground state energy E and (b) the ionization rate w for the hydrogen atom (dashed line, blue circles) and positronium (full line, orange squares, crosses) as functions of the strength of external electric field F . The lines, full symbols and crosses represent the analytical values (formulae), numerical results obtained by the WPP method and those obtained by the CR method, respectively. Green circles represent the results for positronium obtained by scaling the numerical data for hydrogen. Vertical gray lines mark the field strengths F^* dividing the tunnelling and over-the-barrier domains for each atom. For comparison, the annihilation rates for para- and ortho-positronium, w_{ann}^{p-Ps} and w_{ann}^{o-Ps} , are shown in the inset (red lines) in plot (b).

wave function $\psi(\mathbf{r}, 0)$ is set to be the ground state wave function of the field-free atom. In this case the spectrum reduces to a single Lorentzian corresponding to the lowest state and $|c(t)|^2 = e^{-wt}$, where $w = \Gamma/\hbar$ is the corresponding decay rate (hereafter we put $\hbar = 1$). Then, Γ (or w) can be determined more precisely by calculating the gradient of $\ln(|c(t)|^2)$. This method was used here to calculate the lowest state energies and widths of hydrogen and positronium in electric field described by Hamiltonian (1).

3.3. The complex-rotation method

A resonant state $\psi(\mathbf{r})$ can be regarded as an extension of the concept of bound state in a sense that it is an eigensolution of the Schrödinger equation which asymptotically behaves as a purely outgoing wave ($\psi(\mathbf{r})$ is not square integrable, see figure 1) with complex eigenenergy E_{res} . The real and imaginary parts of E_{res} determine the energy (position) and the width of the resonance, $E = \text{Re}(E_{res})$, $\Gamma = -2 \text{Im}(E_{res})$. The basic idea of the complex rotation method (see e.g.

references [25–27]) is to make the resonance wave function $\psi(\mathbf{r})$ square integrable by a complex rotation of the coordinate, $\psi(\mathbf{r}) \rightarrow \psi_\theta(\mathbf{r}) = \psi(e^{i\theta} \mathbf{r})$, where θ is a real parameter called the ‘rotation angle’. Such a ‘rotated’ state $\psi_\theta(\mathbf{r})$ is an eigenfunction of the so-called complex rotated Hamiltonian H_θ obtained from the original Hamiltonian H by the transformations $\mathbf{r} \rightarrow e^{i\theta} \mathbf{r}$. The spectrum of Hamiltonian (5) (or (1)) can be computed by diagonalizing the corresponding rotated Hamiltonian

$$H_\theta = -\frac{e^{-2i\theta}}{2\mu} \nabla^2 - \frac{e^{-i\theta}}{r} - e^{i\theta} Fz + e^{-3i\theta} V_{hfs} \quad (13)$$

in a square integrable basis which is complete in a sense that it covers the continuous part of the spectrum, too. For this purpose we use the Sturmian basis [28].

4. Results

In the first step of this analysis we neglect higher order terms in the Hamiltonian and calculate the lowest state energies and widths (ionization rates) for the hydrogen atom and positronium using Hamiltonian (1). These quantities in the range of field strengths from $F = 0$ to 0.25 a.u. ($\approx 1.286 \times 10^{11}$ V, m $^{-1}$), obtained using the formulae and methods described in the previous section, are shown in figure 2. It can be seen that the expressions (11) and (12) approximately reproduce numerical results in the tunnelling regime ($F < F^*$) but fail in the OBI regime ($F > F^*$). The values of the field strength which separate the ionization regimes ($F^* = 0.065$ a.u. for H and $F^* = 0.016$ a.u. for Ps) are determined from equation (2) using the expression (11) or the corresponding numerical values for the lowest state energy. A growing difference between the analytical and numerical results for E and w at $F > F^*$ confirms the fact that equations (11) and (12) are valid only for weak fields, and the values for E and w at stronger fields (especially in the OBI regime) must be determined numerically.

Numerical values for positronium (gross structure) obtained by the WPP method and by the CR method are shown in columns 2–5 of table 1. It can be seen that a difference between the results obtained by these two numerical methods, which is small for $F \sim F^*$ ($|\Delta E/E| < 0.2\%$ for $F < 0.1$ a.u., $\Delta w/w < 0.5\%$ for $F \in (0.02, 0.1)$ a.u.), becomes significant when $F \gg F^*$, especially for energies ($|\Delta E/E| \approx 8.2\%$ and $\Delta w/w \approx 1.7\%$ for $F = 0.25$ a.u.). The small difference at lower field strengths can be attributed to a numerical error (of the WPP method, primarily). However, the significant discrepancy that occurs at very strong fields should be attributed to the fact that the quantities E and $\Gamma/2$, which appear in the Breit–Wigner formula (Lorentz parameters), are not identical to the real and imaginary part of the complex energy, especially for very broad resonances (large Γ) [32]. Namely, the correspondence between resonant states and complex poles of the scattering matrix makes sense only under the assumption that $\Gamma \ll |E|$ (see e.g. the introduction in reference [33]). Therefore, although the CR calculations introduce a smaller numerical error, the values for E and Γ ,

Table 1. The lowest state energies (E_{Ps} , E_{p-Ps} , E_{o-Ps}) and widths (Γ_{Ps}) of positronium at different strengths of external electric field F (all in atomic units) obtained by the WPP method and by the CR method. Quantities E_{Ps} , E_{p-Ps} and E_{o-Ps} are the lowest state energies for: positronium calculated without a HFS contribution, para- and ortho-positronium calculated using only the term with delta-function in expression (10), respectively. The quantity E_{hfs} in the last column is the HFS of the lowest state energy of positronium, determined as $E_{o-Ps} - E_{p-Ps}$.

F	E_{Ps} (WPP)	Γ_{Ps} (WPP)	E_{Ps} (CR)	Γ_{Ps} (CR)	E_{p-Ps} (CR)	E_{o-Ps} (CR)	E_{hfs}
0	-0.25	0	-0.25	0	-0.2500133	-0.2499823	3.1053×10^{-5}
0.01	-0.25188	2×10^{-6}	-0.2518858	1.94635×10^{-6}	-0.2518988	-0.2518685	3.0220×10^{-5}
0.02	-0.25875	2.121×10^{-3}	-0.2587803	2.26983×10^{-3}	-0.2587919	-0.2587649	2.7001×10^{-5}
0.03	-0.26866	1.484×10^{-2}	-0.2686678	1.49579×10^{-2}	-0.2686785	-0.2686535	2.4945×10^{-5}
0.04	-0.27743	3.560×10^{-2}	-0.2776272	3.57081×10^{-2}	-0.2776376	-0.2776133	2.4289×10^{-5}
0.05	-0.28464	6.033×10^{-2}	-0.2850625	6.06145×10^{-2}	-0.2850728	-0.2850487	2.4140×10^{-5}
0.06	-0.29055	8.757×10^{-2}	-0.2911676	8.77519×10^{-2}	-0.2911779	-0.2911538	2.4140×10^{-5}
0.07	-0.29555	0.1157	-0.2961905	0.1161592	-0.2962008	-0.2961766	2.4199×10^{-5}
0.08	-0.29989	0.1448	-0.3003339	0.1453131	-0.3003444	-0.3003201	2.4319×10^{-5}
0.09	-0.30374	0.1751	-0.3037541	0.1749071	-0.3037645	-0.3037401	2.4378×10^{-5}
0.10	-0.30722	0.2034	-0.3065706	0.2047509	-0.3065811	-0.3065566	2.4468×10^{-5}
0.11	-0.31035	0.2343	-0.3088764	0.2347219	-0.3088869	-0.3088624	2.4527×10^{-5}
0.12	-0.31328	0.2646	-0.3107449	0.2647381	-0.3107555	-0.3107309	2.4527×10^{-5}
0.13	-0.31599	0.2951	-0.3122348	0.2947434	-0.3122454	-0.3122208	2.4557×10^{-5}
0.14	-0.31850	0.3257	-0.3133938	0.3246994	-0.3134043	-0.3133798	2.4527×10^{-5}
0.15	-0.32087	0.3564	-0.3142612	0.3545786	-0.3142717	-0.3142472	2.4498×10^{-5}
0.16	-0.32305	0.3871	-0.3148696	0.3843615	-0.3148801	-0.3148557	2.4408×10^{-5}
0.17	-0.32509	0.4180	-0.3152467	0.4140357	-0.3152571	-0.3152328	2.4348×10^{-5}
0.18	-0.32701	0.4487	-0.3154157	0.4435906	-0.3154262	-0.3154019	2.4259×10^{-5}
0.19	-0.32879	0.4794	-0.3153969	0.4730203	-0.3154073	-0.3153832	2.4110×10^{-5}
0.20	-0.33047	0.5100	-0.3152075	0.5023201	-0.3152178	-0.3151938	2.3961×10^{-5}
0.21	-0.33206	0.5403	-0.3148625	0.5314882	-0.3148727	-0.3148489	2.3842×10^{-5}
0.22	-0.33355	0.5705	-0.3143751	0.5605221	-0.3143853	-0.3143616	2.3663×10^{-5}
0.23	-0.33495	0.6000	-0.3137570	0.5894222	-0.3137670	-0.3137436	2.3454×10^{-5}
0.24	-0.33627	0.6288	-0.3130183	0.6181881	-0.3130283	-0.3130050	2.3246×10^{-5}
0.25	-0.33763	0.6576	-0.3121682	0.6468209	-0.3121781	-0.3121551	2.3007×10^{-5}

obtained by the WPP method, are closer in meaning to those in experiments.

For comparison with the ionization rate, the annihilation rates for p-Ps ($w_{ann}^{p-Ps} = 1.935 \times 10^{-7}$ a.u.) and o-Ps ($w_{ann}^{o-Ps} = 1.704 \times 10^{-10}$ a.u.) are shown in the inset in figure 2(b). The field strengths leading to the same values for the ionization rates are $F \approx 0.0085$ a.u. and 0.0062 a.u., respectively, i.e. both of them are in the middle of the tunnelling domain. Since the ionization rate increases with the field strength, in the OBI regime it becomes much higher than the annihilation rates.

In the next step we calculate the lowest state energies and widths for positronium in the electric field by taking into account the HFS. For this purpose we use the CR method and rotated Hamiltonian (13) with terms (9) and (10) for p-Ps (singlet) and o-Ps (triplet), respectively. The calculations for o-Ps have shown that the term in V_{hfs} , which is proportional to $1/r^3$, gives much smaller contribution to the HFS (for about two orders of magnitude) than the term with delta-function. This fact is in agreement with the assumption from the last paragraph of section 2.2 which validates expression (10) as a good approximation. Moreover, if we do not require high accuracy, we can neglect the term $\sim 1/r^3$ and perform the calculations using only the second term (with delta-function) in equation (6). The values for the lowest state energies of p-Ps (E_{p-Ps}) and o-Ps (E_{o-Ps}) obtained in this way and their differences $E_{hfs}(F) = E_{o-Ps}(F) - E_{p-Ps}(F)$ are given in the last

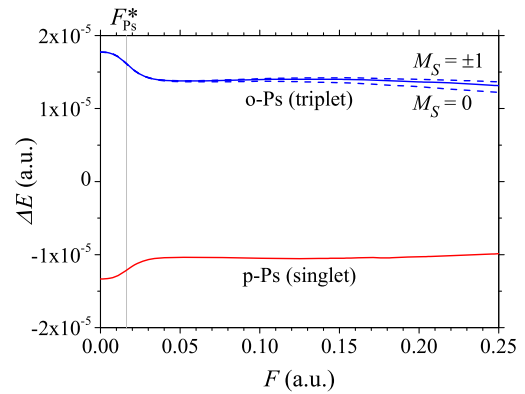


Figure 3. HFS of the lowest state energy of positronium in electric field. The p-Ps and o-Ps lowest state energies relative to the corresponding gross structure energy ($\Delta E_{p-Ps,o-Ps} = E_{p-Ps,o-Ps} - E_{Ps}$), as functions of the field strength, are represented by the red and blue curves, respectively. The dashed blue lines represent the values for o-Ps which are obtained using the full expression (10) for $M_S = 0$ and $M_S = \pm 1$ separately, whereas the full blue line is obtained using only the term with delta-function.

three columns of table 1. These values (relative to the corresponding gross structure energy), as well as those for o-Ps obtained using expression (10) for $M_S = 0$ and $M_S = \pm 1$, are shown in figure 3. It can be seen that the HFS, compared to the field-free value ($E_{hfs}(0) \approx 3.1053 \times 10^{-5}$ a.u. ≈ 0.845 meV),

decreases significantly in the tunnelling domain and at the beginning of the OBI domain ($F \sim 2F_{\text{Ps}}^*$) takes the value that is about 20% lower than the initial one. As the field strength increases further, this splitting varies rather slowly, but there is an additional splitting of the triplet level that is increasing ($(E_{\text{o-Ps}}^{M_S=\pm 1} - E_{\text{o-Ps}}^{M_S=0})/E_{\text{hfs}} \approx 6.3\%$ at $F = 0.25$ a.u.).

The behaviour of HFS in the electric field can be explained by the change of form of the lowest state wave function of positronium when it is placed in the field. The HFS in the range $F < 2F_{\text{Ps}}^*$ can be estimated applying the first order perturbation theory, using V_{hfs} (without the term $\sim 1/r^3$) as the perturbation. This approach gives

$$E_{\text{hfs}}(F) \approx \frac{14}{3} \pi \alpha^2 |\psi(0; F)|^2, \quad (14)$$

where $\psi(0; F)$ is the value of the lowest state wave function of positronium in the field of strength F for $r = 0$. Using equation (14) one sees that the observed decrease of HFS, while increasing F , is a direct consequence of the decrease of electron density at the positron position ($|\psi(0; F)|^2$). The latter can be explained by the fact that the density distribution in electric field shifts towards the barrier and thereby decreases at $r = 0$.

The widths of the lowest states of p-Ps and o-Ps are determined simultaneously with the corresponding energies. These values are not shown in table 1, but they can be approximated by linear fits: $\Gamma_{\text{p-Ps}}(F) \approx \Gamma_{\text{Ps}}(F) - 2.6 \cdot 10^{-4}F$ and $\Gamma_{\text{o-Ps}}(F) \approx \Gamma_{\text{Ps}}(F) + 3.4 \cdot 10^{-4}F$ (in a.u.). It should be noted that, unlike E_{hfs} , which can be precisely determined in the experiment by measuring the frequency of absorbed/emitted radiation, corrections to the ionization rate are not related to similar quantities and, therefore, are not as significant as corrections to the energy.

5. Scaling properties

Approximate expressions (11) and (12) for the ground state energy E and the ionization rate w can be written in the form

$$\tilde{E} = -\frac{1}{2} - \frac{9}{4}\tilde{F}^2, \quad (15)$$

$$\tilde{w} = \frac{4}{\tilde{F}} \exp\left(-\frac{2}{3\tilde{F}}\right), \quad (16)$$

where

$$\tilde{E} = E/\mu, \quad \tilde{w} = w/\mu, \quad \tilde{F} = F/\mu^2, \quad (17)$$

are the mass-scaled values for energy, ionization rate and field strength. These scaling properties follow from the invariance of equations of motion for the system described by Hamiltonian (1) under simultaneous transformations

$$\begin{aligned} \mu &\rightarrow \tilde{\mu} = \mu/\lambda, \\ t &\rightarrow \tilde{t} = \lambda t, \\ \mathbf{r} &\rightarrow \tilde{\mathbf{r}} = \lambda \mathbf{r}, \\ \mathbf{p} &\rightarrow \tilde{\mathbf{p}} = \mathbf{p}/\lambda, \end{aligned} \quad (18)$$

$$E \rightarrow \tilde{E} = E/\lambda,$$

$$F \rightarrow \tilde{F} = F/\lambda^2$$

when we take $\lambda = \mu$.

The invariance of the equations of motion for Hamiltonian (1) under transformations (18) extends the validity of scaling properties (17) to their exact solutions (numerical values for E and w calculated within the gross structure). The confirmation of this assumption is the coincidence of numerical results for positronium and scaled numerical results for hydrogen with scaling parameter $\lambda = \mu = 1/2$ (see figure 2). Thus, instead of direct calculation, the gross structure values for E and w for positronium can be obtained immediately by scaling the corresponding numerical data for hydrogen (see e.g. references [29–31]). Recent measurements of the ionization rates for positronium in Rydberg states [9] have shown that these rates are consistent with the scaled values obtained for hydrogen, which implies that the reduced mass scaling is valid, and that for practical purposes the scaled hydrogen rates can be used to describe positronium experiments. Of course, if we need the values with the HFS, the calculations must be performed directly for positronium.

6. Summary and conclusions

In this paper we studied the ionization of positronium in the external electric field of strengths belonging both to the tunnelling and the OBI regimes. The lowest state energy E and its width Γ (ionization rate w) as functions of the field strength are calculated using two different numerical methods: the WPP method and the CR method. The results obtained within the gross structure (i.e. by neglecting the fine and hyperfine structure and other higher order corrections) are in a good agreement and confirm the validity of the approximate expressions (11) and (12) for energy and width at weak fields. For extremely strong fields, however, a difference between the results obtained by these two numerical methods becomes significant. This discrepancy can be attributed to different formulations of quantities E and Γ in the theoretical backgrounds of the two methods.

The ionization rates are compared with the annihilation rates for p-Ps and o-Ps. These rates were found to be comparable at field strengths belonging to the tunnelling domain, but in the OBI domain the ionization rate largely prevails over the annihilation rates. Accordingly, it is expected that at these field strengths the majority of positronium atoms will be ionized before e^-e^+ pair annihilates.

The HFS of the positronium ground state in an electric field is calculated using the CR method and the Hamiltonian for relative motion of positronium with the spin–spin coupling and annihilation interaction terms. It is found that in the tunnelling domain and at the beginning of the OBI domain the HFS decreases, as the field strength increases, but after that it varies slowly. There is, however, an additional splitting of triplet levels that increases with the field strength. As the field strength increases further, this splitting varies rather slowly,

but here an additional splitting of triplet levels occurs, whose rate is comparable to this variation.

Since the higher order terms in Hamiltonian are not affected by the electric field, the variation of HFS is a direct consequence of the wave function dependence on the field strength. This means that the HFS values for positronium determined experimentally at different field strengths could be used to estimate how the electron density at the positron position ($|\psi(0)|^2$), which is the quantity that gives the annihilation rate, depends on the field strength.

Finally, it is demonstrated that the gross structure values of E and Γ for positronium and for the hydrogen atom, obtained either by approximate expressions or numerically, are related by scaling transformations and can be used to determine the corresponding quantities for other hydrogen-like exotic atoms (muonium, for example).

Acknowledgments

The authors thank P-A Hervieux for helpful discussion. This work was supported by the Ministry of Education, Science and Technological Development of Republic of Serbia under Project No. 171020.

ORCID iDs

N S Simonović  <https://orcid.org/0000-0002-3319-9904>

References

- [1] Rich A 1981 *Rev. Mod. Phys.* **53** 127
- [2] Namba T 2012 *Prog. Theor. Exp. Phys.* **2012** 04D003
- [3] Ishida A, Namba T, Asai S, Kobayashi T, Saito H, Yoshida M, Tanaka K and Yamamoto A 2014 *Phys. Lett. B* **734** 338
- [4] Deutsch M 1953 *Proc. of the American Academy of Arts and Sciences, The Rumford Bicentennial* (Cambridge: American Academy of Arts and Sciences) vol 82 pp 331–43
- [5] Alonso A M, Cooper B S, Deller A, Hogan S D and Cassidy D B 2015 *Phys. Rev. Lett.* **115** 183401
- [6] Alonso A M, Cooper B S, Deller A, Hogan S D and Cassidy D B 2016 *Phys. Rev. A* **93** 012506
- [7] Landau L D and Lifshitz E M 1991 *Quantum Mechanics* (Oxford: Pergamon) p 96
- [8] Damburg R J and Kolosov V V 2011 *Theoretical Studies of Hydrogen Rydberg Atoms in Electric Fields (Rydberg States of Atoms and Molecules)* ed R F Stebbings and F B Dunning (Cambridge: Cambridge University Press)
- [9] Alonso A M, Gurung L, Sukra B A D, Hogan S D and Cassidy D B 2018 *Phys. Rev. A* **98** 053417
- [10] Milošević M Z and Simonović N S 2015 *Phys. Rev. A* **91** 023424
- [11] Milošević M Z and Simonović N S 2016 *J. Phys. B: At. Mol. Opt. Phys.* **49** 175001
- [12] Bunjac A, Popović D B and Simonović N S 2016 *Eur. Phys. J. D* **70** 116
- [13] Deutsch M and Brown S C 1952 *Phys. Rev.* **85** 1047
- [14] Ritter M W, Egan P O, Hughes V W and Woodle K A 1984 *Phys. Rev. A* **30** 1331
- [15] Chu S, Mills A P Jr and Hall J L 1984 *Phys. Rev. Lett.* **52** 1689
- [16] Fee M S, Mills A P, Chu S, Shaw E D, Danzmann K, Chichester R J and Zuckerman D M 1993 *Phys. Rev. Lett.* **70** 1397
- [17] Conti R S, Hatamian S, Lapidus L, Rich A and Skalsey M 1993 *Phys. Lett. A* **177** 43
- [18] Hagen D, Ley R, Weil D, Werth G, Arnold W and Schneider H 1993 *Phys. Rev. Lett.* **71** 2887
- [19] Ley R, Hagen D, Weil D, Werth G, Arnold W and Schneider H 1994 *Hyperfine Interact.* **89** 327
- [20] Zatorski J 2008 *Phys. Rev. A* **78** 032103
- [21] Eides M I and Shelyuto V A 2017 *Phys. Rev. A* **96** 011301(R)
- [22] Gurung L, Babij T J, Hogan S D and Cassidy D B 2020 *Phys. Rev. Lett.* **125** 073002
- [23] Berestetskii V B, Lifshitz E M and Pitaevskii L P 1982 *Quantum Electrodynamics (Course of Theoretical Physics vol 4)* 2nd edn (Oxford: Heinemann)
- [24] Bunjac A, Popović D B and Simonović N S 2017 *Phys. Chem. Chem. Phys.* **19** 19829
- [25] Ho Y K 1983 *Phys. Rep.* **99** 1
- [26] Moiseyev N 1998 *Phys. Rep.* **302** 211
- [27] Buchleitner A, Grémaud B and Delande D 1994 *J. Phys. B: At. Mol. Opt. Phys.* **27** 2663
- [28] Avery J and Avery J 2006 *Generalized Sturmians and Atomic Spectra* (Singapore: World Scientific)
- [29] Nicolaidis C A and Themelis S I 1992 *Phys. Rev. A* **45** 349
- [30] Scrinzi A 2000 *Phys. Rev. A* **61** 041402
- [31] Milošević M Z and Simonović N S 2014 *Proc. of the 27th Summer School and Int. Symp. on the Physics of Ionized Gases (SPIG)*, ed D Marić, A R Milosavljević and Z Mijatović (Belgrade: Institute of Physics and SASA) pp 22–5 (<http://spig2014.ipb.ac.rs/doc/SPIG2014-book-online.pdf>)
- [32] Klaiman S and Moiseyev N 2010 *J. Phys. B: At. Mol. Opt. Phys.* **43** 185205
- [33] Nussenzweig H M 1959 *Nucl. Phys.* **11** 499



On the selective multiphoton ionization of sodium by femtosecond laser pulses: A partial-wave analysis



A. Bunjac, D.B. Popović, N.S. Simonović*

Institute of Physics, University of Belgrade, Pregrevica 118, 11080 Belgrade, Serbia

ARTICLE INFO

Article history:

Received 21 August 2020

Received in revised form 27 January 2021

Accepted 27 January 2021

Available online 2 February 2021

Communicated by A. Eisfeld

Keywords:

Femtosecond laser pulse

Multiphoton ionization

Freeman resonance

Partial wave analysis

ionization channel

ABSTRACT

Multiphoton ionization of sodium by femtosecond laser pulses of 800 nm wavelength in the range of laser peak intensities belonging to the over-the-barrier ionization domain is studied. Photoelectron momentum distributions and the energy spectra are determined numerically by solving the time dependent Schrödinger equation for three values of the laser intensity from this domain. The positions of peaks related to Freeman resonances in the calculated spectra agree with the peak positions in the spectra obtained experimentally by Hart et al. [7]. A partial wave analysis of these peaks revealed that each peak is a superposition of the contributions of photoelectrons produced by the resonantly enhanced multiphoton ionization via different intermediate states. It is demonstrated that at appropriate laser intensities the selective ionization, which occurs predominantly through a single intermediate state, is possible.

© 2021 Elsevier B.V. All rights reserved.

1. Introduction

Strong-field ionization of the alkali-metal atoms has been studied intensively over the past decade and earlier, both experimentally and theoretically including *ab initio* numerical calculations [1–9]. A specific feature of this group of atoms – a low ionization potential, which ranges from $I_p \approx 3.89$ eV (for cesium) to 5.39 eV (for lithium), causes that a considerably smaller number of photons of a given energy $\hbar\omega$ is required for their photoionization than for the ionization of other atoms. For example, with the laser wavelength of around 800 nm ($\hbar\omega \approx 1.55$ eV) it takes four photons to ionize an alkali-metal atom, unlike the case of frequently used noble gases where this number is of the order of ten. Since for a dipole transition requiring N photons the lowest order perturbation theory predicts that the photon absorption rate is $W \sim I^N$ if $I \ll I_a$, where I is the laser intensity and $I_a = 3.50945 \times 10^{16}$ W/cm² is the atomic unit value for intensity, measurable effects in experiments with multiphoton ionization (MPI) of alkali can be observed at relatively low laser intensities, available in table-top laser systems. The perturbative treatment, however, is not applicable at higher intensities which can be achieved today. One indication of the nonperturbative regime is the so-called above threshold ionization (ATI) [10–12] in which the atom absorbs more photons than the minimum required. By increasing

the intensity over a certain value, W does not follow further the prediction of perturbation theory.

At a sufficiently high intensity the electric component of the laser field becomes comparable with the Coulomb field of atomic core, opening up another ionization mechanism – the tunnel ionization. In this case the field distorts the atomic potential forming a potential barrier through which the electron can tunnel. Multiphoton and tunneling ionization regimes are distinguished by the value of Keldysh parameter [13] which can be written as $\gamma = \sqrt{I_p}/(2U_p)$, where $U_p = e^2 F^2 / (4m_e \omega^2)$ is the ponderomotive potential of ejected electron with mass m_e and charge e . The value of the electric field F in the expression for γ corresponds to the peak value of laser intensity. Multiphoton and tunneling regimes are characterized by $\gamma \gg 1$ (low-intensity, short-wavelength limit) and $\gamma \ll 1$ (high-intensity, long-wavelength limit), respectively. The transition regime at $\gamma \approx 1$ for alkali-metal atoms is reached at considerably lower intensities than for other atoms, again due to the small ionization potential I_p . The experiments accessing the strong-field regime with alkali [3,6,7,9] have revealed that the commonly used strong-field ionization models in the form of a pure MPI or tunnel ionization cannot be strictly applied. The problem, however, goes beyond by using an *ab initio* numerical method for solving the time-dependent Schrödinger equation (TDSE).

At even larger laser intensities the field strength overcomes the atomic potential. This can be considered as the limiting case of tunnel ionization when the barrier is suppressed below the energy of atomic state. This regime is usually referred to as over-

* Corresponding author.

E-mail address: simonovic@ipb.ac.rs (N.S. Simonović).

the-barrier ionization (OBI). Such a barrier suppression takes place independently of the value of Keldysh parameter. For neutral atoms the threshold value of field strength for OBI is estimated as $F_{\text{OBI}} \approx I_p^2/4$ (in atomic units). F_{OBI} values for alkali, determined more accurately, are given in Ref. [14]. For example, the laser peak intensity that corresponds to the OBI threshold for sodium is about 3.3 TW/cm^2 ($F_{\text{OBI}} = 0.0097 \text{ a.u.}$ [14], $I = I_a F^2$), while the value of Keldysh parameter for the sodium atom interacting with the radiation of this intensity and 800 nm wavelength is $\gamma = 3.61$. Thus, the OBI threshold in this case belongs to the MPI regime. Previous experiments and theoretical studies have already mentioned this peculiar situation for sodium and other alkali [3–7,9]. In addition, it is demonstrated that at intensities above the OBI threshold most of atoms will be ionized before the laser peak intensity is reached [5]. Thus, the ionization occurs at the leading edge of the pulse only, that is equivalent to the ionization by a shorter pulse.

A remarkable feature of the photoelectron energy spectrum (PES) obtained using short (sub-picosecond) laser pulses is the existence of substructures in ATI peaks known as Freeman resonances [15,16]. The mechanism which is responsible for occurrence of these substructures is the dynamic (or AC) Stark shift [10,11,17] which brings the atomic energy levels into resonance with an integer multiple of the photon energy. In this case the resonantly enhanced multiphoton ionization (REMPI) [11,12,18]) takes place, increasing the photoelectron yield, and one observes peaks at the corresponding values of photoelectron energy. Thus, the peaks in the PES can be related to REMPI occurring via different intermediate states.

The resonant dynamic Stark shift of energy levels corresponding to sodium excited states nl ($n \leq 6$), relative to its ground state ($3s$) energy, is recently calculated for the laser intensities up to 7.9 TW/cm^2 and wavelengths in the range from 455.6 to 1139 nm [8]. These data are used to predict the positions of REMPI peaks in the PES of sodium interacting with an 800 nm laser pulse. Freeman resonances in the PES of alkali-metal atoms have been studied in papers [1–9], mentioned at the beginning of this section, where a number of significant results have been reported.

The dynamic Stark shift is an important mechanism in the strong-field quantum control of various atomic and molecular processes [19–22]. Focusing on the MPI of atoms, a particular challenge is the selective ionization of an atom through a single intermediate state which could produce a high ion yield. By increasing simply the laser intensity one increases the yield, but also spreads the electron population over multiple states [16] and, in turn, reduces the selectivity. Krug et al. [2] demonstrated that chirped pulses can be an efficient tool in strong-field quantum control of multiple states of sodium at the MPI. Hart et al. [7] have shown that improved selectivity and yield could be achieved by controlling the resonant dynamic Stark shift via intensity of the laser pulse of an appropriate wavelength ($\sim 800 \text{ nm}$).

In this paper we study the photoionization of sodium by the laser pulse of 800 nm wavelength and 57 fs full width at half maximum (FWHM) with the peak intensities ranging from 3.5 to 8.8 TW/cm^2 , which belong to OBI domain in the MPI regime. These values were chosen for comparison with the experiment by Hart et al. [7]. Using the single-active-electron approximation we calculate the corresponding photoelectron momentum distribution (PMD) and the PES by solving numerically the TDSE and perform a similar analysis as it has been done in Refs. [1–9]. In order to make a deeper insight into the ionization process, in addition, we perform a partial-wave analysis of the calculated PMD. In the next section we describe the model and in Sec. 3 consider the excitation scheme and ionization channels. In Sec. 4 we analyze the calculated photoelectron momentum distribution and energy spectra. A summary and conclusions are given in Sec. 5.

2. The model

Singly-excited states and the single ionization of the alkali-metal atoms are, for most purposes, described in a satisfactory manner using the single-active-electron (SAE) approximation. The valence electron is here weakly bound and can be considered as moving in an effective core potential. One of the simplest models for the effective core potential, applicable for the alkali-metal atoms, is the Hellmann pseudopotential [23] which reads (in atomic units)

$$V_{\text{core}}(r) = -\frac{1}{r} + \frac{A}{r} e^{-ar}. \quad (1)$$

The parameters $A = 21$ and $a = 2.54920$ [14] provide the correct value for the ionization potential of sodium $I_p = 5.1391 \text{ eV} = 0.18886 \text{ a.u.}$ and reproduce approximately the energies of singly-excited states [24] (deviations are less than 1%). The associated eigenfunctions $\psi_{nlm}(\mathbf{r}) = \mathcal{R}_{nl}(r)Y_{lm}(\Omega)$ are one-electron approximations of these states. Here, the radial functions $\mathcal{R}_{nl}(r)$ are originally characterized by the quantum number $n_{\text{SAE}} = 1, 2, \dots$ and the orbital quantum number l , but for convenience, instead of the quantum number n_{SAE} , we use the principal quantum number of the valence electron in the full multielectron model of the sodium atom $n = n_{\text{SAE}} + 2 = 3, 4, \dots$

Assuming that the field effects on the core electrons can be neglected (the so-called frozen-core approximation [14]), the Hamiltonian describing the dynamics of valence (active) electron of the sodium atom in an alternating field, whose electric component is $F(t) \cos \omega t$, reads (in atomic units)

$$H = -\frac{1}{2}\nabla^2 + V_{\text{core}}(r) - F(t)z \cos \omega t. \quad (2)$$

We consider the linearly polarized laser pulse whose amplitude of the electric field component (field strength) has the form

$$F(t) = F_{\text{peak}} \sin^2(\pi t/T_p), \quad 0 < t < T_p, \quad (3)$$

otherwise $F(t) = 0$. Here ω , F_{peak} and T_p are the frequency of the laser field, the peak value of F and the pulse duration ($2 \times \text{FWHM} = 114 \text{ fs} \approx 4713 \text{ a.u.}$), respectively. Since the system is axially symmetric, the magnetic quantum number m of the active electron is a good quantum number for any field strength. In the sodium ground state (when $F = 0$) the orbital and magnetic quantum numbers are equal to zero and in our calculations we set $m = 0$.

Photoabsorption processes were simulated by solving numerically the TDSE for the active electron wave function $\psi(\mathbf{r}, t)$, assuming that at $t = 0$ the atom is in the ground state represented by the lowest eigenstate of Hamiltonian (2) with $F = 0$. Photoexcitation can be studied by the method of time dependent coefficients (TDC), where the wave function $\psi(\mathbf{r}, t)$ expands in a finite basis consisting of functions $\psi_{nl0}(\mathbf{r})$. In this approach the populations of atomic states are the squares of absolute values of expansion coefficients $c_{nl}(t)$, determined by solving the corresponding set of equations numerically. This method, however, cannot be used to calculate photoionization because the basis of atomic states does not include the continuum states. An adequate alternative for this purpose is the wave-packet propagation method on a spatial grid. Here we use the second-order-difference (SOD) scheme [25] adapted to cylindrical coordinates (ρ, φ, z) , see Refs. [8,26]. Due to the axial symmetry of the system, Hamiltonian (2) and the electron's wave function do not depend on the angle φ and the dynamics reduces to two degrees of freedom (ρ and z). The calculations were performed on a 6144×12288 grid in the wave-packet propagation domain $\rho, |z| \leq L = 3000 \text{ a.u.}$ and the propagation time was about $1.3 T_p$ with the step $\Delta t = 0.002 \text{ a.u.}$

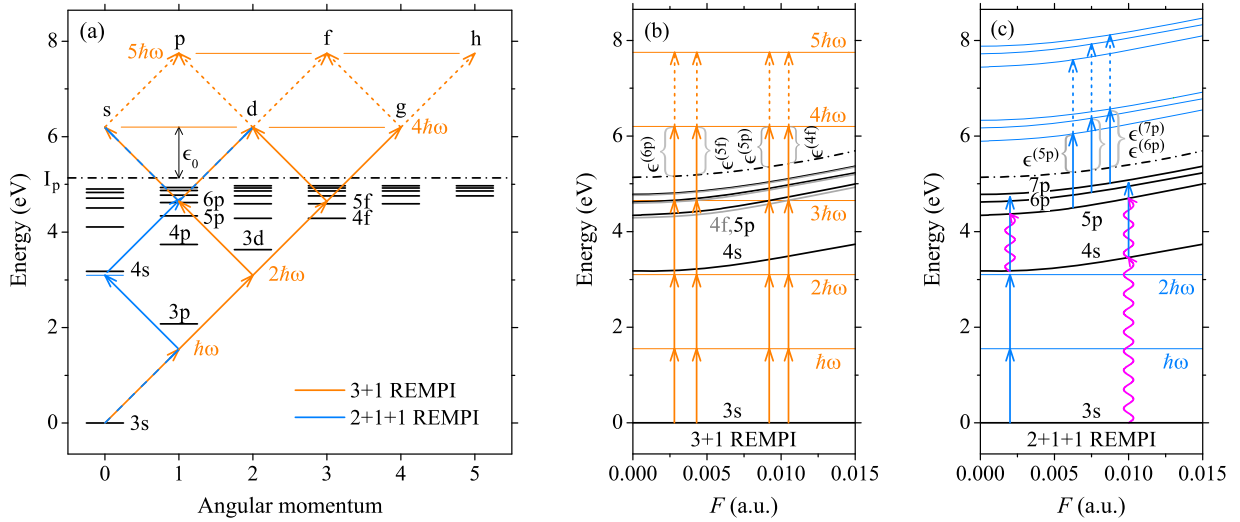


Fig. 1. (a) The unperturbed energy levels (short black lines) corresponding to singly excited states of sodium [24] relative to its ground state (3s) and possible four-photon and five-photon absorption pathways (arrows) from the ground state to continuum for the radiation of 800 nm wavelength ($\hbar\omega \approx 1.55$ eV). The continuum boundary is drawn by the dash-dot line and ϵ_0 is the excess energy of photoelectrons produced in the nonresonant four-photon ionization. (b) Energy levels corresponding to 4s and P states (black curves) and to F states (gray curves), as functions of the field strength, and 3+1 REMPI pathways via intermediate states 4f, 5p, 5f and 6p (orange arrows). $\epsilon^{(nl)}$ are the corresponding photoelectron excess energies. (c) Energy levels corresponding to 4s and P states as functions of the field strength (black curves) and 2+1+1 REMPI pathways via near resonant (at weak fields) 3s \rightarrow 4s transition and subsequent excitation of P states (blue arrows). The wave lines represent nonresonant transitions related to Rabi oscillations between the corresponding states. (For interpretation of the colors in the figure(s), the reader is referred to the web version of this article.)

The absorbing potential of the form $-0.03i(r-r_0)^2$ in the area $r > r_0 = L - 100$ a.u. was used to suppress the reflection of the wave packet from the domain boundaries.

3. Energy scheme and photoionization channels

The lowest energy levels corresponding to singly-excited states of sodium and possible multiphoton absorption pathways during the interaction of the atom with a laser radiation of 800 nm wavelength ($\hbar\omega = 0.05695$ a.u. ≈ 1.55 eV) are shown in Fig. 1(a). At this wavelength there exist three dominant REMPI channels: (i) (3+1)-photon ionization via excitation of 5p, 6p and 7p states, giving rise to photoelectrons with s and d-symmetry; (ii) (3+1)-photon ionization via excitation of 4f, 5f and 6f states, producing photoelectrons with d and g-symmetry; (iii) (2+1+1)-photon ionization via nearly resonant two-photon transition 3s \rightarrow 4s and subsequent excitation of P-states, giving rise again to photoelectrons with s and d-symmetry [2,7].

3.1. Estimation of the photoelectron excess energy. The nonresonant MPI

Theoretically, if the MPI occurs by absorbing N photons, the excess energy of ejected electrons in the weak field limit is $\epsilon^{(0)} = N\hbar\omega - I_p$. At stronger fields, however, the dynamic Stark shift of the ground state (δE_{gr}), as well as that of the continuum boundary (δE_{cb}), change effectively the ionization potential I_p to $I_p - \delta E_{gr} + \delta E_{cb}$ and the excess energy becomes dependent on the field strength (see Fig. 1(b))

$$\epsilon(F) = N\hbar\omega - I_p + \delta E_{gr}(F) - \delta E_{cb}(F). \quad (4)$$

This equation, using quadratic approximation $\delta E \approx -\alpha(\omega)F^2/4$ [11], reads

$$\epsilon(F) \approx N\hbar\omega - I_p - \left(\alpha_{gr}^{stat} + \frac{e^2}{m_e \omega^2} \right) \frac{F^2}{4}, \quad (5)$$

where the dynamic polarizability $\alpha(\omega)$ in the ground state and at the continuum boundary is approximated by its static value for the sodium ground state $\alpha_{gr}^{stat} = 162.7$ a.u. [27] and by its asymptotic value in the high frequency limit $\alpha_{cb}(\omega) \approx -e^2/(m_e \omega^2)$ [11],

respectively. Thus, $\delta E_{cb} \approx U_p$, where U_p is the ponderomotive potential of the active electron, whereas $\delta E_{gr} \approx -0.53 U_p$.

When the MPI is induced by a laser pulse, the field strength varies from 0 to F_{peak} and back producing photoelectrons of different energies, but with the maximum yield at $\epsilon(F_{peak})$ (for a given N). This peak in the PES corresponds to the nonresonant N -photon ionization and its position can be estimated by formula (5) with $F = F_{peak}$.

3.2. 3+1 REMPI channels

Formula (5) is also useful for estimating the positions of REMPI peaks in the PES. Replacing the variable F with the value F_{nl} at which the atomic state nl shifts in the three-photon resonance with the laser field, this formula for $N = 4$ estimates the excess energy $\epsilon^{(nl)}$ of photoelectrons produced in the 3+1 REMPI via this state (see Fig. 1(b)). The values F_{nl} for states 4p, 4f, 5p, 5f and 6p in the case of laser field of 800 nm wavelength are determined in a previous work [8]. These values, together with the corresponding values for $\epsilon^{(nl)}$ estimated by formula (5) are given in Table 1.

Rewriting the resonance condition $E_{nl}(F_{nl}) - E_{gr}(F_{nl}) = 3\hbar\omega$ in the form $E_{nl}(F_{nl}) = 3\hbar\omega - I_p + \delta E_{gr}(F_{nl})$ and inserting it into Eq. (4) (with $N = 4$ and $F = F_{nl}$), one has

$$\epsilon^{(nl)} = E_{nl}(F_{nl}) - \delta E_{cb}(F_{nl}) + \hbar\omega. \quad (6)$$

Since the dynamic Stark shift for the high lying levels takes approximately the same value as that for the continuum boundary ($\delta E_{nl}(F) \approx \delta E_{cb}(F) \approx U_p(F)$), the photoelectron energy at the 3+1 REMPI via considered state will be

$$\epsilon^{(nl)} \approx E_{nl}^{(0)} + \hbar\omega, \quad (7)$$

where $E_{nl}^{(0)}$ is the energy of the state nl for the field-free atom. The positions of REMPI maxima in the PES are, therefore, almost independent on the peak intensity of the laser pulse, in contrast to the position of the nonresonant four-photon ionization maximum $\epsilon(F_{peak})$. The values for $\epsilon^{(nl)}$ obtained by Eq. (7) are shown in the last column of Table 1. Since usually $\delta E_{nl} + \delta E_{gr} > 0$ (at least for P and F states, see Fig. 1(b)), the states which can be shifted into

Table 1

Energies $E_{nl}^{(0)}$ of singly excited P and F-states (nl from 4p to 7p) of the field free sodium atom [24], field strengths F_{nl} at which these states shift into the three-photon resonance with the laser field of 800 nm wavelength ($E_{nl}(F_{nl}) - E_{3s}(F_{nl}) = 3\hbar\omega$, $\hbar\omega \approx 1.55$ eV) [8] and the excess energies $\epsilon^{(nl)}$ of photoelectrons produced in the 3+1 REMPI via these states, obtained by Eq. (5). The values for $\epsilon^{(nl)}$ obtained by formula (7), which are also related to 2+1+1 REMPI via 4s and subsequent excitation of P intermediate states, are shown in the fifth column.

state (nl)	$E_{nl}^{(0)}$ (eV)	F_{nl} (a.u.)	$\epsilon^{(nl)}$ (eV)	$E_{nl}^{(0)} + \hbar\omega$ (eV)
4p	-1.386	0.0148	0.358	(0.164)
4f	-0.851	0.0105	0.707	0.699
5p	-0.795	0.0092	0.789	0.755
5f	-0.545	0.0043	1.001	1.005
6p	-0.515	0.0028	1.035	1.035
6f	-0.378	-	-	1.172
7p	-0.361	-	-	1.189

three-photon resonance are those with $E_{nl}^{(0)} \leq 3\hbar\omega - I_p$ (for the wavelength of 800 nm these states are 4f, 5p, 5f, 6p, but not 7p and 6f, which are only near resonant at small values of F). As a consequence the REMPI maxima are in the spectrum located below the theoretical value for photoelectron energy in the weak field limit ($\epsilon^{(nl)} \leq \epsilon^{(0)}$).

3.3. The 2+1+1 REMPI channel

Earlier experimental and theoretical studies [2,7] have indicated that a particularly important role in the MPI of sodium using the radiation of around 800 nm wavelength has the 2+1+1 REMPI via nearly resonant two-photon transition $3s \rightarrow 4s$ and subsequent excitation of P states. Our previous calculations [8] have shown that this two-photon transition is close to be resonant at the values of field strength when the dynamic Stark shift is small (see Fig. 1(c)). The TDC calculations at the field strength $F = 0.002$ a.u. confirm that the transfer of population from the ground (3s) to 4s state, compared to other excited states, is significant (see Fig. 2(a)). This transfer is also high at stronger fields (see Fig. 2(c) for $F = 0.01$ a.u.), which can be explained by strong Rabi oscillations between these two states. The population from 4s state flows further

to state 5p (as a consequence of Rabi oscillations between these states) and to states 6p and 7p (by the near resonant one-photon absorption), see Fig. 1(c). Since $\delta E_{4s}(F) \approx \delta E_{np}(F) \approx \delta E_{cb}(F)$, differences $E_{np} - E_{4s}$ and $E_{cb} - E_{np}$ are almost independent of F , and transitions $4s \rightarrow np$ and subsequent ionization occur at all values of the field strength, producing the photoelectrons with s and d-symmetry and excess energies given by Eq. (7). Therefore, the photoelectrons produced in the 2+1+1 REMPI and in the 3+1 REMPI via the same intermediate P state cannot be distinguished either by angular momentum or by energy.

Relative contributions of these two ionization channels in the total photoelectron yield can be theoretically estimated from the populations of sodium P states. Fig. 2 shows the populations of the 4s, 4f and 5p states over time, excited by the continuous radiation of 800 nm wavelength, which were calculated using the TDC method in the basis of SAE orbitals with $n = 3, \dots, 7$ and $l = 0, 1, 2, 3$ (17 states, ending with 7p). The plots (a) and (c) are obtained taking into account all allowed transitions between the orbitals, while the plots (b) and (d) are determined taking into account all transitions except those related to 4s state. One can see that the presence of transition $3s \rightarrow 4s$, which is nearly resonant at $F = 0.002$ a.u., significantly increases the population of P states at this field strength, but does not affect the F states. Contrarily, at $F = 0.01$ a.u. this transition does not affect significantly the population of higher states. Based on this, we conclude that at smaller values of the field strength ($F < 0.004$ a.u.) the 2+1+1 process dominates over the 3+1 one, but at stronger fields it is rather suppressed.

4. Photoionization by femtosecond pulses

4.1. Photoelectron momentum distribution

The photoelectron momentum distribution (PMD) is given by $|\bar{\psi}(\mathbf{k})|^2$, where $\bar{\psi}(\mathbf{k})$ is the momentum representation of the photoelectron wave function $\psi(\mathbf{r}, t)$ at a time $t \geq T_p$ (here we take $t = 6000$ a.u. ≈ 145 fs). The function $\bar{\psi}(\mathbf{k})$ is obtained by projecting the wave function $\psi(\mathbf{r}, t)$ onto the continuum states of the

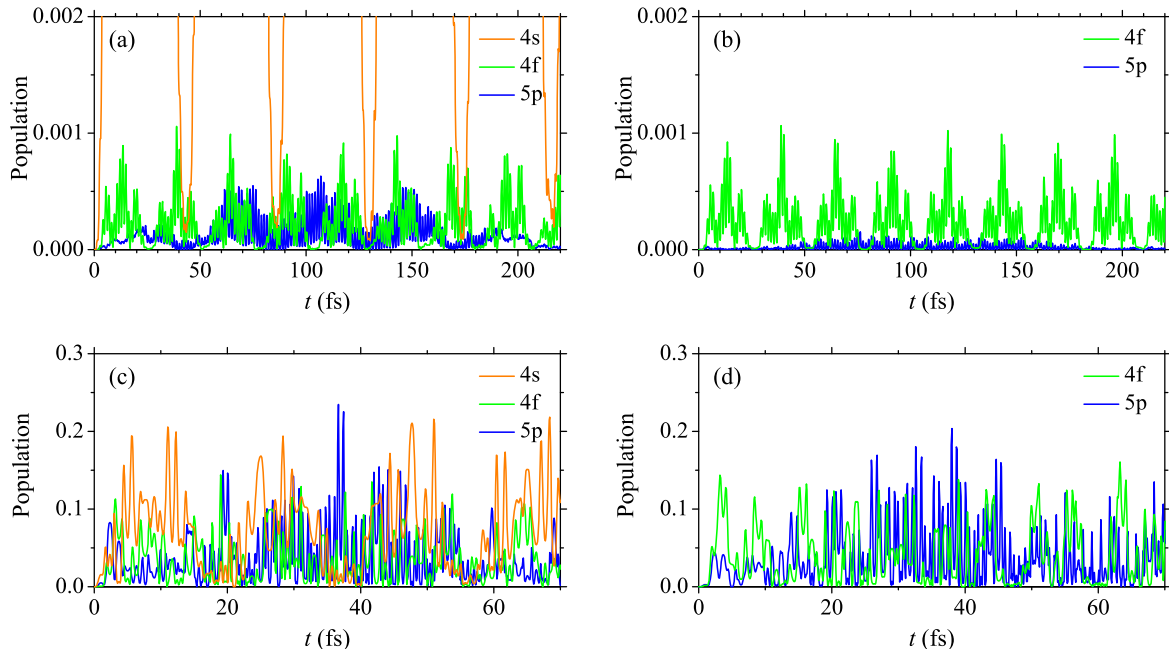


Fig. 2. Populations of 4s, 4f and 5p states of the sodium atom under the influence of 800 nm wavelength continuous laser of the field strength: (top) $F = 0.002$ a.u. and (bottom) $F = 0.01$ a.u., calculated by the TDC method: (left) using the basis of 17 lowest S, P, D and F sodium states, and (right) using the same basis, but without the 4s state.

field-free atom with definite values of \mathbf{k} . These continuum states are solutions of the Schrödinger equation for the active electron in the spherically symmetric potential (1) which satisfy the incoming boundary condition and can be written as the partial wave expansion [28]

$$\phi_{\mathbf{k}}^{(-)}(\mathbf{r}) = \sqrt{\frac{2}{\pi}} \frac{1}{k} \sum_{l,m} i^l e^{-i\Delta_l} \frac{u_l(k,r)}{r} Y_{lm}(\Omega) Y_{lm}^*(\Omega_{\mathbf{k}}). \quad (8)$$

The functions $u_l(k,r) = r\mathcal{R}_l(k,r)$ are numerically determined solutions of the radial equation for given values of the orbital quantum number l and energy $\epsilon = \hbar^2 k^2 / 2m_e$, while Δ_l is the scattering phase shift for the l th partial wave. This shift is the sum of the Coulomb phase shift $\sigma_l = \arg \Gamma(l+1+i\eta)$, where $\eta = -1/k$ (for k given in atomic units), and the phase shift δ_l due to the short-range term in the potential (1). The values of δ_l can be determined by matching the numerical solution $u_l(k,r)$ to its asymptotic form $\cos \delta_l F_l(\eta, kr) + \sin \delta_l G_l(\eta, kr)$, where $F_l(\eta, kr)$ and $G_l(\eta, kr)$ are the regular and irregular Coulomb functions [29]. In the case of potential (1) we found $\delta_l \approx -2, -0.4, -0.05$ and 0 radians for $l = 0, 1, 2$ and $l \geq 3$, respectively. Thus, the photoelectron wave function in momentum representation reads

$$\bar{\psi}(\mathbf{k}) = \langle \phi_{\mathbf{k}}^{(-)} | \psi(t) \rangle = \sqrt{\frac{2}{\pi}} \frac{1}{k} \sum_l (-i)^l e^{i\Delta_l} Y_{10}(\vartheta_{\mathbf{k}}) I_l(k), \quad (9)$$

where

$$I_l(k) = 2\pi \int_{-\infty}^{\infty} \int_{-\infty}^{\infty} \frac{u_l(k,r)}{r} Y_{10}(\vartheta) \psi(\rho, z) \rho d\rho dz, \quad (10)$$

assuming that $r = \sqrt{\rho^2 + z^2}$ and $\cos \vartheta = z/r$. Note that in Eq. (9) there is no summation over the quantum number m since the wave function $\psi(\mathbf{r}, t)$ is characterized by the value $m = 0$. Integral $I_l(k)$ is calculated numerically on the same (ρ, z) -grid as $\psi(\mathbf{r}, t)$.

Fig. 3 shows the calculated PMD for the photoionization of sodium by 800 nm wavelength laser pulse of the form (3) with $T_p = 114$ fs (≈ 4713 a.u., FWHM = 57 fs) for three values of the peak intensity: 3.5, 4.9 and 8.8 TW/cm² (the corresponding field strengths are: $F_{\text{peak}} = 0.0100, 0.0118$ and 0.0158 a.u.).

The radial (k) dependence of the PMD contains information about the photoelectron energies $\epsilon = \hbar^2 k^2 / 2m_e$. The dashed semi-circles of radii $k_0 = 0.279$ a.u. ($\epsilon^{(0)} = 1.060$ eV) and $k'_0 = 0.438$ a.u. ($\epsilon^{(0')} = 2.610$ eV), drawn in the PMD plots, mark the asymptotic values of momenta (energies) of the photoelectrons generated in the nonresonant MPI with four and five photons, respectively, in the weak field limit. Compared to these values, the radial maxima of PMD determined numerically are shifted toward smaller k -values. The origin of these local maxima is twofold. Some of them are related to the nonresonant MPI for different numbers of absorbed photons, while others can be attributed to the REMPI (Freeman resonances). The shift of nonresonant maxima $\delta k = \hbar^{-1} \sqrt{2m_e \epsilon(F_{\text{peak}}) - k_0}$, referring to Eq. (5), is determined by the dynamic Stark shift of the ground state and the continuum boundary at the given laser peak intensity. The positions of Freeman resonances are, on the other hand, almost independent on the field strength, but they are also located below k_0 due to inequality $\epsilon^{(nl)} \leq \epsilon^{(0)}$ discussed in Sec. 3.2.

The angular structure of the PMD, the so-called photoelectron angular distribution (PAD), carries information about the superposition of accessible emitted partial waves, which, according to selection rules for the four-photon absorption, can be s, d and g-waves (see Fig. 1(a)). Indeed, apart from the strong emission along the laser polarization direction ($\vartheta = 0^\circ$ and 180°), which can be

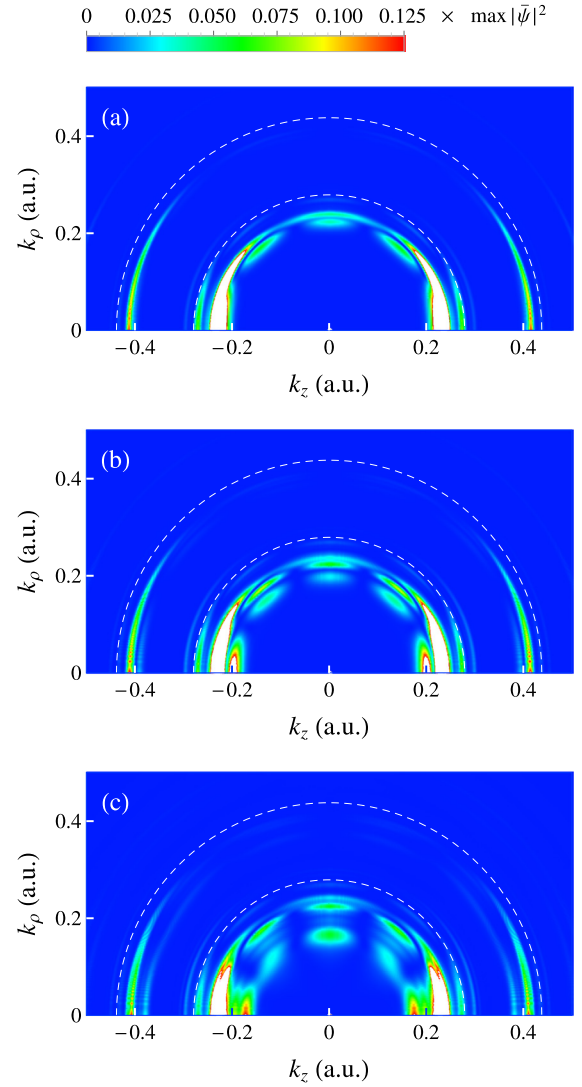


Fig. 3. Photoelectron momentum distribution $|\bar{\psi}(\mathbf{k})|^2$ (arbitrary units) in the photoionization of sodium by the laser pulse ($\lambda = 800$ nm, $T_p = 2 \times \text{FWHM} = 114$ fs) of the form (3) calculated at $t = 145$ fs for three values of the laser peak intensity: (a) 3.5 TW/cm², (b) 4.9 TW/cm² and (c) 8.8 TW/cm². The blue area corresponds to the value $|\bar{\psi}(\mathbf{k})|^2 = 0$, while the white area is the cutoff of the distribution at 12.5% of its maximum value. The dashed semi-circles of radii $k_0 = 0.279$ a.u. and $k'_0 = 0.438$ a.u. correspond to the asymptotic values of the photoelectron momentum in the weak field limit after absorption of four and five photons (the threshold and the 1st ATI order), respectively.

attributed to all three partial waves, the PADs also show maxima at $\vartheta = 90^\circ$, which characterize d and g-waves and at $\vartheta \approx 45^\circ$ and 135° , which characterize the g-wave. Analogously, accessible emitted partial waves for the five-photon absorption can be p, f and h-waves (see Fig. 1(a)).

4.2. Partial probability densities and photoelectron energy spectra

In order to determine the partial probability densities and the PES, we rewrite the expression (9) in the form

$$\bar{\psi}(\mathbf{k}) = \sum_l \Phi_l(k) Y_{10}(\vartheta_{\mathbf{k}}), \quad (11)$$

where

$$\Phi_l(k) = \sqrt{\frac{2}{\pi}} \frac{1}{k} (-i)^l e^{i\Delta_l} I_l(k) \quad (12)$$

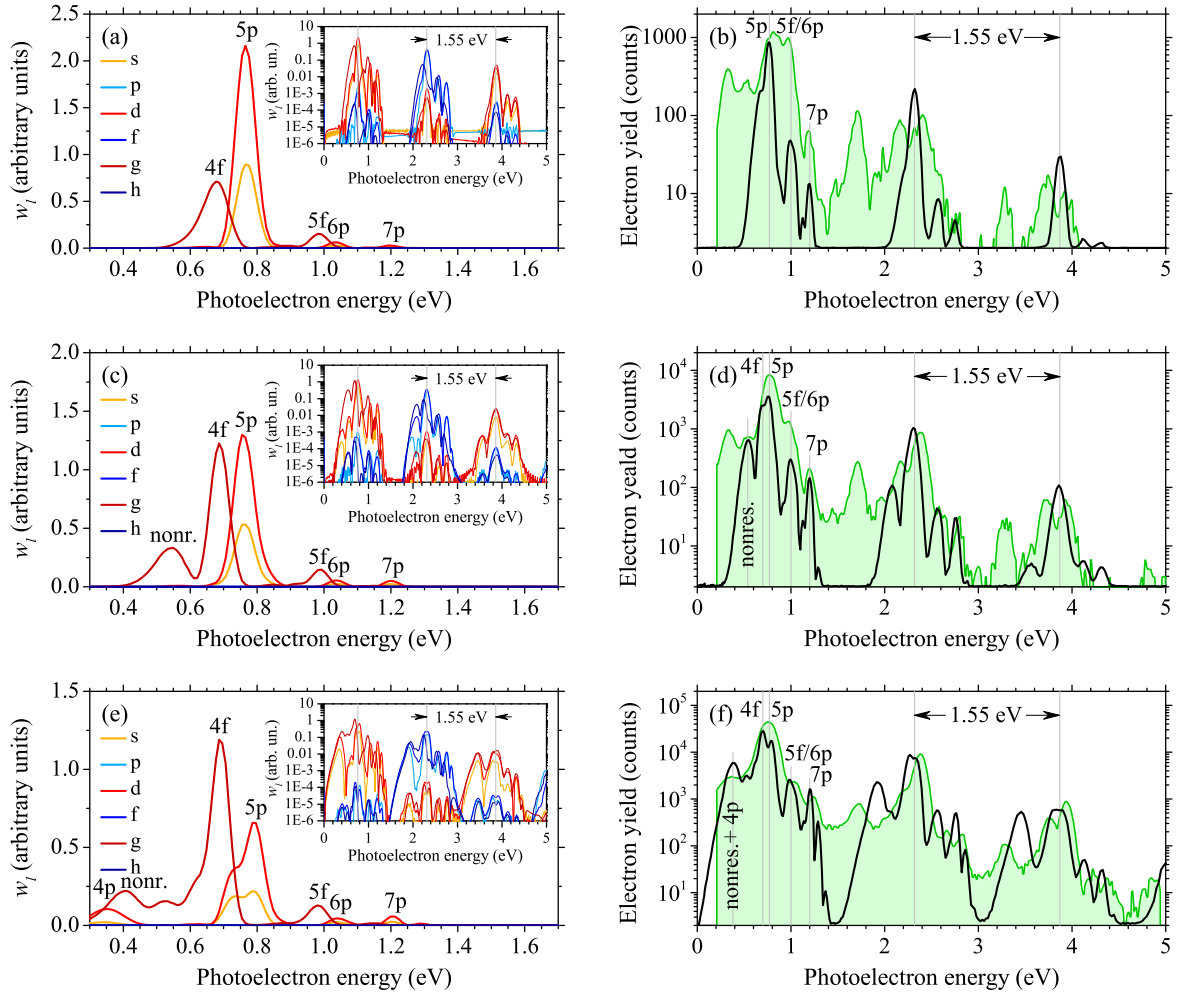


Fig. 4. Partial probability densities w_l for $l = 0, \dots, 5$ (left column) and the total probability density w (right column, black line), as functions of the photoelectron energy $\epsilon = \hbar^2 k^2 / 2m_e$, obtained for three values of the laser peak intensity: (a,b) 3.5 TW/cm^2 , (c,d) 4.9 TW/cm^2 , (e,f) 8.8 TW/cm^2 . Experimental results (electron yield) [7] are represented by green lines (right column). The total probability densities are rescaled for comparison with the experimental results. Thin vertical lines mark the positions of the 5p resonance in the threshold and higher order ATI peaks, as well as the positions of the nonresonant peak and the 4f, 5f/6p and 7p resonances in the threshold peak.

are the radial functions in momentum representation. Thus, the partial radial probability densities of photoelectrons in momentum space are

$$w_l(k) = |\Phi_l(k)|^2 k^2 = \frac{2}{\pi} |I_l(k)|^2 \quad (13)$$

and the total radial probability density is the sum $w(k) = \sum_l w_l(k)$. The quantities w_l for $l = 0, \dots, 5$, as functions of the photoelectron excess energy $\epsilon = \hbar^2 k^2 / 2m_e$, are shown in the left column of Fig. 4 for three values of the laser peak intensity: 3.5 , 4.9 and 8.8 TW/cm^2 . The corresponding total probability densities w represent the PES for these three values of laser intensity. They are shown in the right column of Fig. 4 together with the corresponding spectra obtained experimentally [7].

The spectra, both the calculated and experimental, exhibit typical ATI structure with prominent peaks separated by the photon energy $\hbar\omega \approx 1.55 \text{ eV}$. Fig. 4 (right column) shows the peaks corresponding to the lowest three orders of ATI (MPI by $4 + s$ photons, $s = 0, 1, 2$) which are located approximately at $\epsilon = 0.76 \text{ eV} + s\hbar\omega$. As expected, the peak intensity decreases with the increase of ATI order. Compared to the threshold peak ($s = 0$), the reduction coefficient is 0.2 - 0.3 for $s = 1$ and 0.02 - 0.03 for $s = 2$. The partial wave analysis recovers the character of these peaks. The insets in Fig. 4 (left column) clearly show that the dominant contribution in the total probability density around the threshold peak

($s = 0$, $\epsilon \approx 0.76 \text{ eV}$) and around the second-order ATI peak ($s = 2$, $\epsilon \approx 3.86 \text{ eV}$) comes from the partial waves with even l (s , d , g -waves). Thus, the photoelectrons with these energies are generated by absorbing an even number of photons ($N = 4$ and 6). Contrarily, in the vicinity of the first-order ATI peak ($s = 1$, $\epsilon \approx 2.31 \text{ eV}$) the partial waves with even l are suppressed and those with odd l (p , f , h -waves) dominate. Therefore, in this case odd number of photons is absorbed (here $N = 5$). Each ATI peak, in addition, has an internal structure in the form of local (sub)peaks which can be attributed to the nonresonant MPI and to the REMPI via different excited states. The positions of these subpeaks in the calculated spectra, especially those belonging to the threshold peak ($s = 0$), agree well with the peak positions in the spectra obtained experimentally by Hart et al. [7]. A small displacement of the experimental value for the distance between the threshold and the first ATI peak from the theoretical value $\hbar\omega$.

4.3. Nonresonant photoionization

The position of the nonresonant threshold peak (four-photon ionization maximum) predicted by formula (7) for laser peak intensities 3.5 , 4.9 and 8.8 TW/cm^2 is $\epsilon(F_{\text{peak}}) = 0.74 \text{ eV}$, 0.61 eV and 0.26 eV , respectively. This peak is visible in the numerically determined spectra shown in Fig. 4. Since the energy of photoelectrons

produced by the nonresonant MPI does not depend on l , a feature of the nonresonant peak is that the maxima of contributing partial densities w_l have the same positions on the energy axis. At the laser peak intensity of 3.5 TW/cm^2 , however, the nonresonant peak overlaps with the most prominent REMPI peak (see Fig. 4(a,b)) and it is difficult to estimate the position of former from the numerical data. The position of this peak at intensities 4.9 TW/cm^2 and 8.8 TW/cm^2 is 0.54 eV and 0.41 eV (numerical values), respectively (see Fig. 4(c-f)). A discrepancy between the values obtained by formula (7) and from numerical calculations (especially at $I = 8.8 \text{ TW/cm}^2$) is attributed to the approximative character of the former. In addition, it should be mentioned that in experimental spectra the nonresonant peak is less prominent (almost invisible). This observation is reported also in an earlier work presenting a comparison between calculated and experimental data for the photoionization of lithium [5]. Nonresonant peaks of the first and of the second ATI order can be observed in Fig. 4, too, at positions which are shifted by one and two-photon energy relative to the threshold peak at a given laser intensity.

4.4. Resonantly enhanced multiphoton ionization

In contrast to nonresonant peaks the positions of REMPI peaks (Freeman resonances), as explained in Sec. 3, are almost independent of the laser peak intensity. For the most prominent peak at $\epsilon \approx 0.76 \text{ eV}$ the intermediate P and F states are the states 5p and 4f, whereas for the subpeaks at $\epsilon \approx 1 \text{ eV}$ and at $\epsilon \approx 1.2 \text{ eV}$ these are the states 6p and 5f and the states 7p and 6f, respectively. Note, however, that for the radiation of 800 nm wavelength the transfer of population from the ground state to states 7p and 6f is only near resonant ($E_{7p}, E_{6f} > 3\hbar\omega - I_p$, see Fig. 1(b)) and, strictly speaking, the four-photon ionization via these states is not 3+1 REMPI (see Sec. 3.2). In this case formula (5) is not applicable, but the photoelectron energy can be estimated using relation (7).

Here we focus on the main subpeak of the threshold peak (around 0.76 eV). Taking into account all three ionization pathways (see the first paragraph in Sec. 3) and the fact that photoelectrons produced in the 3+1 and 2+1+1 REMPI via P states cannot be distinguished (Sec. 3.3), the electron outgoing wave in the energy domain of this peak can be written as the superposition of two wave-packets

$$\bar{\psi} = \bar{\psi}^{(5p)} + \bar{\psi}^{(4f)}, \quad (14)$$

which, according to Fig. 1(a), have forms

$$\bar{\psi}^{(5p)} = \Phi_0^{(5p)} Y_{00} + \Phi_2^{(5p)} Y_{20}, \quad (15)$$

$$\bar{\psi}^{(4f)} = \Phi_2^{(4f)} Y_{20} + \Phi_4^{(4f)} Y_{40}. \quad (16)$$

Since states 5p and 4f shift into the three-photon resonance at different field strengths (see Table 1 and Fig. 1(b)), wave packets (15) and (16) are formed in different phases of the laser pulse and characterized by different mean energies ($\approx 0.8 \text{ eV}$ and 0.7 eV , respectively, referring to Table 1).

Expression (14) with components (15), (16) is compatible with the partial wave expansion of function $\bar{\psi}$. Fig. 4(a,c,e) demonstrates that the outgoing wave in the domain of threshold peak decomposes into s, d and g-waves

$$\bar{\psi} = \Phi_0 Y_{00} + \Phi_2 Y_{20} + \Phi_4 Y_{40}. \quad (17)$$

Radial functions Φ_l and the corresponding partial probability densities w_l are determined numerically using formulae (12) and (13), respectively. The positions of maxima of $w_l(\epsilon)$ (see Table 2) confirm the existence of two electron wave-packets with different mean energies. The photoelectrons with s and d-symmetry have

Table 2

Photoelectron energies ϵ at which the partial probability densities w_l ($l = 0, 2, 4$) shown in Fig. 4(a,c,e) take maximal values w_l^m and the ratios w_l^m/w_0^m ($l = 2, 4$).

partial wave:	s ($l = 0$)	d ($l = 2$)	g ($l = 4$)		
I (TW/cm^2)	ϵ (eV)	ϵ (eV)	w_2^m/w_0^m	ϵ (eV)	w_4^m/w_0^m
3.5	0.77	0.76	2.40	0.68	0.79
4.9	0.76	0.76	2.45	0.68	2.30
8.8	0.78	0.79	3.00	0.69	4.55

a higher mean energy ($\sim 0.8 \text{ eV}$) than those with g-symmetry ($\sim 0.7 \text{ eV}$). Referring to Table 1, these two energies characterize the photoelectrons produced in the REMPI via 5p and 4f states ($\epsilon^{(5p)}$ and $\epsilon^{(4f)}$). Since the maxima of $w_2(\epsilon)$ and $w_0(\epsilon)$ almost coincide, we conclude that s-electrons and the majority of d-electrons belong to the same channel, i.e. they are generated in the 3+1 (or 2+1+1) REMPI via 5p state. Thus, the contribution of d-electrons in the wave packet (16) is minor ($\Phi_2^{(4f)} \approx 0$). Then, comparing expansion (17) and expressions (14), (15), (16), we get $\Phi_0^{(5p)} = \Phi_0$, $\Phi_2^{(5p)} \approx \Phi_2$ and $\Phi_4^{(4f)} = \Phi_4$.

A similar analysis indicates that the subpeak at $\epsilon \approx 1 \text{ eV}$ is related to 3+1 REMPI via states 5f and 6p, while that at $\epsilon \approx 1.2 \text{ eV}$ is related to 3+1 (or 2+2+1) REMPI via 7p state (or sequence $4s \rightarrow 7p$) and much less to 3+1 REMPI via state 6f. Finally, note that for 8.8 TW/cm^2 laser intensity an additional peak arises at $\epsilon \approx 0.35 \text{ eV}$ (see Fig. 4(e)), which can be related to the 3+1 REMPI via state 4p [8]. Then, the peak at $\epsilon \approx 0.39 \text{ eV}$ in the PES (Fig. 4(f)) can be attributed to the overlap between this resonant peak and the nonresonant peak at $\epsilon \approx 0.41 \text{ eV}$.

4.5. Selective enhancement of photoionization channels

Partial-wave analysis of the photoelectron wave function revealed that each subpeak of the threshold peak and succeeding ATI peaks, shown in Fig. 4(b,d,f), contains contributions of three REMPI channels, i.e. it is a superposition of three Freeman resonances. Here we examine their relative share in the electron yield and the possibility for selective ionization of atom through a single channel.

At the laser peak intensity $I = 3.5 \text{ TW/cm}^2$ the maximum contribution in the peak around 0.76 eV comes from the electrons of d-symmetry (see Fig. 4(a)). At $I = 4.9 \text{ TW/cm}^2$ the electrons of d and g-symmetry have approximately equal contributions to this peak (Fig. 4(c)), while at intensity $I = 8.8 \text{ TW/cm}^2$ the maximum contribution comes from the electrons of g-symmetry (Fig. 4(e), see also the ratios of w_l maxima shown in Table 2). The contribution of s-electrons in this peak is 2.4-3 times smaller than the contribution of d-electrons. The contributions of s, d and g-electrons in the peaks at $\epsilon \approx 1 \text{ eV}$ and $\epsilon \approx 1.2 \text{ eV}$ do not change significantly with the laser intensity. The peak at $\epsilon \approx 1 \text{ eV}$ is built predominantly by the electrons of g-symmetry, while the maximum contribution to the peak at $\epsilon \approx 1.2 \text{ eV}$ comes from the electrons of d-symmetry. These results indicate that for $F \leq F_{\text{OBI}}$ dominant ionization channel in the peak around 0.76 eV is the 3+1 or, more likely, 2+1+1 REMPI via 5p state, while for $F > F_{\text{OBI}}$ it is the 3+1 REMPI via 4f state. For the peaks around 1 eV and 1.2 eV , dominant channels are the 3+1 REMPI via 5f state and the 2+1+1 REMPI via 7p state, respectively.

These findings are verified by calculating the populations of the unperturbed atomic states nl (i.e. transition probabilities $|\langle nl|\psi(t)\rangle|^2$) during the pulse, while solving the TDSE. Fig. 5 shows the populations of relevant S, P and F states during the pulse of 3.5 TW/cm^2 and 8.8 TW/cm^2 peak intensity. Although $I = 3.5 \text{ TW/cm}^2$ corresponds to the OBI threshold, for this peak intensity there is still a significant population of atoms which are not ionized at all phases of the pulse (see the left side of Fig. 5). The

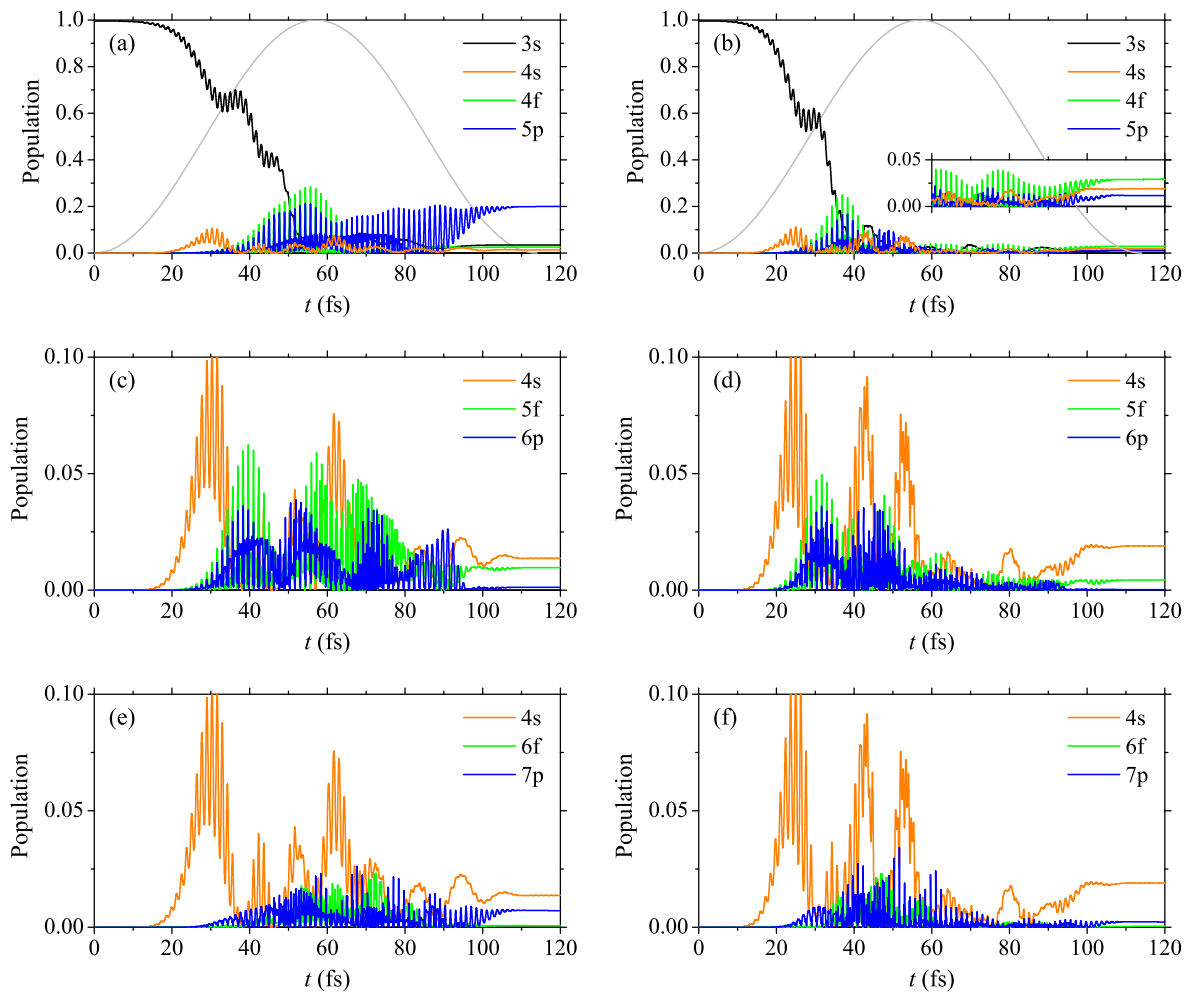


Fig. 5. Populations of the unperturbed ground (3s) and excited states 4s, 4f, 5p, 5f, 6p, 6f and 7p of sodium during the 114 fs laser pulse of 800nm wavelength with peak intensities 3.5 TW/cm^2 (left column) and 8.8 TW/cm^2 (right column), calculated by the wave-packet propagation method. The gray line represents normalized envelope $F(t)/F_{\text{peak}}$ of the pulse.

population of states 5p and 7p is here higher than that of states 4f and 6f, respectively, but the population of state 5f is higher than the population of state 6p. Contrarily, at $I = 8.8 \text{ TW/cm}^2$ most atoms after the first half of the pulse are ionized (see the right side of Fig. 5). Among the atoms that were not ionized the population of states 4f and 5f in this case is higher than that of states 5p and 6p, respectively, while the population of state 7p is again higher than the population of state 6f. These observations fully agree with the findings concerning the photoionization channels.

The populations at different phases of the laser pulse can be well understood from diagrams (b) and (c) in Fig. 1. Diagram (b) predicts and Fig. 5(a,b) confirms that three-photon transitions from the ground state to states 4f and 5p are resonant with the radiation of 800 nm at the field strength $F \approx 0.01 \text{ a.u.}$ (see also Table 1), which takes place in the middle of the laser pulse when $I = 3.5 \text{ TW/cm}^2$ and at $T_p/3$ and $2T_p/3$ for $I = 8.8 \text{ TW/cm}^2$. States 5f and 6p, on the other hand, shift into resonance at smaller values of the field strength, which are reached at the beginning and at the end of pulse (see Fig. 5(c,d)). Contrarily, the three-photon transitions from the ground state to states 6f and 7p are not resonant with the radiation of 800 nm, but 2+1-photon transition $3s \rightarrow 4s \rightarrow 7p$ is near resonant in the weak field limit. Since the dynamic Stark shift for P states grows with the field strength approximately as the shift for 4s state (see Fig. 1(c)), the transition $4s \rightarrow 7p$ remains near resonant and occurs during the whole pulse (see Fig. 5(e,f)). This is supported by the fact that populating the

4s state continues at higher field strengths due to Rabi oscillations between this and the ground state. In addition, the transitions $4s \rightarrow 5p$ and $4s \rightarrow 6p$, which also occur due to Rabi oscillations, partially contribute to the population of 5p and 6p states.

5. Summary and conclusions

In this paper we studied the photoionization of sodium by femtosecond laser pulses of 800 nm wavelength in the range of field strengths belonging to the over-the-barrier ionization domain and analyzed possibilities for selective resonantly enhanced multiphoton ionization through a single channel. Using the single-active-electron approximation we calculated the photoelectron momentum distributions by solving numerically the time dependent Schrödinger equation for these pulse parameters. In order to determine the contribution of different ionization channels to the total photoelectron yield, a partial wave analysis of the outgoing wave function in momentum representation was performed from which the partial probability densities w_l as functions of the photoelectron energy ϵ were obtained. The total density $\sum_l w_l(\epsilon)$ then represents the photoelectron energy spectrum. The spectra calculated for the pulses of 800 nm wavelength, 57 fs duration (FWHM) and $3.5\text{--}8.8 \text{ TW/cm}^2$ peak intensity agree well with the spectra obtained experimentally by Hart et al. [7]. This holds for the positions of both REMPI and ATI peaks.

The partial wave analysis of the spectral peaks related to Freeman resonances revealed that each peak is a superposition of the contributions of photoelectrons from different ionization channels. We found that at the laser peak intensity of 3.5 TW/cm^2 dominant contribution in the main peak (around 0.76 eV) comes from d-electrons, while at the intensity of 8.8 TW/cm^2 the electrons of g-symmetry dominate. In this way, by changing the laser intensity, one can select the main ionization channel. We have shown that in the first case it is combined 3+1 and 2+1+1 REMPI via 5p state, while in the second case it is the 3+1 REMPI via 4f state. In contrast to the main peak, the structure of local peaks around 1 eV and 1.2 eV is not sensitive to the laser intensity. The peak at 1 eV is related to 3+1 REMPI via the states 5f and 6p, whereas the dominant ionization channel for the peak around 1.2 eV is 2+1+1 REMPI via the near resonant 4s state and subsequently excited 7p state. These findings were justified by calculating the populations of excited states during the pulse. The selectivity might be further improved by choosing more appropriate pulse parameters (that is feasible with modern Ti:sapphire lasers enabling pulse-shaping, phase-locking, spectral broadening, amplification, etc.) leading to a better resonance between intermediate states and the laser field.

CRedit authorship contribution statement

Andrej Bunjac: Methodology, Software, Calculation, Investigation, Reviewing and Editing; **Duška Popović:** Conceptualization, Investigation, Reviewing and Editing; **Nenad Simonović:** Supervision, Conceptualization, Methodology, Investigation, Writing, Original draft preparation.

Declaration of competing interest

The authors declare that they have no known competing financial interests or personal relationships that could have appeared to influence the work reported in this paper.

Acknowledgements

This work was done in the Laboratory for Atomic Collision Processes, Institute of Physics Belgrade, under Project No. OI171020 of the Ministry of Education, Science and Technological Development of the Republic of Serbia. Numerical simulations were run on the PARADOX-IV supercomputing facility at the Scientific Computing Laboratory, National Center of Excellence for the Study of

Complex Systems, Institute of Physics Belgrade, supported in part by the Ministry of Education, Science and Technological Development of the Republic of Serbia under project No. OI171017.

References

- [1] M. Wollenhaupt, M. Krug, J. Köhler, T. Bayer, C. Sarpe-Tudoran, T. Baumert, *Appl. Phys. B* 95 (2009) 245.
- [2] M. Krug, T. Bayer, M. Wollenhaupt, C. Sarpe-Tudoran, T. Baumert, S.S. Ivanov, N.V. Vitanov, *New J. Phys.* 11 (2009) 105051.
- [3] M. Schuricke, G. Zhu, J. Steinmann, K. Simeonidis, I. Ivanov, A. Kheifets, A.N. Grum-Grzhimailo, K. Bartschat, A. Dorn, J. Ullrich, *Phys. Rev. A* 83 (2011) 023413.
- [4] S.-D. Jheng, T.F. Jiang, *J. Phys. B, At. Mol. Opt. Phys.* 46 (2013) 115601.
- [5] T. Morishita, C.D. Lin, *Phys. Rev. A* 87 (2013) 063405.
- [6] M. Schuricke, K. Bartschat, A.N. Grum-Grzhimailo, G. Zhu, J. Steinmann, R. Moshhammer, J. Ullrich, A. Dorn, *Phys. Rev. A* 88 (2013) 023427.
- [7] N.A. Hart, J. Strohaber, A.A. Kolomenskii, G.G. Paulus, D. Bauer, H.A. Schuessler, *Phys. Rev. A* 93 (2016) 063426.
- [8] A. Bunjac, D.B. Popović, N.S. Simonović, *Phys. Chem. Chem. Phys.* 19 (2017) 19829.
- [9] P. Wessels, B. Ruff, T. Kroker, A.K. Kazansky, N.M. Kabachnik, K. Sengstock, M. Drescher, J. Simonet, *Commun. Phys.* 1 (2018) 32.
- [10] M.H. Mittleman, *Introduction to the Theory of Laser-Atom Interactions*, Plenum Press, New York, 1982.
- [11] N.B. Delone, V.P. Krainov, *Multiphoton Processes in Atoms*, Vol. 13, Springer, Heidelberg, 2000.
- [12] C.J. Joachain, N.J. Kylstra, R.M. Potvliege, *Atoms in Intense Laser Fields*, Cambridge University Press, Cambridge, 2012.
- [13] L.V. Keldysh, *Zh. Eksp. Teor. Fiz.* 47 (1964) 1945.
- [14] M.Z. Milošević, N.S. Simonović, *Phys. Rev. A* 91 (2015) 023424.
- [15] R.R. Freeman, P.H. Bucksbaum, H. Milchberg, S. Darack, D. Schumacher, M.E. Geusic, *Phys. Rev. Lett.* 59 (1987) 1092.
- [16] G.N. Gibson, R.R. Freeman, T.J. McIlrath, *Phys. Rev. Lett.* 69 (1992) 1904.
- [17] N.B. Delone, V.P. Krainov, *Phys. Usp.* 42 (1999) 669.
- [18] F. Grossmann, *Theoretical Femtosecond Physics*, Springer-Verlag, Berlin, 2008.
- [19] H. Rabitz, R. de Vivie-Riedle, M. Motzkus, K. Kompa, *Science* 288 (2000) 824.
- [20] M. Shapiro, P. Brumer, *Principles of the Quantum Control of Molecular Processes*, Wiley, New York, 2003.
- [21] B.J. Sussman, D. Townsend, M.Yu. Ivanov, A. Stolow, *Science* 314 (2006) 278.
- [22] J. González-Vázquez, I.R. Sola, J. Santamaria, V.S. Malinovsky, *Chem. Phys. Lett.* 431 (2006) 231.
- [23] H. Hellmann, *J. Chem. Phys.* 3 (1935) 61.
- [24] J.E. Sansonetti, *J. Phys. Chem. Ref. Data* 37 (2008) 1659.
- [25] A. Askar, A.S. Cakmak, *J. Chem. Phys.* 68 (1978) 2794.
- [26] A. Bunjac, D.B. Popović, N.S. Simonović, *Eur. Phys. J. D* 71 (2017) 208.
- [27] J. Mitroy, M.S. Safronova, C.W. Clark, *J. Phys. B, At. Mol. Opt. Phys.* 43 (2010) 202001.
- [28] B. Fetić, W. Becker, D.B. Milošević, *Phys. Rev. A* 102 (2020) 023101.
- [29] A.R. Barnett, in: K. Bartschat (Ed.), *Computational Atomic Physics. Electron and Positron Collisions with Atoms and Ions*, Springer, Berlin, 1996, pp. 181–202.



Analysis of the asymmetry of Autler–Townes doublets in the energy spectra of photoelectrons produced at two-photon ionization of atoms by strong laser pulses

A. Bunjac^a , D. B. Popović^b , and N. S. Simonović^c 

Institute of Physics, University of Belgrade, Pregrevica 118, 11080 Belgrade, Serbia

Received 1 November 2022 / Accepted 29 November 2022

© The Author(s), under exclusive licence to EDP Sciences, SIF and Springer-Verlag GmbH Germany, part of Springer Nature 2022

Abstract. We analyzed the asymmetry of Autler–Townes doublets in the calculated photoelectron energy spectra for the two-photon ionization of the hydrogen atom by an intense short laser pulse that resonantly couples its ground state with the excited 2p state. The spectra are calculated applying the method of time-dependent amplitudes using two approaches of different level of approximation. The first approach involves solving a complete set of equations for amplitudes, which, in addition to amplitudes of coupled (1s, 2p) and continuous states, also includes the amplitudes of other discrete (nonessential) states. The second approach is the three-level model that includes only the amplitudes of the two coupled states and those of continuum states. By comparing the spectra obtained using these two approaches it is confirmed that the shift of the Autler–Townes doublets, which exists only in the spectra obtained by solving the full set of equations, can be attributed to the AC Stark shift, which is a consequence of the coupling with nonessential states. Finally, it was found that the asymmetry in the intensity of the Autler–Townes doublet components, which appears in the spectra obtained using both computational approaches, is primarily due to the decrease in the transition probability between the 2p and continuum states with increasing photoelectron energy.

1 Introduction

Multiphoton ionization of an atom by a laser field that resonantly couples its ground state to an excited state can serve as a probe for the field induced Rabi dynamics of the coupled states. In the time-dependent picture this dynamics is manifested as the periodic transfer of population from one state to another—the so-called Rabi flopping (see e.g. [1]), but in the frequency domain it leads to a splitting of the resonant peak in the photoabsorption spectrum, known as the Autler–Townes (AT) doublet. Before the availability of coherent light sources this splitting was first detected in the absorption spectrum of a molecule using radiation from the radio frequency domain [2].

Apart from the photoabsorption spectra, the AT splitting can also be detected in the energy spectra of photoelectrons produced at multiphoton ionization of atoms and molecules. However, despite theoretical predictions to observe it at short wavelengths [3–8], its direct observation at XUV wavelengths has been reported only recently, after the free-electron lasers with high temporal and spatial coherence became avail-

able [9]. Applying intense pulses from such a source, one-photon Rabi oscillations are successfully induced between the ground state and an excited state of the atom, particularly if the carrier frequency of the source is resonant for the transition between these states. A second photon from the same pulse can further ionize the atom from the excited state, so finally we have resonant two-photon ionization. The emitted photoelectrons coherently probe the dynamics of the coupled states and the photoelectron energy spectrum (PES) reveals the AT doublet.

A detailed theoretical analysis of the AT splitting, instead of a simple doublet, predicts a multiple-peak pattern in the PES [5–8], as well as additional effects such as energy shift and asymmetry of the pattern [3, 4, 7, 8]. An explanation for the multiple-peak structure, which has been proposed in previous studies [6], is the so-called dynamic interference of photoelectrons emitted on the rising and falling sides of the pulse with a time delay. However, subsequent analysis has shown that this explanation is not adequate in the general case [10, 11], which is also confirmed by our recent calculations [12].

In this paper, we focus on the analysis of shift and asymmetry of AT doublets, taking as an example the resonant two-photon ionization of hydrogen atoms by short laser pulses. In order to get more pronounced

^a e-mail: bunjac@ipb.ac.rs

^b e-mail: duska@ipb.ac.rs

^c e-mail: simonovic@ipb.ac.rs (corresponding author)

effects, we have chosen pulses of higher intensity and shorter duration than previously used. In the next section we present two computational approaches with different degrees of approximation for calculating the populations of atomic states and the photoelectron energy spectra. Both approaches are based on the method of time-dependent amplitudes, whereby the first solves the full set of equations for amplitudes, while the second takes into account only two resonantly coupled states and continuum states. In Sect. 3 we present the results obtained within these approaches and analyze the above effects in the AT splitting. A summary and conclusions are given in Sect. 4.

2 Model and computational approaches

The populations of atomic states during the interaction of the atom with the laser pulse, including their final values when the pulse has expired, and the photoelectron energy spectra, that are the subject of the analysis carried out in the next section, were obtained by solving the time-dependent Schrödinger equation (in atomic units)

$$i \frac{d}{dt} |\psi(t)\rangle = (H_0 + z\mathcal{E}(t)) |\psi(t)\rangle. \tag{1}$$

Here $|\psi(t)\rangle$ is the non-stationary atomic state at time t , H_0 is the Hamiltonian of the field-free (bare) atom, $\mathcal{E}(t)$ is the electric field component of the laser pulse and z is the projection of the electron-nucleus distance in the field direction. The term $z\mathcal{E}(t)$ describes the atom-field interaction in the dipole approximation using the length gauge. We consider a linearly polarized laser pulse whose electric field component reads

$$\mathcal{E}(t) = \mathcal{E}_0 g(t) \cos \omega t, \tag{2}$$

where \mathcal{E}_0 is the peak value of the field strength, ω is the laser carrier frequency and the function $g(t)$ determines the shape of the pulse envelope.

Equation (1) is solved numerically assuming that the atom is initially in its ground state, i.e. $|\psi(t_0)\rangle = |1s\rangle$, where t_0 is a time before the beginning of the interaction. Since the atom interacting with the field (2) has axial symmetry, the z-projection of the electron angular momentum l_z is a constant of motion and the magnetic quantum number m is a good quantum number. Thus, the state $|\psi(t)\rangle$ is at any time t characterized by the value $m = 0$, which characterizes the ground state of the bare atom. Unless otherwise stated, atomic units (a.u.) are used throughout the paper.

2.1 The full set of equations for amplitudes

The state of the hydrogen atom at time t interacting with a laser field can be written as the superposition of eigenstates of the commuting observables H_0 , l^2 , and l_z

$$|\psi(t)\rangle = \sum_{n,l} c_{nl}(t) |nl\rangle + \int \sum_l c_{\varepsilon l}(t) |\varepsilon l\rangle d\varepsilon, \tag{3}$$

where $c_{nl}(t)$ and $c_{\varepsilon l}(t)$ are the time-dependent amplitudes for the population of discrete and continuum eigenstates, $|nl\rangle \equiv |nlm\rangle$ and $|\varepsilon l\rangle \equiv |\varepsilon lm\rangle$ with $m = 0$, respectively.

By substituting expansion (3) in Schrödinger equation (1) and projecting the result onto each eigenstate, one obtains the following set of equations for the amplitudes

$$\begin{aligned} i\dot{c}_{nl} &= E_n c_{nl}(t) + \mathcal{E}(t) \sum_{n',l'} \langle nl|z|n'l'\rangle c_{n'l'}(t) \\ &+ \mathcal{E}(t) \int \sum_{l'} \langle nl|z|\varepsilon l'\rangle c_{\varepsilon l'}(t) d\varepsilon, \\ i\dot{c}_{\varepsilon l} &= \varepsilon c_{\varepsilon l}(t) + \mathcal{E}(t) \sum_{n',l'} \langle \varepsilon l|z|n'l'\rangle c_{n'l'}(t) \\ &+ \mathcal{E}(t) \int \sum_{l'} \langle \varepsilon l|z|\varepsilon' l'\rangle c_{\varepsilon' l'}(t) d\varepsilon', \end{aligned} \tag{4}$$

where E_n and ε are the values of the discrete and continuum energy levels of the bare atom, respectively.

By representing the integral over ε by the sum over a set of its discretized values ε_i and neglecting the continuum-continuum interaction, the set of integro-differential equations (4) reduces to the following set of differential equations

$$\begin{aligned} i\dot{c}_{nl} &= E_n c_{nl}(t) + \mathcal{E}(t) \sum_{n',l'} \langle nl|z|n'l'\rangle c_{n'l'}(t) \\ &+ \mathcal{E}(t) \sum_{i,l'} \langle nl|z|\varepsilon_i l'\rangle c_{\varepsilon_i l'}(t) \Delta\varepsilon, \\ i\dot{c}_{\varepsilon_i l} &= \varepsilon c_{\varepsilon_i l}(t) + \mathcal{E}(t) \sum_{n',l'} \langle \varepsilon_i l|z|n'l'\rangle c_{n'l'}(t). \end{aligned} \tag{5}$$

At the laser peak intensities up to few hundred TW/cm² that we consider here, in the expansion (3) it is sufficient to use the set of discrete states $|nl\rangle$ with $n \leq 7$ and $l = 0, \dots, n - 1$, and s and d discretized continuum states (see Fig. 1) with energies in the interval from 5 to 8.6 eV with the step $\Delta\varepsilon = 0.01$ eV. The restriction to s and d continuum state justifies the neglect of the continuum-continuum interaction since the matrix elements between states of the same parity (here s and d) are equal to zero. The expressions for matrix elements $\langle nl|z|n'l'\rangle$ and $\langle nl|z|\varepsilon l'\rangle$ are given in Appendix A.

The quantities $|c_{nl}(t)|^2$ can be interpreted as the populations of atomic states $|nl\rangle$ after the interaction of the atom with the laser field which has ended at time t . Thus, the populations of states $|nl\rangle$, after time t_{ex} when we assume that the laser pulse has expired, are $|c_{nl}(t_{\text{ex}})|^2$. Analogously, the quantity $|c_{\varepsilon l}(t_{\text{ex}})|^2$ represents the probability density of finding the atomic elec-

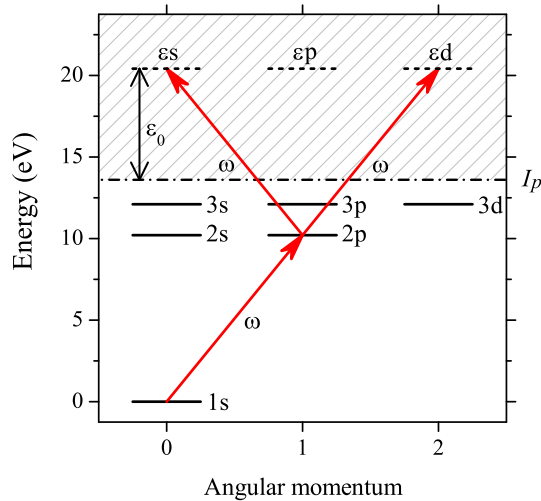


Fig. 1 Energy level scheme of the hydrogen atom and the two-photon absorption paths for transitions from the ground (1s) state to the final continuum states (εs and εd) via one-photon resonant excitation of 2p state

tron in the continuum state $|\varepsilon l\rangle$ after the pulse has expired.

Since the photoelectron yield at a given energy ε is proportional to the total probability density of finding the electron in continuum states corresponding to this energy, the photoelectron energy spectrum (PES) is adequately represented by the distribution

$$w(\varepsilon) = \sum_l |c_{\varepsilon l}(t_{\text{ex}})|^2, \tag{6}$$

which in the considered case practically reduces to formula $w(\varepsilon) = |c_{\varepsilon s}(t_{\text{ex}})|^2 + |c_{\varepsilon d}(t_{\text{ex}})|^2$.

2.2 The three-level model

In the case of resonant or near resonant excitation of an intermediate state (here 2p), the other excited states are nonessential and at weak fields their role in the ionization process may be neglected, i.e. the process may be adequately described within the three-level model (E_1, E_2, ε) [6]. Then, the atomic state at time t reads

$$|\psi(t)\rangle = C_{1s}(t)|1s\rangle + C_{2p}(t)e^{-i\omega t}|2p\rangle + e^{-2i\omega t} \int [C_{\varepsilon s}(t)|\varepsilon s\rangle + C_{\varepsilon d}(t)|\varepsilon d\rangle] d\varepsilon, \tag{7}$$

where $C_{1s}(t)$, $C_{2p}(t)$ and $C_{\varepsilon l}(t)$ are the time-dependent amplitudes for the population of states $|1s\rangle$ (ground state), $|2p\rangle$ (intermediate state) and $|\varepsilon l\rangle$, $l = 0, 2$ (continuum states), respectively. In this expansion the states $|2p\rangle$ and $|\varepsilon l\rangle$ have been multiplied with the phase factors $e^{-i\omega t}$ and $e^{-2i\omega t}$ in order to simplify the set of equations for the amplitudes. By comparing Eqs. (3) and (7), one sees that $C_{1s}(t) = c_{1s}(t)$, $C_{2p}(t) = e^{i\omega t} c_{2p}(t)$ and $C_{\varepsilon l}(t) = e^{2i\omega t} c_{\varepsilon l}(t)$. Since the

difference between the C and c sets of amplitudes is only in the phase factors, both sets adequately determine the populations of atomic states and photoelectron yield.

If we set the ground state energy to zero ($E_1 = 0$, as shown in Fig. 1), by inserting Eq. (7) in the Schrödinger equation (1) and applying the rotating wave approximation [1], we obtain the following system of equations for the amplitudes

$$\begin{aligned} i\dot{C}_{1s} &= \frac{1}{2} D^* \mathcal{E}_0 g(t) C_{2p}(t), \\ i\dot{C}_{2p} &= \frac{1}{2} D \mathcal{E}_0 g(t) C_{1s}(t) + (E_2 - \omega) C_{2p}(t) \\ &\quad + \frac{1}{2} \mathcal{E}_0 g(t) \int [d_{\varepsilon s}^* C_{\varepsilon s}(t) + d_{\varepsilon d}^* C_{\varepsilon d}(t)] d\varepsilon, \\ i\dot{C}_{\varepsilon s} &= \frac{1}{2} d_{\varepsilon s} \mathcal{E}_0 g(t) C_{2p}(t) + (I_p + \varepsilon - 2\omega) C_{\varepsilon s}(t), \\ i\dot{C}_{\varepsilon d} &= \frac{1}{2} d_{\varepsilon d} \mathcal{E}_0 g(t) C_{2p}(t) + (I_p + \varepsilon - 2\omega) C_{\varepsilon d}(t). \end{aligned} \tag{8}$$

Note that, by taking $E_1 = 0$, the energies of the 2p and final continuum states are $E_2 = 0.375 \text{ a.u.} = 10.204 \text{ eV}$ and $I_p + \varepsilon$, respectively, where $I_p = 0.5 \text{ a.u.} = 13.606 \text{ eV}$ is the ionization potential of the hydrogen atom. Here $D = \langle 2p|z|1s\rangle$ and $d_{\varepsilon l} = \langle \varepsilon l|z|2p\rangle$ are the dipole transition matrix elements for the excitation of the 2p state and for its subsequent ionization, respectively.

Using formal solutions of the third and fourth of Eq. (8)

$$C_{\varepsilon l}(t) = -\frac{i}{2} \mathcal{E}_0 d_{\varepsilon l} \int_{-\infty}^t e^{-i(I_p + \varepsilon - 2\omega)(t-t')} g(t') C_{2p}(t') dt', \tag{9}$$

where $l = 0, 2$, and the local approximation which assumes that the main contribution of the integral over t' stems from the times around $t' \sim t$ [13, 14], the last term in the second of Eq. (8) reduces to

$$\begin{aligned} &\frac{1}{2} \mathcal{E}_0 g(t) \int [d_{\varepsilon s}^* C_{\varepsilon s}(t) + d_{\varepsilon d}^* C_{\varepsilon d}(t)] d\varepsilon \\ &= -\pi i \frac{|d_{\varepsilon 0}|^2 \mathcal{E}_0^2}{4} g^2(t) C_{2p}(t), \end{aligned} \tag{10}$$

where $|d_{\varepsilon 0}|^2 = |d_{\varepsilon 0s}|^2 + |d_{\varepsilon 0d}|^2$ and $\varepsilon_0 = 2\omega - I_p$. Note also that the third and the fourth of Eq. (8) are equivalent. Namely, dividing them by $d_{\varepsilon s}$ and $d_{\varepsilon d}$, respectively, they reduce to the same equation for the scaled amplitude $\tilde{C}_\varepsilon(t) = C_{\varepsilon s}(t)/d_{\varepsilon s} \equiv C_{\varepsilon d}(t)/d_{\varepsilon d}$ (which also follows from Eq. (9)).

Finally, one obtains the set of equations

$$\begin{aligned} i\dot{C}_{1s} &= \frac{1}{2} \Omega_0^* g(t) C_{2p}(t), \\ i\dot{C}_{2p} &= \frac{1}{2} \Omega_0 g(t) C_{1s}(t) + \left[E_2 - \frac{i}{2} \Gamma g^2(t) - \omega \right] C_{2p}(t), \end{aligned}$$

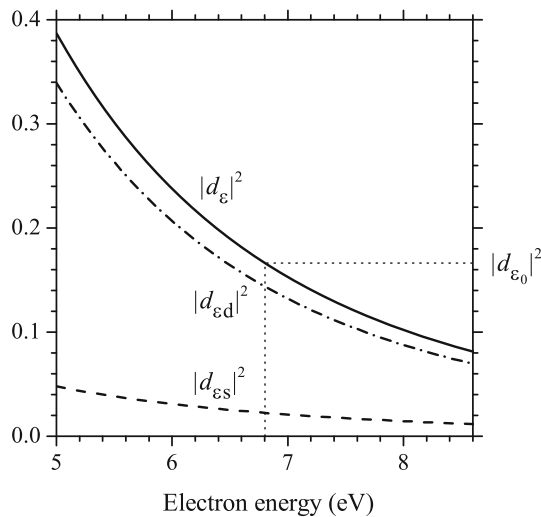


Fig. 2 The squares of modula of the dipole matrix elements for transitions from the 2p state to continuum states εs and εd (dashed and dash-dot lines, respectively), determined by Eq. (18), and their sum $|d_\varepsilon|^2$ (full line) in the energy interval $\varepsilon \in (6.4, 7.2)$ eV. The vertical and horizontal dotted lines mark the resonant energy $\varepsilon_0 = 6.803$ eV and the corresponding value of $|d_\varepsilon|^2$ ($|d_{\varepsilon_0}|^2 = 0.1663$ a.u.), respectively

$$i\dot{\tilde{C}}_\varepsilon = \frac{1}{2}\mathcal{E}_0g(t)C_{2p}(t) + (\varepsilon - \varepsilon_0)\tilde{C}_\varepsilon(t), \tag{11}$$

where $\Omega_0 = D\mathcal{E}_0$ is the frequency of Rabi flopping between the populations of states 1s and 2p at the peak value of laser intensity and

$$\Gamma = 2\pi \left| \frac{d_{\varepsilon_0}\mathcal{E}_0}{2} \right|^2 \tag{12}$$

is the ionization rate of the intermediate resonant state |2p>. The imaginary term $-\frac{i}{2}\Gamma g^2(t)$ describes the losses of the population of the intermediate state by the ionization into all final electron continuum states $|\varepsilon l\rangle$.

The PES can be determined applying formula (6), which here takes the form

$$w(\varepsilon) = |d_\varepsilon|^2 |\tilde{C}_\varepsilon(t_{\text{ex}})|^2, \tag{13}$$

where $|d_\varepsilon|^2 = |d_{\varepsilon s}|^2 + |d_{\varepsilon d}|^2$. The values of the dipole matrix elements for transitions from the 1s to the 2p state and from the 2p state to continuum states are determined using Eqs. (17)–(21). The matrix element for the transition 1s \rightarrow 2p is $D = 0.7449$ a.u., while the values of $|d_\varepsilon|^2$ for $\varepsilon \in (5, 8.6)$ eV are shown in Fig. 2. The resonant excitation of the 2p state and the subsequent ionization occurs if the laser carrier frequency is $\omega = 0.375$ a.u., which coincides with the transition frequency between the 1s and 2p states (in the weak field limit). The photon energy corresponding to this frequency is 10.204 eV and the expected kinetic energy of the ejected electrons is $\varepsilon_0 = 0.25$ a.u. = 6.803 eV.

In the next section it will be shown that the approximate results obtained using the three-level model, in which the exact values for $|d_\varepsilon|^2$ are replaced by the value of $|d_{\varepsilon_0}|^2$, as it was the case in previous studies [6], are sufficient for a qualitative analysis of spectra. The values of the matrix elements for transitions from the 2p state to continuum s and d states at the energy ε_0 are $d_{\varepsilon_0 s} = (0.1469 - 0.0296 i)$ a.u. and $d_{\varepsilon_0 d} = (-0.0749 - 0.3717 i)$ a.u., respectively. These values give $|d_{\varepsilon_0}|^2 = 0.1663$ a.u. and the quotient $|d_{\varepsilon_0 s}|^2/|d_{\varepsilon_0 d}|^2 = 0.1563$ which estimates the relative ratio of s and d-electrons in the photoelectron yield.

3 Results

Using the methods described in the previous section, we analyze the populations of atomic states and photoelectron energy spectra for the two-photon ionization of the hydrogen atom by the laser pulse (2) of the gaussian form

$$g(t) = e^{-t^2/\tau^2} \tag{14}$$

with $\tau = 6$ fs and the carrier frequency $\omega = 0.375$ a.u. which is resonant for the transition 1s \rightarrow 2p.

Figure 3 shows the evolution of the populations of atomic states 1s and 2p, calculated for the pulse of peak intensity $I_0 = 25$ TW/cm² ($I_0 = \mathcal{E}_0^2/(8\pi\alpha)$, $\alpha = 1/137$) for which approximately 1.5 Rabi cycles during the pulses are completed. The populations shown in panel (a) were obtained using the method of time-dependent amplitudes described in Sect. 2.1, i.e. by solving the system of Eq. (5) for the recommended set of amplitudes, while those in panel (b) were obtained applying the three-level model described in Sect. 2.2, i.e. by solving the system of Eq. (11). Beside the populations of the 1s and 2p states, in the panel (a) the populations of the states 2s and 3d are shown, too. The populations of other states are significantly smaller and, for this reason, not shown in the figure. A good agreement between the results for the populations of the states 1s and 2p in the panels (a) and (b), as well as relatively small values for populations of other (non-essential) states, confirm the validity of the three-level model, particularly for describing the electron dynamics in the discrete-state subspace.

Figure 4 shows the final populations of the ground and intermediate states, using $t_{\text{ex}} = 3\tau$ for the gaussian pulse (14), as functions of the peak intensity I_0 in the domain of 0.02–400 TW/cm². The values obtained using the computational approaches described in Sects. 2.1 and 2.2 practically coincide and for this reason they are represented in the figure by the same lines. The vertical dashed lines indicate the values of I_0 at which the atom manages to complete an integer number of Rabi cycles during the pulse.

Figure 5 shows the photoelectron energy spectra calculated for the laser peak intensities which are in Fig. 4 indicated by the vertical dashed lines. The spectra

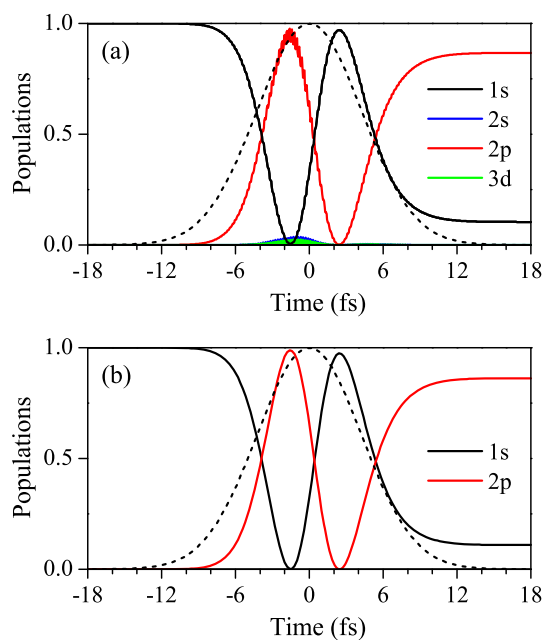


Fig. 3 **a** Populations of the ground state (1s) and the excited states 2s, 2p and 3d of the hydrogen atom during the action of the gaussian laser pulse of 25 TW/cm^2 peak intensity, $\tau = 6 \text{ fs}$ and $\omega = 0.375 \text{ a.u.}$, calculated by solving the set of Eq. (5). **b** Populations of the ground state (1s) and the excited state 2p of the hydrogen atom during the action of the same pulse, calculated by solving the set of Eq. (11) (the three-level model). The dashed line represents the envelope of the laser pulse. For the chosen peak intensity the populations perform approximately 1.5 Rabi cycles during the pulse

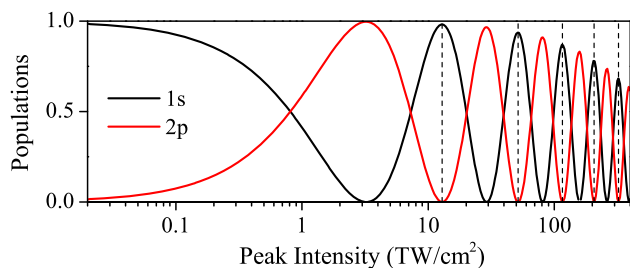


Fig. 4 Populations of the ground (1s) and the excited 2p state of hydrogen, after the laser pulse has expired, as functions of the laser peak intensity. The results are obtained using the gaussian pulse of the carrier frequency $\omega = 0.375 \text{ a.u.}$ (which corresponds to the photon energy of 10.204 eV) and $\tau = 6 \text{ fs}$. The vertical dashed lines indicate the peak intensities at which an integer number of Rabi cycles is completed during the pulse

in panel (a) are determined by solving the system of Eq. (5) and applying Eq. (6), while those in panel (b) are obtained by solving the system of Eq. (11) (the three-level model) and applying Eq. (13) with $|d_\epsilon|^2$ values shown in Fig. 2 (solid red lines) and, alternatively, with $|d_\epsilon|^2 \approx |d_{\epsilon_0}|^2$ (dotted lines). It can be seen that, regardless of the calculation method, for each value of I_0 the spectrum consists of a pattern exhibiting the AT

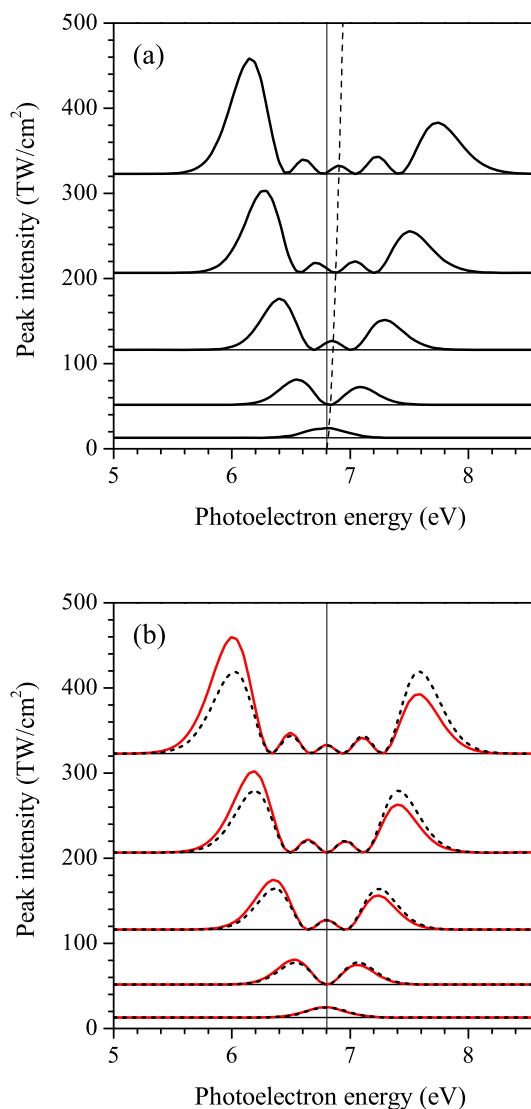


Fig. 5 Calculated photoelectron energy spectra for two-photon ionization of the hydrogen atom by gaussian laser pulses of 6 fs duration, 10.203 eV photon energy, and peak intensities indicated in Fig. 4 by vertical dashed lines. The spectra in panel (a) are determined by solving the full set of Eq. (5) with recommended number of states (see the text in Sect. 2.1), while those in panel (b) are obtained using the three-level model with exact $|d_\epsilon|^2$ values (solid red lines) and with $|d_\epsilon|^2 \approx |d_{\epsilon_0}|^2$ (dashed lines). The weak field value of the photoelectron energy $\epsilon_0 = 6.803 \text{ eV}$ is marked by the vertical thin line. The dashed line in panel (a) shows the shift of the spectral patterns (AT doublets) which is a slowly increasing function of the laser peak intensity

splitting. An exception is the pattern for the laser peak intensity corresponding to one Rabi cycle during the pulse. Namely, the separation between the components of the AT doublet (the edge peaks) is proportional to the field strength [2], and in the one-cycle case this separation is of the same order as the widths of the components.

A notable difference between the spectra shown in panels (a) and (b) of Fig. 5 is a shift of the AT doublets to higher values of the photoelectron energy that exists in the former and does not exist in the latter spectra. The shift increases with the laser peak intensity and can be attributed to the dynamic (AC) Stark shift that is a consequence of coupling of the ground and resonant states with nonessential states [7, 8]. Since the last states do not participate in the three-level model, the AC Stark shift is not included and the AT doublets calculated using such an approximate model are not shifted.

Another difference between the spectra obtained using approaches of different degrees of approximation is in the intensity of the AT doublet components. In the spectra obtained using the three-level model with the approximation $|d_\varepsilon|^2 = |d_{\varepsilon_0}|^2$, the edge peaks are of the same intensity, but in the spectra obtained by the method of time-dependent amplitudes with a larger number of states (panel (a)) and those obtained using the three-level model with exact values for $|d_\varepsilon|^2$, the right peak is lower than the left one. According to Refs. [7, 8] the AC Stark shift could be an explanation for this kind of asymmetry, too. Namely, the carrier frequency, which is resonant for the transition $1s \rightarrow 2p$, is due to the Stark shift slightly different from the field-free resonant frequency $\omega = 0.375$ a.u., and this detuning may be a reason for the asymmetry [5]. However, our calculations performed within the three-level model with exact values for $|d_\varepsilon|^2$ reproduce very well the asymmetry obtained by the full calculations. Therefore, we conclude that, although the asymmetry in the intensity of the AT doublet components may be partially caused by the AC Stark shift, it is primarily due to the change of the values of matrix elements $d_{\varepsilon l}$ with the photoelectron energy ε .

4 Summary and conclusions

In this paper we analyzed the shift and asymmetry of Autler–Townes doublets observed in the photoelectron energy spectra in the case of two-photon ionization of the hydrogen atom by intense short laser pulses of the carrier frequency which is resonant with the transition $1s \rightarrow 2p$. These doublets are a manifestation of the field induced Rabi flopping of population between the resonantly coupled $1s$ and $2p$ (essential) states, but also they carry information about other atomic (nonessential) states and transitions to continuum states. The spectra were calculated applying the method of time-dependent amplitudes using two approaches of different level of approximation. The first approach involves solving a complete set of equations for amplitudes, which, apart from the amplitudes of essential and continuum states, also include the amplitudes of non-essential states. The second approach is the three-level model that includes only the amplitudes of the two essential states ($1s$, $2p$) and those of continuum states. Thus, the AC Stark shift which is a consequence of the coupling

of essential states with non-essential ones, can appear only in spectra obtained using the first approach, which was confirmed by the calculations. The asymmetry in the intensity of the Autler–Townes doublet components appears both in the results obtained by the first approach and in the results obtained using the three-level model with exact values of the dipole matrix elements for transitions between the $2p$ and continuum states. Thus, we conclude that this asymmetry is primarily a consequence of the decrease in the probability of transitions between the $2p$ and continuum states with increasing photoelectron energy.

Acknowledgements This work was supported by Ministry of Education, Science and Technological Development of Republic of Serbia and by the COST Action No. CM18222 (AttoChem).

Author contributions

All authors contributed to the study conception, material preparation, data collection and its analysis. The first draft of the manuscript was written by the corresponding author (N.S.S). All authors read and approved the final manuscript.

Data Availability Statement This manuscript has no associated data or the data will not be deposited. [Author’s comment: The datasets generated during and/or analysed during the current study are available from the corresponding author on reasonable request.]

Appendix A: Matrix elements for dipole transitions

The matrix elements that occur in Eqs. (4), (5) and (8) are conveniently calculated using the coordinate representation for the discrete and continuum energy eigenstates of the bare atom

$$\begin{aligned} |nl\rangle \rightarrow \psi_{nl}(\mathbf{r}) &= R_{nl}(r)Y_{l0}(\Omega), \\ |\varepsilon l\rangle \rightarrow \psi_{\varepsilon l}(\mathbf{r}) &= \sqrt{\frac{2}{\pi k}} i^l e^{-i\sigma_l(k)} \frac{F_l(\eta, kr)}{r} Y_{l0}(\Omega), \end{aligned} \quad (15)$$

where $R_{nl}(r)$ and $Y_{l0}(\Omega)$ are the radial wave functions of hydrogen and the spherical harmonics with $m = 0$, respectively, whereas $\sigma_l = \arg \Gamma(l+1+i\eta)$ and $F_l(\eta, kr)$ are the Coulomb phase shift and the regular Coulomb functions [15], where $\eta = -1/k$ and $k = \sqrt{2\varepsilon}$ (in atomic units). Then

$$\langle nl|z|n'l'\rangle = \int \psi_{nl}^*(\mathbf{r}) r \cos \vartheta \psi_{n'l'}(\mathbf{r}) d^3\mathbf{r} = I_{nl,n'l'}^{(\text{dis})} J_{l'l}, \quad (17)$$

$$\begin{aligned} \langle nl|z|\varepsilon l'\rangle &= \int \psi_{nl}^*(\mathbf{r}) r \cos \vartheta \psi_{\varepsilon l'}(\mathbf{r}) d^3 \mathbf{r} \\ &= \sqrt{\frac{2}{\pi k}} i^{l'} e^{-i\sigma_{l'}(k)} I_{nl,\varepsilon l'}^{(\text{cont})} J_{l'l'}, \end{aligned} \quad (18)$$

where

$$I_{nl,n'l'}^{(\text{dis})} = \int_0^\infty R_{nl}(r) R_{n'l'}(r) r^3 dr, \quad (19)$$

$$I_{nl,\varepsilon l'}^{(\text{cont})} = \int_0^\infty R_{nl}(r) F_{l'}(\eta, kr) r^2 dr, \quad (20)$$

$$J_{l'l'} = \int_\Omega Y_{l0}(\Omega) Y_{l'0}(\Omega) \cos \vartheta d\Omega. \quad (21)$$




References

1. D.A. Steck, Quantum and Atom Optics, <http://steck.us/teaching>. Accessed 24 Sept 2020 (revision 0.13.4)
2. S.H. Autler, C.H. Townes, Phys. Rev. **100**, 703 (1955)
3. K.J. LaGattuta, Phys. Rev. A **47**, 1560–1563 (1993)
4. M.G. Girju, K. Hristov, O. Kidun, D. Bauer, J. Phys. B **40**, 4165 (2007)
5. D. Rogus, M. Lewenstein, J. Phys. B **19**, 3051 (1986)
6. P.V. Demekhin, L.S. Cederbaum, Phys. Rev. A **86**, 063412 (2012)
7. A.D. Müller, E. Kutscher, A.N. Artemyev, L.S. Cederbaum, P.V. Demekhin, Chem. Phys. **509**, 145 (2018)
8. A. Tóth, A. Csehi, J. Phys. B: At. Mol. Opt. Phys. **54**, 035005 (2021)
9. S. Nandi, E. Olofsson, M. Bertolino, S. Carlström, F. Zapata, D. Busto, C. Callegari, M. Di Fraia, P. Eng-Johnsson, R. Feifel, G. Gallician, M. Gisselbrecht, S. Maclot, L. Neoričić, J. Peschel, O. Plekan, K.C. Prince, R.J. Squibb, S. Zhong, P.V. Demekhin, M. Meyer, C. Miron, L. Badano, M.B. Danailov, L. Giannessi, M. Manfredda, F. Sottocorona, M. Zangrando, J.M. Dahlström, Nature **608**, 488 (2022)
10. M. Baghery, U. Saalmann, J.M. Rost, Phys. Rev. Lett. **118**, 143202 (2017)
11. W.C. Jiang, J. Burgdörfer, Opt. Express **26**, 19921 (2018)
12. N.S. Simonović, D.B. Popović, A. Bunjac, To be published
13. P.V. Demekhin, L.S. Cederbaum, Phys. Rev. A **83**, 023422 (2011)
14. P.V. Demekhin, L.S. Cederbaum, Phys. Rev. A **88**, 043414 (2013)
15. A.R. Barnett, in *Computational Atomic Physics, Electron and Positron Collisions with Atoms and Ions*, ed. by K. Bartschat (Springer, Berlin, 1996), pp.181–202

Springer Nature or its licensor (e.g. a society or other partner) holds exclusive rights to this article under a publishing agreement with the author(s) or other rightsholder(s); author self-archiving of the accepted manuscript version of this article is solely governed by the terms of such publishing agreement and applicable law.

Article

Manifestations of Rabi Dynamics in the Photoelectron Energy Spectra at Resonant Two-Photon Ionization of Atom by Intense Short Laser Pulses

Nenad S. Simonović , Duška B. Popović  and Andrej Bunjac 

Institute of Physics, University of Belgrade, Pregrevica 118, 11080 Belgrade, Serbia

* Correspondence: simonovic@ipb.ac.rs

Abstract: We study the Rabi flopping of the population between the ground and excited 2p states of the hydrogen atom, induced by intense short laser pulses of different shapes and of carrier frequency $\omega = 0.375$ a.u. which resonantly couples the two states, and manifestations of this dynamics in the energy spectra of photoelectrons produced in the subsequent ionization of the atom from the excited state. It is found that, for Gaussian, half-Gaussian and rectangular pulses, characterized by the same pulse area, the final populations take the same values and the spectra consist of similar patterns having the same number of peaks and approximately the same separation between the prominent edge (Autler–Townes) peaks. The additional analysis in terms of dressed states showed that the mechanism of formation of multiple-peak structures during the photoionization process is the same regardless of the pulse shape. These facts disprove the hypothesis proposed in earlier studies with Gaussian pulse, that the multiple-peak pattern appears due to dynamic interference of the photoelectrons emitted with a time delay at the rising and falling sides of the pulse, since the hypothesis is not applicable to either a half-Gaussian pulse that has no rising part or a rectangular pulse whose intensity is constant.

Keywords: Rabi dynamics; laser pulse; photoionization; photoelectron energy spectrum; Autler–Townes splitting; multiple-peak pattern; dressed states; dynamic interference



Citation: Simonović, N.S.; Popović, D.B.; Bunjac, A. Manifestations of Rabi Dynamics in the Photoelectron Energy Spectra at Resonant Two-Photon Ionization of Atom by Intense Short Laser Pulses. *Atoms* **2023**, *11*, 20. <https://doi.org/10.3390/atoms11020020>

Academic Editors: Himadri S. Chakraborty and Hari R. Varma

Received: 12 December 2022

Revised: 16 January 2023

Accepted: 18 January 2023

Published: 23 January 2023



Copyright: © 2023 by the authors. Licensee MDPI, Basel, Switzerland. This article is an open access article distributed under the terms and conditions of the Creative Commons Attribution (CC BY) license (<https://creativecommons.org/licenses/by/4.0/>).

1. Introduction

If an atom, initially being in its ground state, interacts with an alternating field that resonantly couples this state to an excited state, the population will be periodically transferred from one state to another. This effect was first described theoretically by Rabi, who applied it for fermions in rotating magnetic fields [1]. In general, the flopping of the population can be explained by the fact that the eigenstates of the Hamiltonian describing the bare atom are no longer stationary states if the atom interacts with the field. Another consequence of this fact is the splitting of the coupled atomic states into doublets of “dressed states”, whose quasi-energies are separated by the value corresponding to the frequency of Rabi flopping (see, e.g., Ref. [2]). This splitting can be observed in the photoabsorption and photoionization spectra of atoms and molecules. Before the availability of coherent light sources, it was first detected using radiation from the radio frequency domain. In the original observation by Autler and Townes [3], a radio frequency source tuned to the separation between two doublet microwave absorption lines of the OCS molecule was used.

Despite theoretical predictions to observe Rabi dynamics at short wavelengths [4,5] and the availability of intense XUV light sources for more than a decade, direct observation of Rabi dynamics at such short wavelengths has been reported only recently [6]. In the actual experiment, applying intense XUV laser pulses from a free-electron laser with high temporal and spatial coherence, one-photon Rabi oscillations are induced between the ground state and an excited state in helium atoms (pump). Then, a second (probe) photon

from the same pulse ionizes the atom from the excited state (resonant two-photon ionization) or, at higher intensities, two photons can do it from the ground state (nonresonant two-photon ionization). In both cases, the emitted photoelectrons coherently probe the underlying dynamics and the measured signal reveals an Autler–Townes (AT) doublet.

In the above experiment, the AT doublets were built at the resonant two-photon ionization for 1.5 completed Rabi cycles. However, theoretical analysis of the resonant multiphoton ionization for more than two completed Rabi cycles during the pulse predicts the appearance of a multiple-peak pattern in the photoelectron energy spectrum (PES) [7–10]. The number of peaks appearing in the pattern is essentially determined by the pulse area [7]. The area theorem (see Ref. [11] and references therein) actually, relates this quantity to the number of Rabi cycles during the pulse, but numerical calculations have shown that this number, the number of peaks in the radial density of photoelectrons and the number of peaks in the pattern coincide [9]. The coincidence between the first two numbers is easily explained by the propagation of the emitted bunches of photoelectrons, which are separated in time and, thus, separated in space, too. On the other hand, the explanation for the multiple-peak pattern in the spectrum is still under consideration. There is a general agreement that this pattern is a result of the superposition of the contributions of photoelectrons ejected via two dressed states during the pulse action. The situation is simplest in the case of photoionization by a rectangular pulse, where the two contributions have the forms of cardinal sine (sinc) functions of energy, shifted by the value of the corresponding Rabi frequency, and the multiple-peak pattern is a result of their overlap [7] (see also Section 3.3). Conversely, in the case of smooth pulses such as the Gaussian, it is not clear exactly what is happening. The analysis performed within the stationary phase approximation suggested that dynamic interference of the photoelectrons emitted with the same energy, but with a time delay at the rising and falling sides of the pulse, essentially determines the multiple-peak structure (modulations) in the PES [8,12,13]. However, this assumption has been questioned by analyzing the conditions for dynamic interference [14,15], where it was found that they are not always fulfilled, particularly in the case of photoionization from the hydrogen ground state.

To shed more light on the above issue, in this paper we investigate manifestations of Rabi dynamics in the photoelectron energy spectra calculated for resonant two-photon ionization of the hydrogen atom by intense short laser pulses of three different forms—Gaussian, half-Gaussian and rectangular ones. By choosing the carrier frequency of 0.375 a.u. that resonantly couples the hydrogen ground (1s) and excited 2p states, the pulse induces one-photon Rabi oscillations between these states, and a second photon from the same pulse subsequently ionizes the atom from the 2p state. The problem was previously studied by other authors, who also used different forms of the laser pulse (see Refs. [4,5,7–9]), but conditions for the dynamic interference were not considered. The paper is organized in the following way. In the next section, we briefly describe the computational method for calculating the populations of atomic states and the photoelectron energy spectra, based on the three-level model, and present results for resonant two-photon ionization of hydrogen by intense short laser pulses. In Section 3 we analyze the Rabi dynamics and the AT patterns in the spectra in terms of dressed states. A summary and conclusions are given in Section 4.

2. Calculation of Populations of Atomic States and Photoelectron Energy Spectra

The populations of atomic states during the interaction of the atom with the laser pulse, including their final values when the pulse has expired, and the photoelectron energy spectra were obtained by solving the time-dependent Schrödinger equation (in atomic units)

$$i \frac{d}{dt} |\psi(t)\rangle = (H_0 + z\mathcal{E}(t)) |\psi(t)\rangle. \quad (1)$$

Here $|\psi(t)\rangle$ is the non-stationary atomic state at time t , H_0 is the Hamiltonian of the field-free (bare) atom, $\mathcal{E}(t)$ is the electric field component of the laser pulse and z is the

projection of the electron–nucleus distance in the field direction. The term $z\mathcal{E}(t)$ describes the atom–field interaction in the dipole approximation using the length gauge. We consider a linearly polarized laser pulse, whose electric field component reads

$$\mathcal{E}(t) = \mathcal{E}_0 g(t) \cos \omega t, \tag{2}$$

where \mathcal{E}_0 is the peak value of the field strength, ω is the laser carrier frequency, and the function $g(t)$ determines the shape of the pulse envelope.

Below, we solve Equation (1), assuming that the atom is initially in its ground state, i.e., $|\psi(t_0)\rangle = |1s\rangle$, where t_0 is a time before the beginning of the interaction. Since the atom interacting with the field (2) has axial symmetry, the z-projection of the electron angular momentum l_z is a constant of motion and the magnetic quantum number m is a good quantum number for any field strength. Thus, the state $|\psi(t)\rangle$ is at any time t characterized by the value $m = 0$, which characterizes the ground state of the bare atom. Unless otherwise stated, atomic units (a.u.) are used throughout the paper.

2.1. The Three-Level Model

In the case of photoionization which goes via resonant or near-resonant excitation of an intermediate state, which here is 2p, the other excited states are nonessential and at weak fields the process can be adequately described within the three-level model. A computational method for solving Equation (1) within this model is presented in our recent paper [16], and in more detail in Ref. [8]. Here, we give only the basic expressions and the final set of relevant equations.

The atomic state at time t within the three-level model reads

$$|\psi(t)\rangle = C_{1s}(t)|1s\rangle + C_{2p}(t)e^{-i\omega t}|2p\rangle + e^{-2i\omega t} \int [C_{\varepsilon s}(t)|\varepsilon s\rangle + C_{\varepsilon d}(t)|\varepsilon d\rangle] d\varepsilon, \tag{3}$$

where $C_{1s}(t)$, $C_{2p}(t)$ and $C_{\varepsilon l}(t)$ are the time-dependent amplitudes for the population of the ground state $|1s\rangle$, intermediate state $|2p\rangle$ and continuum states $|\varepsilon l\rangle$ ($l = 0, 2$), respectively. The variables ε and l label the kinetic energy and orbital momentum of produced photoelectrons. The states $|2p\rangle$ and $|\varepsilon l\rangle$ have been multiplied with the phase factors $e^{-i\omega t}$ and $e^{-2i\omega t}$ in order to simplify the set of equations for the amplitudes.

If we set the ground state energy E_1 to zero, by inserting Equation (3) in the Schrödinger Equation (1) and applying the rotating wave approximation [2] and the local approximation [8,17], we obtain the set of equations for the amplitudes

$$\begin{aligned} i\dot{C}_{1s} &= \frac{1}{2} \Omega_0^* g(t) C_{2p}(t), \\ i\dot{C}_{2p} &= \frac{1}{2} \Omega_0 g(t) C_{1s}(t) + \left[E_2 - \frac{i}{2} \Gamma g^2(t) - \omega \right] C_{2p}(t), \\ i\dot{C}_{\varepsilon} &= \frac{1}{2} \mathcal{E}_0 g(t) C_{2p}(t) + (\varepsilon - \varepsilon_0) \tilde{C}_{\varepsilon}(t), \end{aligned} \tag{4}$$

where $\Omega_0 = D\mathcal{E}_0$ is the frequency of Rabi flopping between the populations of states 1s and 2p at the peak value of laser intensity, $\Gamma = 2\pi|d_{\varepsilon_0}\mathcal{E}_0/2|^2$ is the ionization rate of the intermediate (near-)resonant state 2p and $\tilde{C}_{\varepsilon}(t) = C_{\varepsilon s}(t)/d_{\varepsilon s} \equiv C_{\varepsilon d}(t)/d_{\varepsilon d}$ is the scaled amplitude for the population of continuum states. Here, $D = \langle 2p|z|1s\rangle$ and $d_{\varepsilon l} = \langle \varepsilon l|z|2p\rangle$ are the dipole transition matrix elements for the excitation of the 2p state and for its subsequent ionization, respectively, and $|d_{\varepsilon}|^2 = |d_{\varepsilon s}|^2 + |d_{\varepsilon d}|^2$. For a given carrier frequency of the laser pulse ω , the expected energy of photoelectrons is $\varepsilon_0 = 2\omega - I_p$, where $I_p = 0.5 \text{ a.u.} = 13.606 \text{ eV}$ is the ionization potential of the hydrogen atom. Note that, by taking $E_1 = 0$, the energies of the 2p and final continuum states are $E_2 = 0.375 \text{ a.u.} =$

10.204 eV and $I_p + \varepsilon$, respectively. Finally, let us state that the formal solution of the third of Equation (4) is

$$\tilde{C}_\varepsilon(t) = -\frac{i}{2} \mathcal{E}_0 \int_{-\infty}^t e^{-i(\varepsilon - \varepsilon_0)(t-t')} g(t') C_{2p}(t') dt'. \quad (5)$$

The quantities $|C_{1s}(t)|^2$ and $|C_{2p}(t)|^2$ can be interpreted, respectively, as the populations of atomic states $|1s\rangle$ and $|2p\rangle$ after the interaction of the atom with the laser field until time t . Thus, the populations of these states, after time t_{ex} when we assume that the laser pulse has expired, are $|C_{1s}(t_{\text{ex}})|^2$ and $|C_{2p}(t_{\text{ex}})|^2$. Analogously, the quantities $|C_{\varepsilon l}(t)|^2$ and $|C_{\varepsilon l}(t_{\text{ex}})|^2$ represent the probability densities of finding the atomic electron in the continuum state $|\varepsilon l\rangle$ (here $l = 0, 2$) after the interaction of the atom with the laser field until time t and after the pulse has expired, respectively. Since the photoelectron yield at a given energy ε is proportional to the total probability density of finding the electron in continuum states corresponding to this energy, the PES is adequately represented by the distribution

$$w(\varepsilon) = |C_{\varepsilon s}(t_{\text{ex}})|^2 + |C_{\varepsilon d}(t_{\text{ex}})|^2 = |d_\varepsilon|^2 |\tilde{C}_\varepsilon(t_{\text{ex}})|^2. \quad (6)$$

The values of the dipole matrix elements for transitions from the 1s to the 2p state and from the 2p state to continuum states are determined applying expressions given in Appendix A in Ref. [16]. The matrix element for the transition $1s \rightarrow 2p$ is $D = 0.7449$ a.u., while the values of $|d_\varepsilon|^2$ are shown in Figure 2 in the same reference. The resonant excitation of the 2p state and the subsequent ionization occurs if the laser carrier frequency is $\omega = 0.375$ a.u., which coincides with the transition frequency between the 1s and 2p states (in the weak field limit). The photon energy corresponding to this frequency is 10.204 eV, and the expected kinetic energy of the ejected electrons is $\varepsilon_0 = 0.25$ a.u. = 6.803 eV. In this case, one has $|d_{\varepsilon_0}|^2 = 0.1663$ a.u. [16]. We will see later that the approximate results obtained using the three-level model, in which the exact values for $|d_\varepsilon|^2$ are replaced by the value of $|d_{\varepsilon_0}|^2$, as used in previous studies [8], are sufficient for a qualitative analysis of spectra.

2.2. Results

The populations of atomic states and the photoelectron energy spectra of the hydrogen atom exposed to the laser pulse of carrier frequency $\omega = 0.375$ a.u. have been calculated using the described method for three pulse shapes: (a) the Gaussian shape

$$g(t) = e^{-t^2/\tau^2} \quad (7)$$

with $\tau = 30$ fs, (b) the half-Gaussian shape

$$g(t) = \begin{cases} 0 & \text{for } t < 0, \\ e^{-t^2/\tau^2} & \text{for } t > 0, \end{cases} \quad (8)$$

with $\tau' = 2\tau = 60$ fs, and (c) the rectangular shape

$$g(t) = \begin{cases} 1 & \text{for } |t| < \tau'', \\ 0 & \text{for } |t| > \tau'', \end{cases} \quad (9)$$

with $\tau'' = \tau\sqrt{\pi}/2 = 26.5868$ fs. The parameters τ , τ' and τ'' are chosen so that for a given value of \mathcal{E}_0 all three pulses have the same value of the pulse area [7]

$$\theta = \Omega_0 \int_{-\infty}^{+\infty} g(t) dt, \quad (10)$$

which here is $\theta = \sqrt{\pi} \Omega_0 \tau = \sqrt{\pi} \Omega_0 \tau' / 2 = 2 \Omega_0 \tau''$. For times when the pulses (7)–(9) expire, we take $t_{\text{ex}} = 3\tau$, $t'_{\text{ex}} = 3\tau'$ and $t''_{\text{ex}} = \tau''$, respectively. Let us state at this point that,

referring to the area theorem [7,11], the number of Rabi cycles completed during the pulse is $N = \theta / (2\pi)$.

Figure 1 shows the evolution of the populations of states 1s and 2p, calculated for pulses of the above three shapes and peak intensity $I_0 = 1 \text{ TW/cm}^2$ ($I_0 = \mathcal{E}_0^2 / (8\pi\alpha)$, $\alpha = 1/137$) for which the pulse area is $\theta = 8.741$ and $N \approx 1.4$. One can see that, although the evolution is different, in accordance with the area theorem [11] the final populations for all three pulses (after they have expired) take the same values.

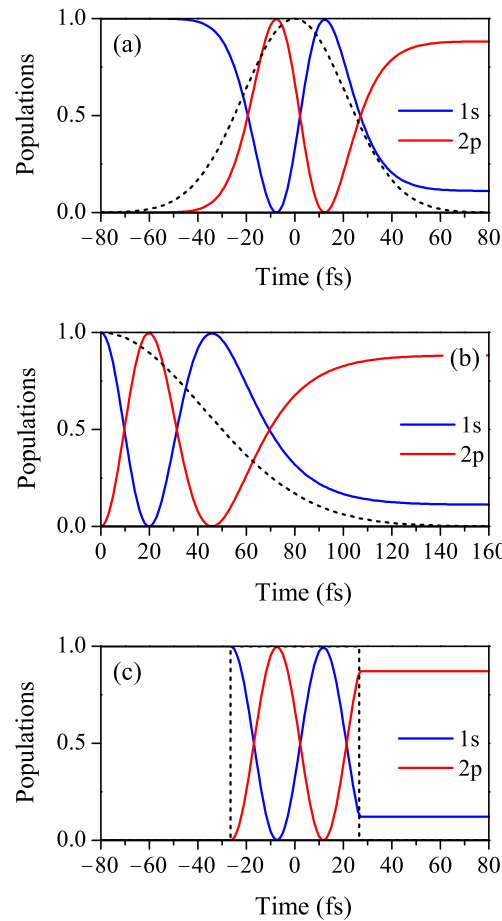


Figure 1. (Color online) The evolution of populations of the ground state (1s) and the excited 2p state during the process of resonant two-photon ionization of hydrogen by: (a) Gaussian laser pulse (7) with $\tau = 30 \text{ fs}$, (b) half-Gaussian pulse (8) with $\tau' = 60 \text{ fs}$ and (c) rectangular pulse (9) with $\tau'' = 26.5868 \text{ fs}$, all of carrier frequency $\omega = 0.375 \text{ a.u.} = 10.203 \text{ eV}$, which is resonant for transition $1s \rightarrow 2p$ and peak intensity of 1 TW/cm^2 . The dashed lines represent the envelopes of the laser pulses. The parameters τ , τ' and τ'' are chosen so that all three pulses have the same value of the pulse area $\theta = 8.741$, for which the populations perform approximately 1.4 Rabi cycles.

Figure 2 shows the final populations of the states 1s and 2p as functions of I_0 in the domain of $10^9\text{--}10^{13} \text{ W/cm}^2$. Again, in agreement with the area theorem, for each peak intensity the final populations of atomic states for the considered three pulses have the same values. Due to this fact, the blue and red lines in Figure 2 represent the populations of the ground and excited states, respectively, obtained for all three pulse shapes. The vertical dashed lines indicate the peak intensities at which an integer number of Rabi cycles during the pulse is completed: $I_0(N) = 0.517, 2.067, 4.650, 8.267, 12.917 \text{ TW/cm}^2$ for $N = 1, 2, 3, 4, 5$, respectively.

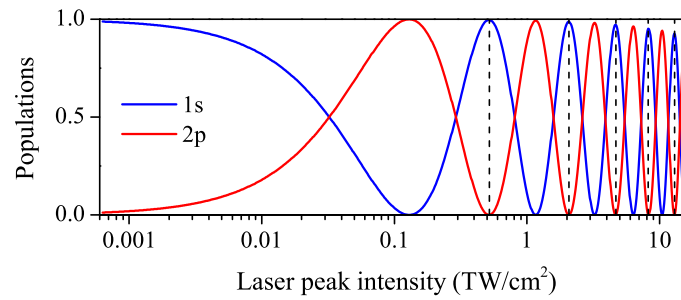


Figure 2. (Color online) Final populations of the ground state (1s) and the excited 2p state of hydrogen at the end of the process of its resonant two-photon ionization, as functions of the laser peak intensity. The results obtained using the Gaussian, half-Gaussian and rectangular pulses (Equations (7)–(9)) of carrier frequency $\omega = 0.375$ a.u. with $\tau = 30$ fs, $\tau' = 60$ fs and $\tau'' = 26.5868$ fs practically coincide and they are represented by common lines. The vertical dashed lines indicate the peak intensities at which an integer number of Rabi cycles during the pulse is completed.

Figure 3 shows the photoelectron energy spectra determined by solving the set of Equation (4) and applying Equation (6) with exact $|d_\epsilon|^2$ values (solid red lines) and with $|d_\epsilon|^2 \approx |d_{\epsilon_0}|^2$ (dashed lines) for: (a) Gaussian pulse (7), (b) half-Gaussian pulse (8) and (c) rectangular pulse (9), with the peak intensities $I_0(N)$, $N = 1, \dots, 5$. Note that the spectra obtained using the approximate value $|d_{\epsilon_0}|^2$ are symmetric, but this is not the case when the exact values for $|d_\epsilon|^2$ are used. The observed asymmetry, which is more pronounced at higher laser field intensities, has recently been studied in several publications [9,16,18]. For each value of I_0 , the PES consist of a pattern exhibiting the AT splitting. The separation between the most prominent edge peaks (AT doublet) increases with the square root of I_0 , i.e., linearly with the peak value of electric field strength. In addition, for the laser peak intensities when more than two Rabi cycles during the pulse are completed, our results confirm the previously reported appearance of a multiple-peak pattern in the calculated PES [7–10].

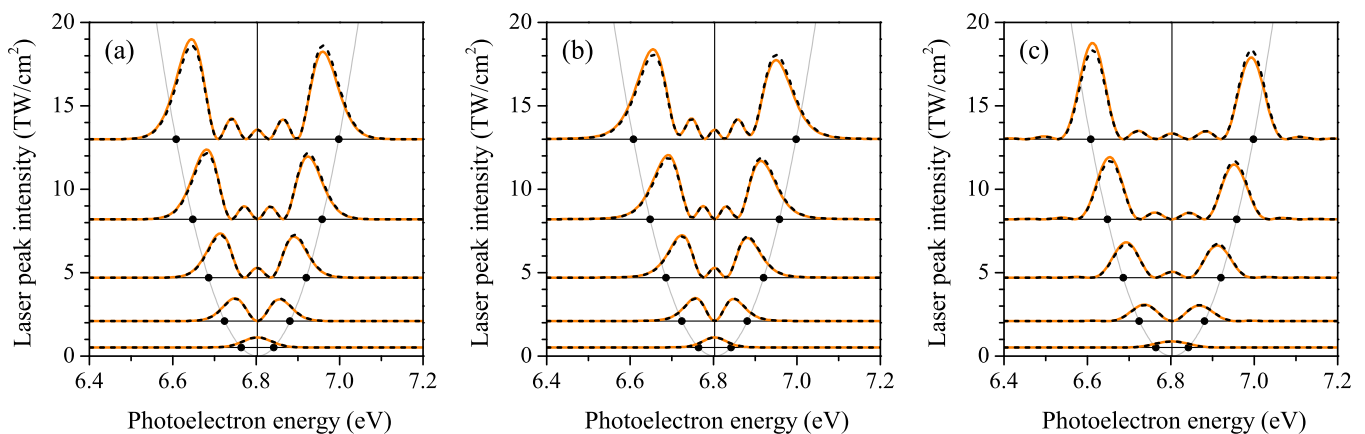


Figure 3. (Color online) Photoelectron energy spectra calculated using the three-level model (Equations (4)–(6)) with exact values of $|d_\epsilon|^2$ (solid orange lines) and with the approximation $|d_\epsilon|^2 \approx |d_{\epsilon_0}|^2$ (dashed lines) for: (a) Gaussian pulse (7), (b) half-Gaussian pulse (8) and (c) rectangular pulse (9), all of carrier frequency $\omega = 0.375$ a.u. and the peak intensities marked in Figure 2 by vertical dashed lines. Black dots mark the real parts of $E_\pm(0) + \epsilon_0$, whose separation ($\approx \Omega_0$) estimates the splitting of the resonant peak.

Demekhin and Cederbaum [8] analyzed the multiple-peak patterns in the PES obtained for the photoionization with the Gaussian pulse. They attributed the appearance of modulations inside the AT doublets to the dynamic interference of two photoelectron waves with the same kinetic energy emitted at two different times during the pulse—at

the time when the pulse is growing and at the time when it decreases. Our calculations, however, show that similar modulations also exist in the case of photoionization with the half-Gaussian pulse, that has no growing part, as well as at the photoionization with the rectangular pulse, whose intensity is constant. Thus, we conclude that the dynamic interference cannot be the principal reason for the modulations in the calculated spectra. This conclusion is supported by the analysis of the conditions for dynamic interference [14,15], where it was found that they are not fulfilled in the case of resonant photoionization via the 2p state (see Figure 3c in Ref. [14]).

3. Analysis of the AT Patterns in Terms of Dressed States

3.1. Dynamics of the Ground and Intermediate States

As the amplitude $\tilde{C}_\varepsilon(t)$ does not appear in the first two of Equation (4), the dynamics of the 1s and 2p states within the three-level model is formally decoupled from the dynamics of continuum states. The equations for these two states can be written in the matrix form

$$i \frac{d}{dt} \begin{pmatrix} C_{1s}(t) \\ C_{2p}(t) \end{pmatrix} = \begin{pmatrix} 0 & \frac{1}{2} \Omega_0^* g(t) \\ \frac{1}{2} \Omega_0 g(t) & -\frac{i}{2} \Gamma g^2(t) \end{pmatrix} \begin{pmatrix} C_{1s}(t) \\ C_{2p}(t) \end{pmatrix}. \quad (11)$$

This matrix equation represents the time-dependent Schrödinger equation that describes the resonantly coupled dynamics of the 1s and 2p states in the basis of the same states in the interaction picture [19]. Using Dirac's formalism, this equation reads

$$i \frac{d}{dt} |\psi_b(t)\rangle = \mathcal{H} |\psi_b(t)\rangle, \quad (12)$$

where $|\psi_b(t)\rangle = e^{iH_0 t} [C_{1s}(t)|1s\rangle + C_{2p}(t)e^{-i\omega t}|2p\rangle] = C_{1s}(t)|1s\rangle + C_{2p}(t)|2p\rangle$ is the bound part of the state (3) in the interaction picture and \mathcal{H} is the interaction Hamiltonian, whose representations in the actual basis are

$$|\psi_b(t)\rangle \rightarrow \begin{pmatrix} C_{1s}(t) \\ C_{2p}(t) \end{pmatrix}, \quad (13)$$

$$\mathcal{H} \rightarrow \begin{pmatrix} 0 & \frac{1}{2} \Omega_0^* g(t) \\ \frac{1}{2} \Omega_0 g(t) & -\frac{i}{2} \Gamma g^2(t) \end{pmatrix}. \quad (14)$$

Since the interaction picture hides the time dependence related to the unperturbed Hamiltonian H_0 , the amplitudes $C_{1s}(t)$, $C_{2p}(t)$ and the Hamiltonian \mathcal{H} are slowly varying quantities. By diagonalizing this Hamiltonian, one obtains two slowly varying complex eigenenergies (quasi-energies)

$$E_\pm(t) = \pm \frac{1}{2} \sqrt{\Omega_0^2 g^2(t) - \Gamma^2 g^4(t)/4} - \frac{i}{4} \Gamma g^2(t) \approx \pm \frac{1}{2} \Omega_0 g(t) - \frac{i}{4} \Gamma g^2(t), \quad (15)$$

which correspond to dressed states

$$|\pm\rangle \approx \frac{1}{\sqrt{2}} (|1s\rangle \pm |2p\rangle). \quad (16)$$

The approximate expressions are applicable if $\Omega_0 \gg \Gamma g(t)$, which is fulfilled if the pulses are not of excessive intensity. Using inverse relations $|1s\rangle = (|+\rangle + |-\rangle)/\sqrt{2}$, $|2p\rangle = (|+\rangle - |-\rangle)/\sqrt{2}$, the state $|\psi_b(t)\rangle$ can be written in the form

$$|\psi_b(t)\rangle = C_+(t)|+\rangle + C_-(t)|-\rangle, \quad (17)$$

where

$$C_\pm(t) = \frac{1}{\sqrt{2}} [C_{1s}(t) \pm C_{2p}(t)]. \quad (18)$$

Note that, due to the presence of an imaginary part in E_{\pm} , the dressed states $|\pm\rangle$ are decaying, i.e., they are two decoupled resonances. The real parts of the quasi-energies move adiabatically apart as the pulse arrives, and towards each other as the pulse expires. More precisely, according to Equation (15), their distance evolves as $E_+(t) - E_-(t) \approx \Omega_0 g(t)$.

3.2. Dynamics of Continuum States

By inserting Equation (17) into Equation (12) and applying the eigenvalue problem $\mathcal{H}|\pm\rangle = E_{\pm}|\pm\rangle$, one obtains equation $i\dot{C}_{\pm} = E_{\pm}(t)C_{\pm}(t)$, which can be solved analytically. Employing the initial conditions $C_{\pm}(-\infty) = 1/\sqrt{2}$, we find

$$C_{\pm}(t) = \frac{1}{\sqrt{2}} e^{-i \int_{-\infty}^t E_{\pm}(t') dt'} = \frac{1}{\sqrt{2}} e^{\mp i \Omega_0 \mathcal{J}_1(t)/2} e^{-\Gamma \mathcal{J}_2(t)/4}, \tag{19}$$

where $\mathcal{J}_n(t) = \int_{-\infty}^t g^n(t') dt'$.

From Equation (18), it follows that $C_{2p}(t) = [C_+(t) - C_-(t)]/\sqrt{2}$, which by substitution in Equation (5) gives

$$\tilde{C}_{\varepsilon}(t) = -\frac{i}{2\sqrt{2}} \mathcal{E}_0 \int_{-\infty}^t e^{-i(\varepsilon-\varepsilon_0)(t-t')} g(t') [C_+(t') - C_-(t')] dt'. \tag{20}$$

Finally, using Equation (6), we obtain

$$\begin{aligned} w(\varepsilon) &= \frac{|d_{\varepsilon}|^2 \mathcal{E}_0^2}{8} \left| \int_{-\infty}^{+\infty} e^{i(\varepsilon-\varepsilon_0)t} g(t) [C_+(t) - C_-(t)] dt \right|^2 \\ &= \left| \frac{d_{\varepsilon} \mathcal{E}_0}{4} \int_{-\infty}^{+\infty} g(t) e^{-\Gamma \mathcal{J}_2(t)/4} [e^{i\phi_+(t)} - e^{i\phi_-(t)}] dt \right|^2, \end{aligned} \tag{21}$$

where $\phi_{\pm}(t) = (\varepsilon - \varepsilon_0)t \mp \Omega_0 \mathcal{J}_1(t)/2$ are the phases of two oscillatory functions in the integrand. This formula gives exactly the same results as Equations (4)–(6), some of them shown in Figure 3, but it provides a deeper insight into the multiple peak structure of the PES.

The AT splitting of the resonant peak in the PES can be roughly estimated from the maximum distance between quasi-energies (15)

$$\Delta_{AT} \equiv \varepsilon_+ - \varepsilon_- \sim E_+(0) - E_-(0) \approx \Omega_0 g_0, \tag{22}$$

where ε_{\pm} are the positions of the AT doublet peaks in the PES and $g_0 \equiv g(0)$ is the maximum value of the envelope $g(t)$ (usually $g_0 = 1$).

Figure 4 shows the time evolution of the photoelectron energy distribution, represented by $|\tilde{C}_{\varepsilon}(t)|^2$ using Equation (20), during the photoionization process of the hydrogen atom by: (a) Gaussian pulse (7), (b) half-Gaussian pulse (8) and (c) rectangular pulse (9), all of them having the carrier frequency of 0.375 a.u. and the peak intensity of 12.917 TW/cm², which leads to five Rabi cycles completed at the end of the pulse ($N = 5$). In all three cases, the number of Rabi cycles performed up to a given instant of time coincides with the number of peaks in the energy distribution at that instant. Thus, the mechanism of formation of a structure with multiple peaks is the same regardless of the shape of the pulse and, therefore, it cannot be dynamic interference of two photoelectron waves emitted during the rising and falling part of the pulse. The appearance of a multiple-peak pattern in the case of rectangular pulse, where an analytical solution is possible, is analyzed in the next subsection.

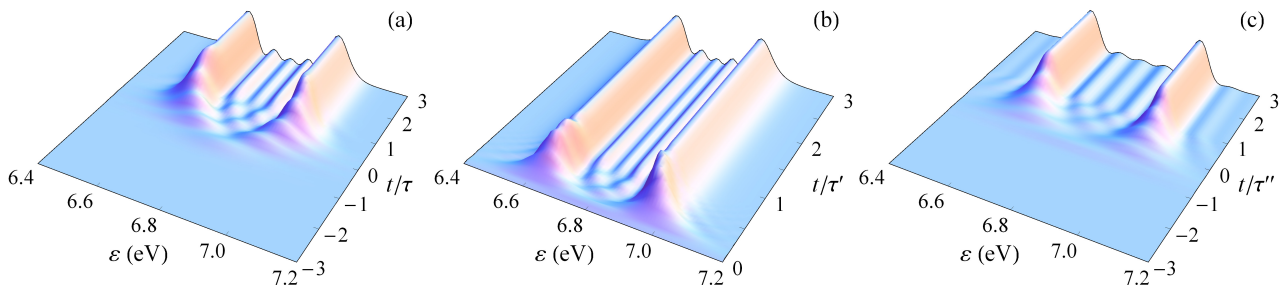


Figure 4. (Color online) Time evolution of the photoelectron energy distribution (in arbitrary units) during the photoionization process of the hydrogen atom by: (a) Gaussian pulse (7), (b) half-Gaussian pulse (8) and (c) rectangular pulse (9) of carrier frequency $\omega = 0.375$ a.u. and peak intensity of 12.917 TW/cm^2 at which the atom completes five Rabi cycles during the pulse.

3.3. Analytical Solution for Rectangular Pulse

The limits of the integral in Equation (21) for the rectangular pulse (9) are reduced to interval $[-\tau'', +\tau'']$, in which $\mathcal{J}_n(t) = \tau'' + t$ and $\phi_{\pm}(t) = (\varepsilon - \varepsilon_0 \mp \Omega_0/2)t \mp \Omega_0\tau''/2$, so that this integral can be solved analytically. Furthermore, since the ionization rate for the laser peak intensities considered here (up to 13 TW/cm^2) is small ($\Gamma < 10^{-4}$ a.u.), it can be neglected and the expression for energy distribution of photoelectrons to a good approximation becomes

$$w(\varepsilon) = \left| \frac{d\varepsilon_0 \mathcal{E}_0}{2} \left(e^{-i\Omega_0\tau''/2} \frac{\sin \delta_+ \tau''}{\delta_+} - e^{i\Omega_0\tau''/2} \frac{\sin \delta_- \tau''}{\delta_-} \right) \right|^2, \quad (23)$$

where $\delta_{\pm} = \varepsilon - \varepsilon_0 \mp \Omega_0/2$. The positions of the two main peaks of this distribution are very close to the positions of the main peaks of partial distributions

$$w_{\pm}(\varepsilon) = \left| \frac{d\varepsilon_0 \mathcal{E}_0}{2} \right|^2 \left(\frac{\sin \delta_{\pm} \tau''}{\delta_{\pm}} \right)^2, \quad (24)$$

whose values are $\varepsilon_{\pm} = \varepsilon_0 \pm \Omega_0/2$. Since the zeros of functions $\sin(\delta_{\pm} \tau'')/\delta_{\pm}$ are $\delta_{\pm} = k\pi/\tau''$, where k are integers, and in agreement with the area theorem $\tau'' = N\pi/\Omega_0$, where N is the number of Rabi cycles during the pulse, the separation of two adjacent zeros is $\Delta\varepsilon = \pi/\tau'' = \Omega_0/N$. Thus, in the interval $(\varepsilon_-, \varepsilon_+)$, whose length here is $\Delta_{AT} = \Omega_0$, there are exactly $N - 1$ zeros and N peaks (see Figure 5 for $N = 5$). The latter explains the coincidence between the number of Rabi cycles during the pulse and the number of peaks in the AT pattern in PES. Obviously, local peaks in distribution (23) also exist in partial distributions (24), i.e., they are not a product of dynamic interference.

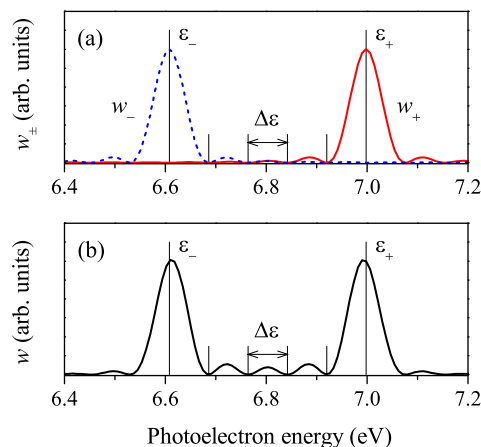


Figure 5. (Color online) (a) Partial distributions $w_{\pm}(\varepsilon)$ and (b) total distribution $w(\varepsilon)$ given by Equations (23) and (24), respectively, for the rectangular laser pulse with $N = \theta/(2\pi) = 5$.

4. Summary and Conclusions

In this paper, we studied the Rabi flopping of the population between the ground (1s) and excited 2p states of the hydrogen atom, induced by intense short laser pulses of different shapes and of carrier frequency $\omega = 0.375$ a.u., which resonantly couples these states, and manifestations of these dynamics in the energy spectra of photoelectrons produced in the subsequent ionization of the atom from its periodically populated/depopulated 2p state. Manifestations of the Rabi dynamics in the spectra are the AT splitting and multiple-peak structure of the AT pattern. The populations of states and spectra were calculated for three different pulse shapes—Gaussian, half-Gaussian and rectangular ones, whose pulse durations were tuned so that, for a given laser peak intensity, their pulse areas have the same value. It was found that, for these pulses, in accordance with the area theorem, the final populations (once the pulses have expired) are the same, and the spectra have similar forms in that they consist of AT patterns with the same number of peaks and with approximately the same separation between the prominent edge (AT) peaks. These facts essentially disprove the assumption that the multiple-peak pattern appears due to dynamic interference of the photoelectrons emitted with the same energy, but with a time delay at the rising and falling sides of the pulse [8,12,13], for the simple reason that a half-Gaussian pulse has no rising part, while the intensity of a rectangular pulse is constant. This conclusion is in agreement with the analysis of the conditions for dynamic interference [14,15], where it was found that they are not fulfilled in the case of resonant photoionization via the 2p state.

The additional analysis in terms of dressed states provided deeper insight into the structure of obtained spectra. This approach implies that the ionization occurs via dressed states, which directly explains the appearance of AT doublets in the PES. Here, the formula for the energy distribution of photoelectrons has the form of the time integral of the sum of two terms with different phase factors corresponding to two dressed states. In the case of rectangular pulse, this integral is analytically solvable and is reduced to the sum of two contributions that have the forms of sinc functions of energy, shifted by the value of the corresponding Rabi frequency. Then, the multiple-peak pattern is simply the result of their overlapping, which explains the matching of the number of completed Rabi oscillations with the number of peaks in the AT pattern. Analysis of the time evolution of the photoelectron energy distribution during the photoionization process showed that the mechanism of formation of multiple-peak structures is the same regardless of the pulse shape and is, therefore, not related to dynamic interference.

Author Contributions: Conceptualization, N.S.S.; methodology, N.S.S.; software, N.S.S. and A.B.; formal analysis, N.S.S., D.B.P. and A.B.; investigation, N.S.S. and D.B.P.; writing—original draft preparation, N.S.S.; writing—review and editing, N.S.S., D.B.P. and A.B. All authors have read and agreed to the published version of the manuscript.

Funding: This research received no external funding.

Data Availability Statement: All the data reported in this work are available from the correspondence author on reasonable request.

Acknowledgments: This work was supported by the COST Action No. CM18222 (AttoChem).

Conflicts of Interest: The authors declare no conflict of interest.

Abbreviations

The following abbreviations are used in this manuscript:

XUV	extreme ultraviolet
AT	Autler–Townes
PES	photoelectron energy spectrum

References

1. Rabi, I.I. Space Quantization in a Gyating Magnetic Field. *Phys. Rev.* **1937**, *51*, 652. [[CrossRef](#)]
2. Steck, D.A. Quantum and Atom Optics. Revision 0.13.4. Available online: <http://steck.us/teaching> (accessed on 24 September 2020).
3. Autler, S.H.; Townes, C.H. Stark Effect in Rapidly Varying Fields. *Phys. Rev.* **1955**, *100*, 703. [[CrossRef](#)]
4. LaGattuta, K.J. Above-threshold ionization of atomic hydrogen via resonant intermediate states. *Phys. Rev. A* **1993**, *47*, 1560–1563. [[CrossRef](#)] [[PubMed](#)]
5. Girju, M.G.; Hristov, K.; Kidun, O.; Bauer, D. Nonperturbative resonant strong field ionization of atomic hydrogen. *J. Phys. B* **2007**, *40*, 4165. [[CrossRef](#)]
6. Nandi, S.; Olofsson, E.; Bertolino, M.; Carlström, S.; Zapata, F.; Busto, D.; Callegari, C.; Di Fraia, M.; Eng-Johnsson, P.; Feifel, R.; et al. Observation of Rabi dynamics with a short-wavelength free-electron laser. *Nature* **2022**, *608*, 488. [[CrossRef](#)] [[PubMed](#)]
7. Rogus, D.; Lewenstein, M. Resonant ionisation by smooth laser pulses. *J. Phys. B* **1986**, *19*, 3051–3059. [[CrossRef](#)]
8. Demekhin, P.V.; Cederbaum, P.V. Coherent intense resonant laser pulses lead to interference in the time domain seen in the spectrum of the emitted particles. *Phys. Rev. A* **2012**, *86*, 063412. [[CrossRef](#)]
9. Müller, A.D.; Kutscher, E.; Artemyev, A.N.; Cederbaum, L.S.; Demekhin, P.V. Dynamic interference in the resonance-enhanced multiphoton ionization of hydrogen atoms by short and intense laser pulses. *Chem. Phys.* **2018**, *509*, 145. [[CrossRef](#)]
10. Tóth, A.; Csehi, A. Probing strong-field two-photon transitions through dynamic interference. *J. Phys. B At. Mol. Opt. Phys.* **2021**, *54*, 035005. [[CrossRef](#)]
11. Fischer, K.A.; Hanschke, L.; Kremser, M.; Finley, J.J.; Müller, K.; Vučković, J. Pulsed Rabi oscillations in quantum two-level systems: Beyond the area theorem. *Quantum Sci. Technol.* **2018**, *3*, 014006. [[CrossRef](#)]
12. Demekhin, P.V.; Cederbaum, L.S. Dynamic Interference of Photoelectrons Produced by High-Frequency Laser Pulses. *Phys. Rev. Lett.* **2012**, *108*, 253001. [[CrossRef](#)] [[PubMed](#)]
13. Demekhin, P.V.; Cederbaum, L.S. ac Stark effect in the electronic continuum and its impact on the photoionization of atoms by coherent intense short high-frequency laser pulses. *Phys. Rev. A* **2013**, *88*, 043414. [[CrossRef](#)]
14. Bagheri, M.; Saalman, U.; Rost, J.M. Essential Conditions for Dynamic Interference. *Phys. Rev. Lett.* **2017**, *118*, 143202. [[CrossRef](#)] [[PubMed](#)]
15. Jiang, W.C.; Burgdörfer, J. Dynamic interference as signature of atomic stabilization. *J. Opt. Express* **2018**, *26*, 19921. [[CrossRef](#)] [[PubMed](#)]
16. Bunjac, A.; Popović, D.B.; Simonović, N.S. Analysis of the asymmetry of Autler-Townes doublets in the energy spectra of photoelectrons produced at two-photon ionization of atoms by strong laser pulses. *Eur. Phys. J. D* **2022**, *76*, 249. [[CrossRef](#)]
17. Demekhin, P.V.; Cederbaum, L.S. Strong interference effects in the resonant Auger decay of atoms induced by intense X-ray fields. *Phys. Rev. A* **2011**, *83*, 023422. [[CrossRef](#)]
18. Zhang, X.; Zhou, Y.; Liao, Y.; Chen, Y.; Liang, J.; Ke, Q.; Li, M.; Csehi, A.; Lu, P. Effect of nonresonant states in near-resonant two-photon ionization of hydrogen. *Phys. Rev. A* **2022**, *106*, 063114. [[CrossRef](#)]
19. Meystre, P.; Sargent, M., III. *Elements of Quantum Optics*, 4th ed.; Springer: Berlin, Germany, 2007.

Disclaimer/Publisher's Note: The statements, opinions and data contained in all publications are solely those of the individual author(s) and contributor(s) and not of MDPI and/or the editor(s). MDPI and/or the editor(s) disclaim responsibility for any injury to people or property resulting from any ideas, methods, instructions or products referred to in the content.

STRONG FIELD MULTIPHOTON IONIZATION OF LITHIUM

A. Bunjac, D. B. Popović and N. S. Simonović

*Institute of Physics, University of Belgrade, P.O. Box 57, 11001 Belgrade,
Serbia*

Abstract. Multiphoton ionization of lithium by 30 fs laser pulses of 785 nm wavelength is studied using a single-electron model where the valence electron moves in an effective core potential and in the external electromagnetic field. The photoelectron momentum distributions and energy spectra are calculated for several field strengths by numerically solving the time-dependent Schrödinger equation. Besides the nonresonant multiphoton ionization, which is the dominating process, structures related to the above threshold ionization are observed in the spectra. The present results are in good agreement with recent experimental and theoretical results.

1. THEORETICAL MODEL

The study of multiphoton ionization (MPI) of atoms, which has a much lower probability than the corresponding single-photon process, became experimentally accessible in last decades after appearance of a new generation of high intensity lasers. The MPI manifests itself as nonresonant multiphoton ionization (NRMPI), above threshold ionization (ATI) and resonantly enhanced multiphoton ionization (REMPI). The theoretical study of such strong field processes exclude any perturbative treatment, that is a valid approach in describing the single-photon ionization. Here we study the MPI of the lithium atom in strong laser fields using a single-electron approximation and solving numerically the time-dependent Schrödinger equation. The calculated photoelectron momentum distributions and energy spectra are compared with recently published experimental and theoretical results [1].

Within the single-electron model and the frozen core approximation the dynamics of the valence (active) electron of lithium atom in an alternating electric field $F(t)$ is described by Hamiltonian (in atomic units)

$$H = \frac{\mathbf{p}^2}{2} + V_{\text{core}}(r) - F(t)z. \quad (1)$$

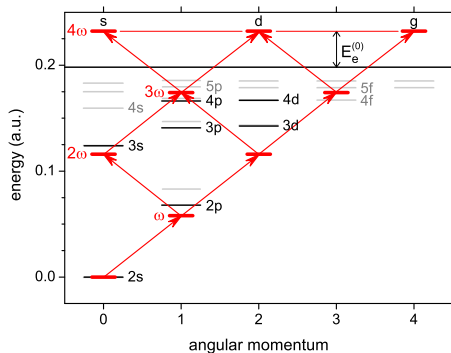


Figure 1. Energy scheme of lithium showing the lowest excited states (black lines - experimental values, gray lines - eigenenergies of pseudopotential (2)) and possible four-photon absorption pathways from the ground state to continuum in the case of laser of 785 nm wavelength ($\omega = 0.05804$ a.u.).

The effective core potential $V_{\text{core}}(r)$ describes the interaction of the valence electron with the atomic core (inner electrons + atomic nucleus). For this purpose we use the Hellmann's pseudopotential [2]

$$V_{\text{core}}(r) = -\frac{1}{r} + \frac{A}{r} e^{-ar}. \quad (2)$$

The parameters $A = 34$ and $a = 3.14331$ [3] provide the correct value for the ionization potential of lithium $I_p = 5.3917$ eV = 0.19814 a.u. and reproduce approximately the energies of singly-excited states (see Fig. 1). Unfortunately, for lithium it is not possible to find a set of parameters providing sufficiently good agreement with experimental values for s and p states simultaneously. In this case the parameters are chosen to get the best agreement for s states.

We consider a linearly polarized laser pulse of the form

$$F(t) = F_{\text{peak}} \sin^2(\pi t/T_p) \cos(\omega t), \quad 0 < t < T_p \quad (3)$$

(otherwise $F(t) = 0$). Here ω , F_{peak} and T_p are the frequency of laser field, the peak value of its electric component and the pulse duration, respectively. Due to the axial symmetry of the system, the magnetic quantum number m of the valence electron is a good quantum number for all values of F (in contrast to the orbital quantum number l). Since the ground state of the field-free lithium atom is characterized by $l = m = 0$, we set $m = 0$ also for $F \neq 0$.

The photoionization process is simulated by calculating the evolution of the wave function of valence electron $\psi(\mathbf{r}, t)$, which is initially ($t = 0$) chosen to be the lowest eigenstate of Hamiltonian (1) (then $F = 0$) that describes the lithium ground state. The evolution is calculated by numerically

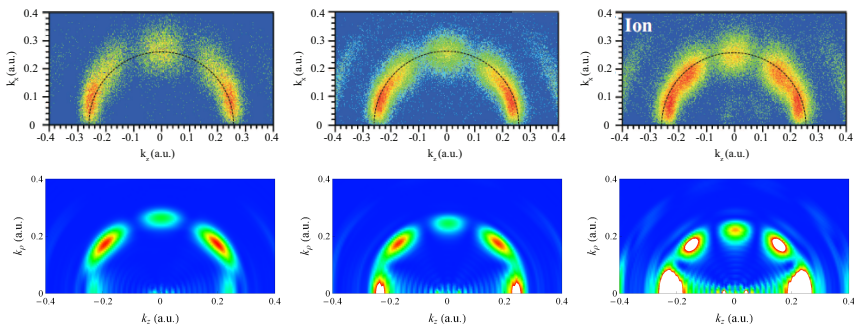


Figure 2. Photoelectron momentum distribution parallel (longitudinal) and transversal (perpendicular) to the polarization direction of 785 nm wavelength laser with 30 fs pulse duration and three different intensities (left: $I = 8 \times 10^{11} \text{ W/cm}^2$, middle: $I = 2 \times 10^{12} \text{ W/cm}^2$, right: $I = 4 \times 10^{12} \text{ W/cm}^2$). Top: experimental data obtained by recoil-ion momentum detection [1]. Bottom: calculated distribution $|\bar{\psi}(\mathbf{k}, t)|^2$ at $t = 1500 \text{ a.u.}$ Dashed semicircle denotes the nominal position of the four-photon line.

integrating the time-dependent Schrödinger equation [4]. The photoelectron momentum distribution (PMD) is obtained from the Fourier transform of the wave function at $t > T_p$ ($\text{PMD} \sim |\bar{\psi}(\mathbf{k}, t)|^2$).

2. RESULTS

Using the described model we study the photoionization of the lithium atom by a 785 nm ($\omega = 0.05804 \text{ a.u.}$, $\hbar\omega = 1.5794 \text{ eV}$) laser pulse of the form (3) with three values of the peak intensities and 30 fs duration ($T_p = 1240 \text{ a.u.}$) and compare our numerical results with recent experimental and numerical results obtained by Schuricke *at al* [1]. The energy level diagram (Fig. 1) illustrates that from the ground state (2s) at least four photons of energy 1.5794 eV are required to reach the continuum. In the low-intensity regime the NRMPI is the dominating process and the expected excess energy of the photoelectrons is $E_e^{(0)} = 0.03403 \text{ a.u.}$ (0.926 eV).

Fig. 2 shows the experimental (top) and calculated (bottom) momentum distributions for three values of the laser field strength. The nodal structure of the observed distributions can be related to superpositions of the accessible emitted partial waves. In the case of four-photon absorption s, d and g partial waves can be emitted (see Fig. 1). Both the experimental and calculated distribution indicate that the d partial wave (two nodes) is dominant at lower laser intensities, whereas the g partial wave is dominant (four nodes) at higher intensities. As expected, the distribution maxima are approximately located at semicircles of radius $k_e^{(0)} = (2E_e^{(0)})^{1/2} = 0.2609 \text{ a.u.}$

Besides NRMPI, already for the lowest intensity considered here, the ATI, i.e. five-photon absorption, can be identified at the radius $k_e^{(0)'} =$

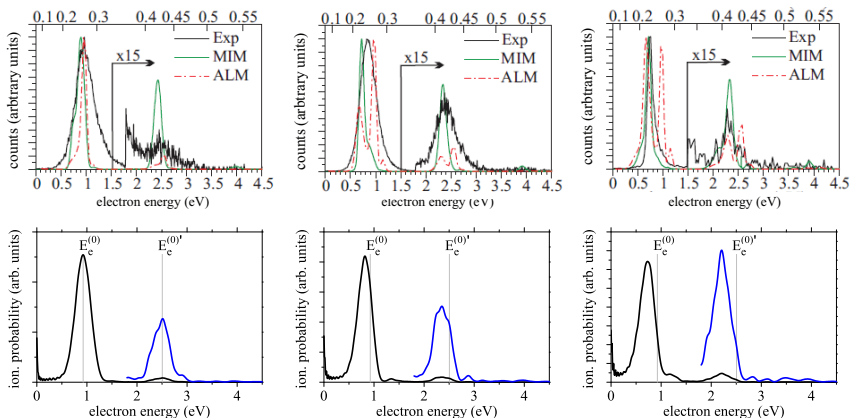


Figure 3. Photoelectron energy spectra extracted from the experimental and theoretical momentum data shown in Fig. 2 (left: $I = 8 \times 10^{11} \text{ W/cm}^2$, middle: $I = 2 \times 10^{12} \text{ W/cm}^2$, right: $I = 4 \times 10^{12} \text{ W/cm}^2$). Top: Results by Schuricke *et al* [1]. Bottom: Present calculations. The count rates and probabilities for energies $E > 0.18 \text{ eV}$ are multiplied by 15.

$(2E_e^{(0)})^{1/2} = 0.4291 \text{ a.u.}$ ($E_e^{(0)'} = E_e^{(0)} + \hbar\omega = 2.5054 \text{ eV}$). In this case p, f and h partial waves can be emitted. The corresponding ATI semicircle contains five nodes which is a feature of h waves.

The photoelectron energy spectrum is obtained by averaging the probability distribution $|\bar{\psi}(\mathbf{k}, t)|^2$ at a time $t > T_p$ along semicircles $k_\rho^2 + k_z^2 = 2E_e$ corresponding to different photoelectron excess energies E_e . The spectra at three values of the field strength, with clearly visible NRMPI and the first ATI peaks, are shown in Fig. 3. The difference between the NRMPI and ATI peak positions and $E_e^{(0)}$ and $E_e^{(0)'}$ values, respectively, can be attributed to the dynamic Stark shift.

Acknowledgements

This work was supported by the COST Action No. CM1204 (XLIC). We acknowledge support from the Ministry of Education, Science and Technological Development of Republic of Serbia under Project No. 171020.

REFERENCES

- [1] M. Schuricke et al, Phys. Rev. A **83**, 023413 (2011).
- [2] H. Hellmann, J. Chem. Phys. **3**, 61 (1935).
- [3] M. Z. Milošević and N. S. Simonović, Phys. Rev. A **91**, 023424 (2015).
- [4] A. Bunjac, D. B. Popović and N. S. Simonović, Phys. Chem. Chem. Phys. **19**, 19829 (2017).

Dynamic Stark shift and multiphoton ionization of sodium by femtosecond laser pulses

A. Bunjac¹, D. B. Popović¹ and N. S. Simonović¹

¹*Institute of Physics, University of Belgrade, Serbia*

e-mail: bunjac@ipb.ac.rs

We study the excitation and multiphoton ionization of sodium induced by strong femtosecond laser pulses [1,2]. The resonant dynamic Stark shift (RDSS) of energy levels and momentum distributions of photoelectrons are determined, both using a wave-packet propagation method. This method is used to determine an RDSS data set for transitions $3s \rightarrow nl$ ($n \leq 6$) in sodium induced by the laser pulse with the peak intensities up to 7.9×10^{12} W/cm² and wavelengths in the range from 455.6 to 1139 nm. The data is applied to analyze the photoelectron spectra (electron yield versus excess energy) of the sodium atom interacting with an 800 nm laser radiation. The momentum distributions of photoelectrons are determined from the calculated electrons' outgoing wave by applying a Fourier transform, and energy spectra are extracted from them. Substructures observed in the recent experimentally measured spectra [3] are successfully reproduced and related to the resonantly enhanced multiphoton ionization (REMPI) via specific (P and F) intermediate states.

REFERENCES

- [1] N. B. Delone, V. P. Krainov, *Multiphoton Processes in Atoms*, Springer (2000).
- [2] C. J. Joachain, N. J. Kylstra, R. M. Potvliege, *Atoms in Intense Laser Fields*, CUP, (2012).
- [3] N. A. Hart et al., Phys. Rev. A 93, 063426 (2016).

Multiphoton ionization of sodium by intense femtosecond laser pulses in the near IR domain

Andrej Bunjac¹, Duška B. Popović¹, Nenad S. Simonović¹

(1) *Institute of physics, University of Belgrade, Pregrevica 118, 11080 Belgrade, Serbia*

Contact: D.B.Popović (duska@ipb.ac.rs)

Abstract. The multiphoton ionization of sodium by the laser pulses of 800 nm wavelength and 57 fs FWHM is studied for laser peak intensities in the range of a few TW/cm². Photoelectron momentum distributions and the energy spectra are determined numerically by solving the time dependent Schrödinger equation. The calculated spectra agree well with the spectra obtained experimentally by Hart et al. [1]. It is shown that the spectral peaks related to the Freeman resonances have contributions from different ionization channels which are characterized by different photoelectron energies and different symmetries of released photoelectron wave-packets.

REFERENCES

[1] N. A. Hart, J. Strohaber et al., *Phys.Rev.A* **93** (2016), 063426

SELECTIVE MULTIPHOTON IONIZATION OF SODIUM BY FEMTOSECOND LASER PULSES

A. BUNJAC, D. B. POPOVIĆ and N. S. SIMONOVIĆ

Institute of Physics, University of Belgrade, Pregrevica 118, 11080 Belgrade, Serbia

Abstract. Multiphoton ionization of sodium by femtosecond laser pulses of 800 nm wavelength is studied in the range of laser peak intensities from 3.5 to 8.8 TW/cm². Photoelectron probability distributions and the energy spectra are determined numerically by solving the time dependent Schrödinger equation. The calculated spectra agree well with recent experimental results. A partial wave analysis of the spectral peaks related to Freeman resonances has shown that under specific conditions the resonantly enhanced multiphoton ionization may be realized through a single energy level.

1. INTRODUCTION

A remarkable feature of the photoelectron energy spectra (PES) obtained at the multiphoton ionization (MPI) of atoms using short (sub-picosecond) laser pulses is the existence of the so-called Freeman resonances. The mechanism which is responsible for occurrence of these spectral structures is the dynamic (or AC) Stark shift which brings the atomic energy levels into resonance with an integer multiple of the photon energy. Freeman et al. (1987) have shown that when atomic states during the laser pulse transiently shift into resonance, the resonantly enhanced multiphoton ionization (REMPI) takes place, increasing the photoelectron yield, and one observes peaks at the corresponding values of photoelectron energy. Thus, the peaks in the PES are related to the REMPI occurring via different intermediate states. A particular challenge would be the selective ionization of the atom through a single energy level which could produce a high ion yield. By increasing the laser intensity one increases the yield, but also spreads the electron population over multiple energy levels and, in turn, reduces the selectivity. Hart et al (2016) have shown that improved selectivity and yield could be achieved by controlling the resonant dynamic Stark shift of sodium states via intensity of the laser pulse of an appropriate wavelength.

Here we study the MPI of the sodium atom by the laser pulse of 800 nm wavelength and 57 fs full width at half maximum (FWHM) with the peak intensities ranging from 3.5 to 8.8 TW/cm², which are the same values as used in the experiment by Hart et al. Using the single-active-electron approximation we calculate the photoelectron probability distribution and the PES by solving numerically the time dependent Schrödinger equation (TDSE). In order to make a deeper insight into the ionization process, we perform, in addition, a partial-wave analysis of the photoelectron outgoing wave.

2. THE MODEL, ENERGY SCHEME AND PHOTOIONIZATION CHANNELS

Within the single-electron model the dynamics of the valence (active) electron of sodium atom in an alternating electric field $F(t)$ is described by Hamiltonian (in atomic units)

$$H = \frac{\mathbf{P}^2}{2} + V_{\text{core}}(r) - F(t)z. \quad (1)$$

The effective core potential $V_{\text{core}}(r)$ describes the interaction of the valence electron with the atomic core (inner electrons + atomic nucleus). For this purpose we use the Hellmann's pseudopotential $V_{\text{core}}(r) = -1/r + A e^{-ar}/r$. The parameters $A = 21$ and $a = 2.54920$ provide the correct value for the ionization potential of lithium $I_p = 5.1391 \text{ eV} = 0.18886 \text{ a.u.}$ and reproduce approximately the energies of singly-excited states (see Fig. 1).

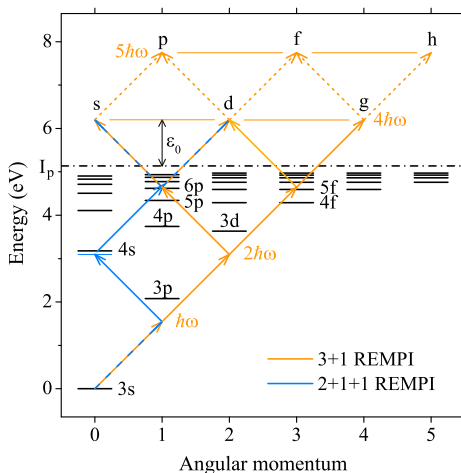


Figure 1: The unperturbed energy levels (short black lines) corresponding to singly excited states of sodium (Sansonet, 2008) relative to its ground state ($3s$) and possible four-photon and five-photon absorption pathways (arrows) from the ground state to continuum for the radiation of 800 nm wavelength ($\hbar\omega \approx 1.55 \text{ eV}$). The continuum boundary is drawn by the dash-dot line and ϵ_0 is the excess energy of photoelectrons produced in the nonresonant four-photon ionization.

We consider a linearly polarized laser pulse of the form

$$F(t) = F_{\text{peak}} \sin^2(\pi t/T_p) \cos(\omega t), \quad 0 < t < T_p \quad (2)$$

(otherwise $F(t) = 0$). Here ω , F_{peak} and T_p are the frequency of laser field, the peak value of its electric component and the pulse duration ($2 \times \text{FWHM}$), respectively. Due to the axial symmetry of the system, the magnetic quantum number m of the valence electron is a good quantum number and we set $m = 0$ (the ground state value).

The photoionization process is simulated by calculating the evolution of the wave function of valence electron $\psi(\mathbf{r}, t)$, which is initially ($t = 0$) chosen to be the lowest eigenstate of Hamiltonian (1) (then $F = 0$) that describes the sodium ground state. The evolution is calculated by integrating the TDSE (see Bunjac et al., 2017).

Fig. 1(a) shows the lowest energy levels corresponding to singly-excited states of sodium and possible multiphoton absorption pathways during the interaction of the atom with a laser radiation of 800 nm wavelength ($\hbar\omega = 0.05695$ a.u. ≈ 1.55 eV). At this wavelength there are three dominant REMPI channels: (i) (3+1)-photon ionization via excitation of 5p, 6p and 7p states, giving rise to photoelectrons with s and d-symmetry; (ii) (3+1)-photon ionization via excitation of 4f, 5f and 6f states, producing photoelectrons with d and g-symmetry; (iii) (3+1+1)-photon ionization via nearly resonant two-photon transition $3s \rightarrow 4s$ and subsequent excitation of P-states, giving rise to photoelectrons with s and d-symmetry.

3. PARTIAL WAVE ANALYSIS

In order to determine the PES, the outgoing part of the active electron wave function $\psi(\mathbf{r}, t)$ at a time $t > T_p$ is transformed from the coordinate to momentum representation $\bar{\psi}(\mathbf{k}, t)$ by the Fourier transform and expanded in terms of partial waves

$$\bar{\psi}(\mathbf{k}) = \sum_l \Phi_l(k) Y_{l0}(\vartheta), \quad (3)$$

where $Y_{l0}(\vartheta)$ are the spherical harmonics with $m = 0$ and $\Phi_l(k) = \int Y_{l0}^*(\vartheta) \bar{\psi}(\mathbf{k}) d\Omega$ are the corresponding radial functions. Using the representation of $\bar{\psi}$ in cylindrical coordinates, the radial functions can be calculated as

$$\Phi_l(k) = 2\pi \int_0^\pi \bar{\psi}(k \sin \vartheta, k \cos \vartheta) Y_{l0}(\vartheta) \sin \vartheta d\vartheta. \quad (4)$$

According to partial wave expansion (3), the radial probability density of photoelectrons in momentum space is the sum $w(k) = \sum_l w_l(k)$, where

$$w_l(k) = |\Phi_l(k)|^2 k^2 \quad (5)$$

are the partial probability densities. These quantities for $l = 0, \dots, 5$, as functions of the photoelectron excess energy $\epsilon = \hbar^2 k^2 / 2m_e$, are shown in the left column of Fig. 2 for three values of the laser peak intensity: 3.5, 4.9 and 8.8 TW/cm². The corresponding total probability densities w represent the PES for these three values of laser intensity. They are shown in the right column of Fig. 2 together with the corresponding spectra obtained experimentally (Hart et al., 2016).

The spectra, both the calculated and experimental, exhibit a typical above threshold ionization (ATI) structure with prominent peaks separated by the photon energy $\hbar\omega \approx 1.55$ eV. Fig. 2 shows the peaks corresponding to lowest three orders of ATI (MPI by $4 + s$ photons, $s = 0, 1, 2$) which are located approximately at $\epsilon = 0.8$ eV + $s\hbar\omega$. The partial wave analysis recovers the character of these peaks. We see in Fig. 2 (left) that for the photoelectron energies around the main peak ($s = 0$, $\epsilon \approx 0.8$ eV) and around the second-order ATI peak ($s = 2$, $\epsilon \approx 3.9$ eV) dominant contributions in the total probability density come from the partial waves with even l (s, d, g-waves). Thus, the photoelectrons with these energies are generated by absorbing an even number of photons ($N = 4$ and 6). Contrarily, in the vicinity of the first-order ATI peak ($s = 1$, $\epsilon \approx 2.35$ eV) the partial waves with even l are suppressed and those with odd l (p, f, h-waves) dominate. Therefore, in this case odd number of photons is absorbed (here $N = 5$).

Fig. 2 (left column) shows that at the laser peak intensity of 3.5 TW/cm^2 dominant contribution in the main peak (around 0.8 eV) comes from d-electrons, while at the intensity of 8.8 TW/cm^2 the electrons of g-symmetry dominate. In conclusion, by changing the laser intensity, one selects the main ionization channel – in the first case this is the 3+1 (or 2+1+1) REMPI via $5p$ state, while in the second case it is the 3+1 REMPI via $4f$ state.

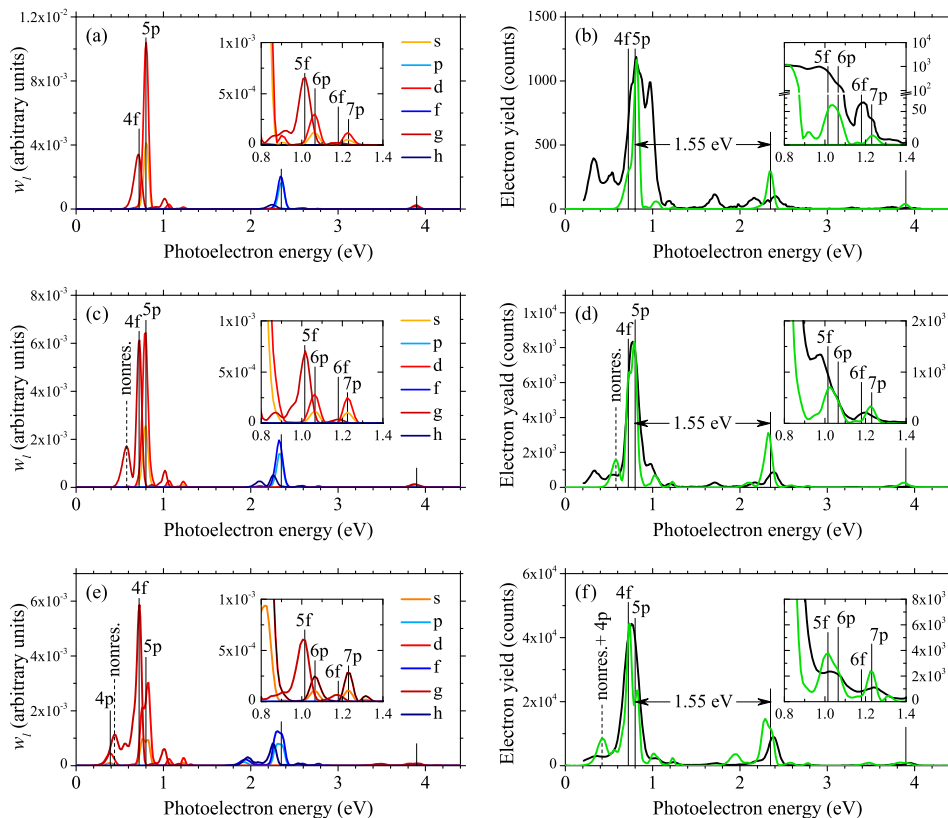


Figure 2: Partial probability densities w_l for $l = 0, \dots, 5$ (left column) and the total probability density w (right column, green line) as functions of the photoelectron energy $\epsilon = \hbar^2 k^2 / (2m_e)$ obtained at three values of the laser peak intensity: (a,b) 3.5 TW/cm^2 , (c,d) 4.9 TW/cm^2 , (e,f) 8.8 TW/cm^2 . Experimental results (Hart et al., 2016) are represented by full black lines (right column). The full vertical lines mark the energies of two REMPI channels (via f and p states) of the threshold peak as well as the position of $5p$ subpeak in the higher order ATI peaks.

References

- Bunjac A., Popović D. B. and Simonović N. S. : 2017, *Phys. Chem. Chem. Phys.*, **19**, 19829.
 Freeman, R. R., Bucksbaum, P. H., Milchberg, H., Darack, S., Schumacher, D. and Geusic, M. E. : 1987, *Phys. Rev. Lett.*, **59**, 1092.
 Hart, N. A., Strohaber, J., Kolomenskii, A. A., Paulus, G. G., Bauer, D., and Schuessler, H. A. : 2016, *Phys. Rev. A* **93**, 063426.
 Sansonetti, J. E. : 2008, *J. Phys. Chem. Ref. Data* **37**, 1659.

HYPERFINE SPLITTING OF THE LOWEST STATE ENERGY OF POSITRONIUM IN STRONG ELECTRIC FIELD

M. Z. MILOŠEVIĆ, A. BUNJAC, D. B. POPOVIĆ and N. S. SIMONOVIĆ

Institute of Physics, University of Belgrade, Pregrevica 118, 11080 Belgrade, Serbia

Abstract. The lowest state energy of positronium in an external electric field is calculated in the range of field strengths belonging to the tunnelling and over-the-barrier ionization regimes, using the wave-packet propagation method and the complex-rotation method. It is found that the hyperfine splitting of this level in the tunnelling domain decreases by increasing the field strength, but in the over-the-barrier domain the additional splitting occurs for triplet states.

1. INTRODUCTION

The electron-positron (e^-e^+) bound system, known as positronium (Ps), is an unstable exotic atom due to a non-negligible probability for annihilation of its constituents (see e.g. Rich et al. 1981). The lifetimes of the singlet (1^1S_0) and triplet (1^3S_1) components of the ground-state of Ps, the so-called para-positronium (p-Ps) and ortho-positronium (o-Ps), are 125 ps and 142 ns, respectively. The ground state energy of Ps is about half of that of hydrogen ($E \approx -6.8$ eV), but its hyperfine splitting (HFS) $E_{o\text{-Ps}} - E_{p\text{-Ps}} = 0.845$ meV, when compared to that for hydrogen, is more than three orders of magnitude larger. This splitting is a consequence of two spin-dependent interactions: (i) the spin-spin coupling (the interaction of individual magnetic momenta of e^- and e^+) and (ii) "the annihilation force" (the possibility of virtual annihilation and re-creation of the e^-e^+ pair, see Deutsch, 1952).

However, when positronium is placed in an electric field, another kind of instability arises – the ionization of Ps by the field. In this case the Coulomb potential of e^-e^+ pair and the external electric field form a potential (Stark) barrier through which the system can decay by tunnelling. The limiting case of this process when the barrier is suppressed below the energy of the atomic state, which takes place at very strong fields, is usually referred to as over-the-barrier ionization (OBI). The HFS of energy levels of Ps, on the other hand, is not directly affected by the external electric field. A weak dependence of HFS on electric field, however, occurs due to the change of form of the lowest state wave function of positronium when the field increases. In order to calculate this effect and the influence of electric field generally, we apply two different numerical methods: the wave-packet propagation (WP) method and the complex-rotation (CR) method, used previously in the studies of ordinary atoms in strong fields (see Bunjac et al., 2017; Milošević and Simonović, 2015).

2. THE MODEL

2. 1. INTERACTION WITH ELECTRIC FIELD

The first step in the analysis of electric field effects on the positronium lowest levels will be the calculation of energies and ionization rates without the HFS terms. The corresponding unperturbed Hamiltonian describing the relative motion of the e^-e^+ pair, placed in the external electric field of strength F , reads (in atomic units)

$$H_0 = -\frac{1}{2\mu}\nabla^2 - \frac{1}{r} - Fz, \quad (1)$$

where r is the inter-particle distance, z is its component in the field direction and μ is the reduced mass which for positronium takes the value $1/2$. When $F \neq 0$ the Coulomb potential $-1/r$ and the external field form the potential barrier with the saddle point of height $V_{\text{sp}} = -2\sqrt{F}$ located at $\mathbf{r}_{\text{sp}} = (0, 0, 1/\sqrt{F})$. Since the potential energy outside the barrier asymptotically tends to $-\infty$, the system can decay by tunnelling at any energy E . Therefore, all bound states of the field-free atom become resonant (autoionizing) states when $F \neq 0$.

As it was already mentioned in Introduction, two ionization regimes can be distinguished: (i) the tunnel ionization (tunnelling) regime, when $E < V_{\text{sp}}$, and (ii) over-the-barrier ionization (OBI) regime, when $E > V_{\text{sp}}$. Here we consider the lowest resonant state which in the limit $F \rightarrow 0$ approaches the ground state of the field-free atom. The value of the field strength which separates the ionization regimes F^* is the root of equation $E(F^*) = V_{\text{sp}}(F^*) \equiv -2\sqrt{F^*}$. Using numerically determined values for the lowest state energy, this equation gives $F^* = 0.016$ a.u. for Ps. Thus, the tunnelling and OBI take place for: (i) $F < F^*$ and (ii) $F > F^*$, respectively.

2. 2. THE SPIN-SPIN COUPLING AND ANNIHILATION INTERACTION

The interactions which lead to the energy splitting between the o-Ps and p-Ps ground states, the spin-spin coupling and the annihilation interaction, are described by two additional terms in the Hamiltonian for relative motion (Berestetskii et al., 1982)

$$V_{\text{ss}} = \frac{\alpha^2}{4} \left[\frac{3(\vec{\sigma}_1 \cdot \mathbf{r})(\vec{\sigma}_2 \cdot \mathbf{r})}{r^5} - \frac{\vec{\sigma}_1 \cdot \vec{\sigma}_2}{r^3} + \frac{8\pi}{3} \vec{\sigma}_1 \cdot \vec{\sigma}_2 \delta(\mathbf{r}) \right], \quad (2)$$

$$V_{\text{ann}} = \frac{\pi\alpha^2}{2} (3 + \vec{\sigma}_1 \cdot \vec{\sigma}_2) \delta(\mathbf{r}). \quad (3)$$

Here $\mathbf{r} = \mathbf{r}_1 - \mathbf{r}_2$ is the relative radius vector of e^-e^+ pair, $\vec{\sigma}_{1,2}$ are the Pauli matrices describing the spin of these two particles and $\alpha = 1/137.036$ is the fine-structure constant. In analogy with ordinary atoms, this energy splitting is called the hyperfine splitting (HFS), although for Ps it is of the same order as the fine structure corrections.

Assuming that the interaction with electric field is fully described by the dipole term $-Fz$, the Hamiltonian for positronium in electric field, which takes into account the HFS, reads

$$H = H_0 + V_{\text{ss}} + V_{\text{ann}} = H_0 + V_{\text{hfs}}. \quad (4)$$

Using relations $\vec{\sigma}_1 \cdot \vec{\sigma}_2 = 2\mathbf{S}^2 - 3$ and $(\vec{\sigma}_1 \cdot \mathbf{r})(\vec{\sigma}_2 \cdot \mathbf{r}) = 2(\mathbf{S} \cdot \mathbf{r})^2 - r^2$, where $\mathbf{S} = (\vec{\sigma}_1 + \vec{\sigma}_2)/2$ is the total spin, and writing $\mathbf{r} = r\mathbf{e}_r$, the HFS term becomes

$$V_{\text{hfs}} = \frac{\alpha^2}{2r^3} [3(\mathbf{S} \cdot \mathbf{e}_r)^2 - \mathbf{S}^2] + \pi\alpha^2 \left(\frac{7}{3} \mathbf{S}^2 - 2 \right) \delta(\mathbf{r}). \quad (5)$$

The matrix which represents operator $(\mathbf{S} \cdot \mathbf{e}_r)^2$ in the basis of singlet/triplet spin states $\{|S, M_S\rangle \mid S = 0, 1; M_S = -S, \dots, S\}$ has quasi-diagonal form

$$(\mathbf{S} \cdot \mathbf{e}_r)^2 = \begin{pmatrix} 0 & 0 & 0 & 0 \\ 0 & \frac{1}{4}(\cos 2\vartheta + 3) & -\frac{\sin 2\vartheta e^{i\varphi}}{2\sqrt{2}} & \frac{1}{2} \sin^2 \vartheta e^{2i\varphi} \\ 0 & -\frac{\sin 2\vartheta e^{-i\varphi}}{2\sqrt{2}} & \sin^2 \vartheta & \frac{\sin 2\vartheta e^{i\varphi}}{2\sqrt{2}} \\ 0 & \frac{1}{2} \sin^2 \vartheta e^{-2i\varphi} & \frac{\sin 2\vartheta e^{-i\varphi}}{2\sqrt{2}} & \frac{1}{4}(\cos 2\vartheta + 3) \end{pmatrix}, \quad (6)$$

while the corresponding matrix of operator \mathbf{S}^2 is diagonal

$$(\mathbf{S}^2)_{SM_S, S'M'_S} = S(S+1) \delta_{SS'} \delta_{M_S M'_S}. \quad (7)$$

Thus, the HFS terms do not couple singlet ($S = 0$) and triplet ($S = 1$) states, but V_{ss} couples the triplet states with different values of M_S .

Since the first diagonal element ($SM_S = S'M'_S = 00$) of matrices (6) and (7) is zero, in the singlet case the spin-dependent terms in Eq. (5) vanish and V_{hfs} reduces to

$$V_{\text{hfs}}^{(S=0)} = -2\pi\alpha^2 \delta(\mathbf{r}). \quad (8)$$

For the triplet case the spin-dependent terms in V_{hfs} are different from zero. Assuming, however, that their contribution is much smaller than the contribution of the term with delta-function, we neglect the M_S -coupling and characterize the lowest state by a definite value of quantum number M_S . In this approximation we keep in the HFS term only diagonal matrix elements $[(\mathbf{S} \cdot \mathbf{e}_r)^2]_{1M_S, 1M_S}$ and $(\mathbf{S}^2)_{1M_S, 1M_S} = 2$ and apply the expression

$$V_{\text{hfs}}^{(S=1)} = \frac{\alpha^2}{2r^3} [3[(\mathbf{S} \cdot \mathbf{e}_r)^2]_{1M_S, 1M_S} - 2] + \frac{8}{3} \pi\alpha^2 \delta(\mathbf{r}). \quad (9)$$

3. RESULTS

The lowest state energy of positronium, calculated using the model without the HFS terms by the WP and CR methods, is shown in Fig. 1(a) in the range of the field strengths from $F = 0$ to 0.25 a.u. ($\approx 1.286 \times 10^{11}$ V/m). A difference between results obtained by these two methods, which becomes significant at very strong fields ($F \gg F^*$), indicates that the resonance mean energy E obtained by the WP method and the real part of complex energy obtained by the CR method do not have the same meaning, particularly for very broad resonances (see Klaiman, 2010).

The lowest state Ps energy with the HFS, i.e. the p-Ps and o-Ps energies as functions of the field strength, are calculated using the CR method. The calculations show that the term in Eq. (9) which is proportional to $1/r^3$ gives much smaller contribution to the HFS (for about two orders of magnitude) than the term with delta-function. This fact is in agreement with the assumption from the previous section

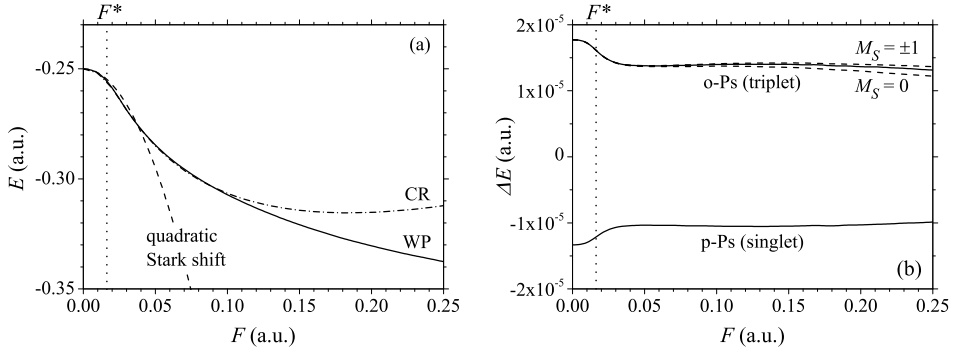


Figure 1: (a) Dependence of the lowest state energy E of positronium on the strength of external electric field F obtained numerically using the wave-packet method (WP) and the complex-rotation method (CR), respectively. For comparison the Stark shift expansion up to the quadratic term is shown (dashed line). The vertical dotted line marks the field strength F^* dividing the tunnelling and OBI domains. (b) Hyperfine splitting of the lowest state energy of Ps in electric field. The p-Ps and o-Ps lowest state energies relative to the unperturbed energy ($\Delta E_{\text{p-Ps}, \text{o-Ps}} = E_{\text{p-Ps}, \text{o-Ps}} - E$), as functions of the field strength. The dashed lines represent the values for o-Ps which are obtained using the complete expression (9) for $M_S = 0$ and $M_S = \pm 1$ separately, whereas the full line is obtained using only the term with delta-function.

which validates Eq. (9) as a good approximation. The p-Ps and o-Ps energies (the later with and without the term $\sim 1/r^3$), relative to the unperturbed energy shown in Fig. 1(a), are presented in Fig. 1(b). It can be seen that in the tunnelling domain and at the beginning of OBI domain the HFS decreases significantly by increasing the field strength, but for $F > 2F^*$ it changes slowly taking the values which are 20-25% smaller than the field-free value. This behaviour can be explained by the change of form of the lowest state wave function of positronium when it is placed in the field. The HFS in the range $F < 2F^*$ can be estimated by applying the first order perturbation theory, using V_{hfs} (without term $\sim 1/r^3$) as the perturbation. This approach gives $E_{\text{hfs}}(F) \approx \frac{14}{3}\pi\alpha^2|\psi(0; F)|^2$, where $\psi(0; F)$ is the value of the lowest state wave function of Ps in the field of strength F for $r = 0$. This relation indicates that the observed decrease of HFS when F increases is a consequence of the decrease of electron density at the positron position ($|\psi(0; F)|^2$), which can be explained by the shift of the density distribution in electric field towards the barrier.

References

- Bunjac A., Popović D. B. and Simonović N. S. : 2017, *Phys. Chem. Chem. Phys.*, **19**, 19829.
Berestetskii, V. B., Lifshitz E. M., Pitaevskii, L. P. : 1982, *Quantum electrodynamics, 2nd ed. (Course of theoretical physics, Vol. 4)*, Butterworth-Heinemann, an imprint of Elsevier, Oxford.
Deutsch, M. and Brown, S. C. : 1952, *Phys. Rev.* **85**, 1047.
Klaiman, S. and Moiseyev, N. : 2010, *J. Phys. B: At. Mol. Opt. Phys.*, **43**, 185205.
Milošević, M. Z. and Simonović, N. S.: 2015, *Phys. Rev. A*, **91**, 023424.
Rich. A. : 1981, *Rev. Mod. Phys.* **53**, 127.

Partial-wave analysis of multiphoton ionization of sodium by short laser pulses in over-the-barrier regime

A. Bunjac, D. B. Popović, N. S. Simonović
Institute of Physics, University of Belgrade, Belgrade, Serbia
simonovic@ipb.ac.rs

Multiphoton ionization of sodium by laser pulses of 800 nm wavelength and 57 fs duration is studied in the range of laser peak intensities belonging to over-the-barrier ionization regime. Photoelectron momentum distributions (PMD, see Figure 1) and energy spectra are determined numerically by solving the time dependent Schrödinger equation [1]. The calculated spectra agree well with the spectra obtained experimentally by Hart et al. [2]. The contributions of photoelectrons with different values of the orbital quantum number in the PMD are determined by expanding the photoelectron wave function in terms of partial waves. Partial wave analysis of the spectral peaks related to Freeman resonances has shown that each peak has photoelectron contributions from different ionization channels which are characterized by different photoelectron energies and different symmetries of released electron wave-packets.

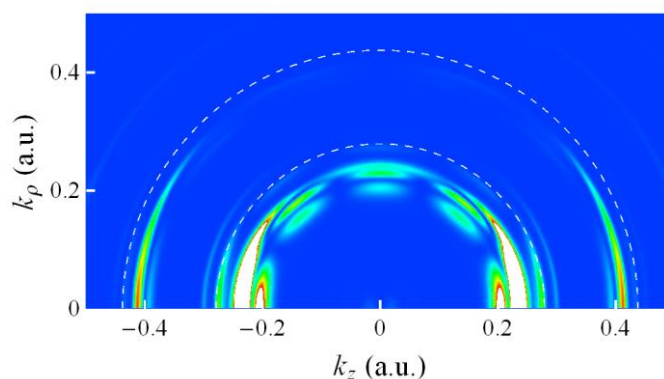


Figure 1: Calculated momentum distribution of photoelectrons produced in the ionization of sodium by the laser pulse of 800 nm wavelength, 57 fs FWHM and 4.9 TW/cm² peak intensity.

References

- [1] A. Bunjac, D. B. Popović and N. S. Simonović, *Phys. Chem. Chem. Phys.* **19**, (2017), 19829
- [2] N. A. Hart, J. Strohaber, A. A. Kolomenskii, G. G. Paulus, D. Bauer, and H. A. Schuessler, *Phys. Rev. A* **93**, (2016), 063426

Partial-wave analysis of the resonantly enhanced multiphoton ionization of sodium by femtosecond laser pulses

Andrej Bunjac, Duška B. Popović, Nenad S. Simonović

Institute of Physics, Pregrevica 118, 11080 Belgrade, Serbia

Contact: D.B.Popović (duska@ipb.ac.rs)

Abstract. We studied resonantly enhanced multiphoton ionization (REMPI) of sodium induced by femtosecond laser pulses of 800 nm wavelength in the range of laser peak intensities belonging to the over-the-barrier ionization domain. The positions of REMPI peaks in the calculated photoelectron energy spectra agree with the peak positions in the spectra obtained experimentally by Hart et al [1]. A partial wave analysis of these peaks revealed that each peak is a superposition of the contributions of photoelectrons produced by REMPI via different intermediate states. We investigated the possibility for selective resonantly enhanced multi photon ionization through a single channel and showed that it is possible to choose the main ionization channel by changing the laser intensity.

REFERENCES

N.A. Hart et al., *Phys. Rev. A* **93** (2016) 063426

Dynamic interference of photoelectrons at multiphoton ionization of atoms by short laser pulses

A. Bunjac, D. B. Popović and N. S. Simonović
Institute of Physics, Belgrade, Serbia
 e-mail:simonovic@ipb.ac.rs

The dynamics of atomic levels resonantly coupled by an intense short laser pulse is studied by calculating numerically the time-dependent amplitudes for the populations of atomic states (both discrete and continuum) [1, 2]. Here we consider the resonant multiphoton ionization of atoms which can be described within the single active electron approximation (hydrogen, alkali), studied earlier using other methods [3, 4]. It is demonstrated that the laser pulse gives rise to two wave packets emitted with a time delay with respect to each other (at the rising and falling sides of the pulse) which interfere in the time domain (see Fig. 1). The interference effects are observed in the energy spectrum and momentum distribution of photoelectrons.

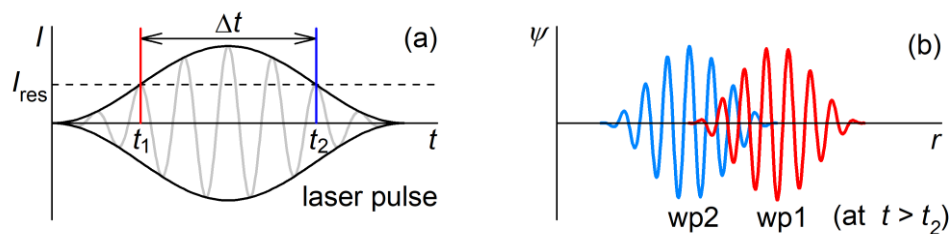


Figure 1. (a) If the intensity I of applied laser field varies, an atomic state can (due to the dynamic Stark shift) transiently shift into resonance, that occurs two times during the pulse (at t_1 and t_2 when $I = I_{\text{res}}$). (b) Then the photoelectrons emitted at the rising and falling sides of the pulse (electron wave packets wp1 and wp2, respectively) interfere due to a time delay $\Delta t = t_2 - t_1$.

REFERENCES

- [1] P. V. Demekhin and L. S. Cederbaum, *Phys. Rev. A* **83**, 023422 (2011).
- [2] P. V. Demekhin and L. S. Cederbaum, *Phys. Rev. A* **86**, 063412 (2012).
- [3] A. Bunjac, D. B. Popović and N. S. Simonović, *Phys. Chem. Chem. Phys.* **19**, 19829 (2017).
- [4] A. Bunjac, D. B. Popović and N. S. Simonović, *Phys. Lett. A* **394**, 127197 (2021).

PHOTOELECTRON ENERGY SPECTRA IN SEQUENTIAL TWO-PHOTON IONIZATION OF HYDROGEN BY GAUSSIAN AND HALF-GAUSSIAN LASER PULSES

N. S. SIMONOVIĆ, D. B. POPOVIĆ and A. BUNJAC

*Institute of Physics, University of Belgrade, Pregrevica 118, 11080 Belgrade, Serbia
E-mail simonovic@ipb.ac.rs*

Abstract. Energy spectra of photoelectrons produced in sequential two-photon ionization of hydrogen by gaussian and half-gaussian laser pulses are studied using a three-level model (1s, 2p, continuum). The spectra show an intensity dependent splitting of the resonant peak and associated modulations. The splitting can be attributed to the existence of two dressed states whose quasi-energies repel each other by the field-induced coupling. The modulations can be explained by the interference of electron waves emitted at different times during the pulse duration.

1. INTRODUCTION

We study the sequential two-photon ionization of the hydrogen atom by an intense short laser pulse and analyze interference effects in the photoelectron energy spectrum (PES). The atom, which was initially in its ground state (1s), is resonantly excited into the intermediate 2p state by the absorption of a single photon of energy $\omega = E_2 - E_1 = 3/8$ a.u. and subsequently ionized by a second photon (see Fig. 1).

In order to determine the populations of atomic states during the action of the laser pulse and after, and to obtain the PES, we calculate the evolution of atomic state $|\psi(t)\rangle$ by solving the time-dependent Schrödinger equation (in atomic units)

$$i \frac{d}{dt} |\psi(t)\rangle = H |\psi(t)\rangle \quad (1)$$

with the initial condition $|\psi(t_0)\rangle = |1s\rangle$. The total Hamiltonian has the form $H = H_0 + W$, where H_0 is the Hamiltonian of the field-free (bare) atom, while the term $W(t)$ describes the atom-field interaction. We consider a linearly polarized laser pulse whose electric component, directed along the z-axis, reads

$$\mathcal{E}(t) = \mathcal{E}_0 g(t) \cos \omega t. \quad (2)$$

$\mathcal{E}_0 g(t)$ is the time-dependent amplitude of the electric field strength, where $g(t)$ is the pulse envelope and ω is the carrier frequency of the pulse. Then the interaction term in the dipole approximation has the form $W(t) = z\mathcal{E}(t)$, where z is the projection of the electron-nucleus distance in the field direction.

2. THE THREE-LEVEL MODEL

2. 1. EQUATIONS FOR THE AMPLITUDES FOR POPULATION OF STATES

In the case of resonant excitation of an intermediate state (here 2p), the other excited states are nonessential and at weak fields their role in the ionization process may be neglected, i.e. the process may be adequately described within the three-level

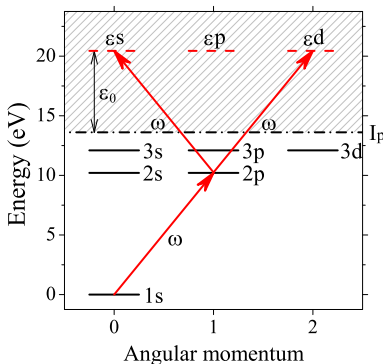


Figure 1: Energy level scheme of the hydrogen atom and the two-photon absorption paths for transitions from the ground ($1s$) state to the final continuum states (εs and εd) via one-photon resonant excitation of $2p$ state.

model ($1s$, $2p$, continuum). Then, the atomic state at time t reads (Demekhin and Cederbaum 2012)

$$|\psi(t)\rangle = a_I(t)|I\rangle + a_R(t)e^{-i\omega t}|R\rangle + \int a_\varepsilon(t)e^{-2i\omega t}|F\varepsilon\rangle d\varepsilon, \quad (3)$$

where $a_I(t)$, $a_R(t)$ and $a_\varepsilon(t)$ are the time-dependent amplitudes for the population of states $|I\rangle \equiv |1s\rangle$ (initial), $|R\rangle \equiv |2p\rangle$ (resonant) and $|F\varepsilon\rangle$ (final), respectively. The states $|R\rangle$ and $|F\varepsilon\rangle$ have been multiplied with the phase factors $e^{-i\omega t}$ and $e^{-2i\omega t}$ in order to simplify the set of equations for the amplitudes.

By inserting Eq. (3) in the Schrödinger equation (1) and applying the rotating wave approximation (Steck 2020) and the local approximation (Demekhin and Cederbaum 2011), one obtains the following set of equations for the amplitudes (Demekhin and Cederbaum 2012)

$$\begin{aligned} i\dot{a}_I &= \frac{1}{2}D^*\mathcal{E}_0g(t)a_R(t), \\ i\dot{a}_R &= \frac{1}{2}D\mathcal{E}_0g(t)a_I(t) + \left(E_R - \frac{i}{2}\Gamma g^2(t) - \omega\right)a_R(t), \\ i\dot{a}_\varepsilon &= \frac{1}{2}d_\varepsilon\mathcal{E}_0g(t)a_R(t) + (I_p + \varepsilon - 2\omega)a_\varepsilon(t), \end{aligned} \quad (4)$$

where $D = \langle R|z|I\rangle$ and $d_\varepsilon = \langle F\varepsilon|z|R\rangle$ are the dipole transition matrix elements for the excitation of the intermediate state and for its subsequent ionization, respectively. Here we set the ground state energy to zero ($E_I = 0$, as in Fig. 1). Then the energies of the resonant and final (continuum) states are $E_R = I_p + E_2 = 3/8$ a.u. and $E_F = I_p + \varepsilon$, where $I_p = 1/2$ a.u. is the ionization potential of the hydrogen atom and ε is the kinetic energy of photoelectrons. The resonant value of ε is $\varepsilon_0 = 2\omega - I_p$ (see Fig. 1). Finally, $\Gamma = 2\pi|d_{\varepsilon_0}/\mathcal{E}_0|^2$ is the ionization rate of the intermediate resonant state $|R\rangle$. The imaginary term $-\frac{i}{2}\Gamma g^2(t)$ describes the losses of the population of the intermediate state by the ionization into all final electron continuum states $|F\varepsilon\rangle$.

2. 2. DRESSED STATES AND THE ENERGY SPLITTING

The resonantly coupled dynamics of states $|I\rangle$ and $|R\rangle$ in the first two of Eqs. (4) is governed by the 2×2 Hamiltonian

$$\mathcal{H} = \begin{pmatrix} 0 & \frac{1}{2}\Omega_0^*g(t) \\ \frac{1}{2}\Omega_0g(t) & -\frac{i}{2}\Gamma g^2(t) \end{pmatrix}, \quad (5)$$

where $\Omega_0 = D\mathcal{E}_0$ is the frequency of Rabi flopping between populations of the coupled states at the peak value of laser intensity. By solving the eigenvalue problem of Hamiltonian (5) we obtain two dressed states as superpositions $|\pm\rangle \approx (|I\rangle \pm |R\rangle)/\sqrt{2}$ and the corresponding complex eigenenergies $E_{\pm}(t) \approx \pm\frac{1}{2}\Omega_0g(t) - \frac{i}{4}\Gamma g^2(t)$. Due to the imaginary parts of E_{\pm} , dressed states $|\pm\rangle$ are decaying, i.e. they are two decoupled resonances. The real parts of E_- and E_+ move apart as the pulse arrives, and towards each other as the pulse expires, estimating the splitting of the resonant peak in the PES $\Delta\varepsilon \sim \Omega_0g_0$, where g_0 is the maximum value of envelope $g(t)$ (usually $g_0 = 1$).

3. RESULTS

The evolution of the ground state of the hydrogen atom exposed to the laser pulse of carrier frequency $\omega = E_R = 3/8 \text{ a.u.} = 10.2 \text{ eV}$ has been calculated for two pulse shapes: (a) the gaussian shape $g(t) = e^{-t^2/\tau^2}$ with $\tau = 30 \text{ fs}$ and (b) the half-gaussian shape $g(t) = e^{-t^2/\tau^2}H(t)$ with $\tau = 60 \text{ fs}$ ($H(t)$ is the Heaviside step function). The computed dipole transition matrix elements for the excitation and ionization, used in Eqs. (4), are $D = 0.744936 \text{ a.u.}$ and $d_{\varepsilon_0} = 0.407759 \text{ a.u.}$ Figure 2 shows the evolution of populations of the ground (1s) and excited 2p state for the pulses of these two shapes and peak intensity $I_0 = 1 \text{ TW/cm}^2$ ($I_0 = \mathcal{E}_0^2/(8\pi\alpha)$, $\alpha = 1/137$), while figure 3 shows the populations of these states as functions of I_0 in the domain of 10^9 - 10^{13} W/cm^2 after the pulses have expired. One can see that the latest populations for the two pulses practically coincide.

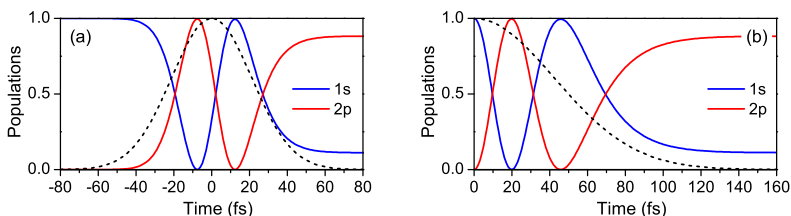


Figure 2: (a) Populations of the ground (1s) and the excited 2p state, calculated as $|a_I(t)|^2$ and $|a_R(t)|^2$, respectively, at the sequential two-photon ionization of hydrogen by a gaussian laser pulse of 1 TW/cm^2 peak intensity, $\tau = 30 \text{ fs}$ and the carrier frequency $\omega = 10.2 \text{ eV}$ which fits to the energy of $1s \rightarrow 2p$ transition. (b) The populations obtained using the half-gaussian pulse with $\tau = 60 \text{ fs}$ and the same frequency and intensity. The dashed lines represent the envelopes of the laser pulses.

Figure 4 shows the photoelectron energy spectra calculated for the two shapes of the laser pulse and the peak intensities I_0 marked in figure 3 by vertical lines. For each value of I_0 the spectra consist of the resonant peak whose splitting, according to relation $\Delta\varepsilon \sim \Omega_0g_0$, increases with the peak value of field strength \mathcal{E}_0 ($\sim \sqrt{I_0}$).

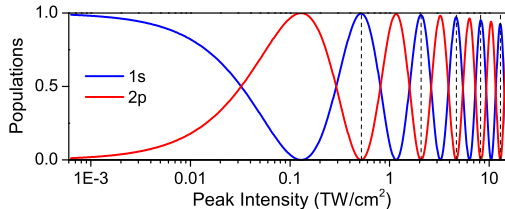


Figure 3: Populations of the ground (1s) and excited 2p state of hydrogen as functions of the laser peak intensity after the laser pulse has expired. The results obtained for the gaussian and half-gaussian pulses of the same carrier frequency $\omega = 10.2$ eV with $\tau = 30$ fs and $\tau = 60$ fs, respectively, which practically coincide, are presented. The vertical dashed lines indicate the peak intensities at which the atom manages to complete an integer number of Rabi cycles during the pulse.

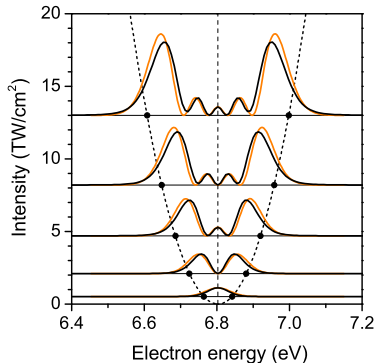


Figure 4: Photoelectron energy spectra represented by distributions $w(\varepsilon) = |a_\varepsilon(3\tau)|^2$ calculated for the gaussian and half-gaussian laser pulses (orange/black lines) with the peak intensities marked in Fig. 3 by vertical lines. Black dots mark the real parts of $E_\pm(0)$, whose separation ($\approx \Omega_0$) estimates the splitting of the resonant peak.

Demekhin and Cederbaum (2012) analyzed the modulations in the PES obtained for the photoionization with the gaussian pulse. They explained the occurrence of modulations between the positions of E_\pm resonances by the interference of two photoelectron waves emitted with the same kinetic energy at two different times – at time when the pulse is growing and at time when it decreases. Our calculations, however, show that similar modulations exist also in the case of photoionization with the half-gaussian pulse, that has no growing part. Based on this, we conclude that the modulations are due to the interference of electron waves emitted all the time during the pulse duration, rather than at two specific times.

References

- Demekhin, P. V., Cederbaum, L. S. : 2011, *Phys. Rev. A*, **83**, 023422.
 Demekhin, P. V., Cederbaum, L. S. : 2012, *Phys. Rev. A*, **86**, 063412.
 Steck, D. A., *Quantum and Atom Optics*, available online at <http://steck.us/teaching> (revision 0.13.4, 24 September 2020).

Interference effects in the sequential two-photon ionization of hydrogen by short laser pulses

N. S. Simonović, D. B. Popović and A. Bunjac
Institute of Physics, University of Belgrade, Serbia
simonovic@ipb.ac.rs

We analyze the splitting of the resonant peak and associated modulations in the photoelectron energy spectrum which occur at sequential two-photon ionization of hydrogen atom whose ground (1s) and excited 2p states are coupled resonantly by a short laser pulse. The spectra as well as the populations of atomic states for different laser peak intensities are determined by solving numerically the time-dependent Schrödinger equation for the atom in the laser field. The results are further analyzed theoretically within the three-level model (1s, 2p, continuum) [1]. It is shown that the splitting can be attributed to the existence of two dressed states whose quasi-energies repel each other by the field-induced coupling [2], while the modulations occur due to the interference of electron waves emitted at different times during the pulse. It is explained why the number of peaks in the interference patterns coincides with the number of Rabi oscillations between the populations of 1s and 2p levels during the pulse.

References

- [1] P. V. Demekhin and L. S. Cederbaum, Coherent intense resonant laser pulses lead to interference in the time domain seen in the spectrum of the emitted particles, *Phys. Rev. A* **86**, (2012), 063412
- [2] Daniel A. Steck, Quantum and Atom Optics, available online at <http://steck.us/teaching> (revision 0.13.4, 24 September 2020)

[↑ Back to Program](#)

Analysis of the photoelectron energy spectra at resonant two-photon ionization of hydrogen atom by intense short laser pulses

Nenad S. Simonović, Duška B. Popović, Andrej Bunjac
Institute of Physics, Pregrevica 118, 11080 Belgrade, Serbia

Contact: D. B. Popović (duska@ipb.ac.rs)

Abstract. We study theoretically the Rabi flopping of the population between the ground and excited 2p states of the hydrogen atom, induced by intense short laser pulses of different shapes and of carrier frequency $\omega = 0.375$ a.u. which resonantly couples the two states, and effects of this dynamics in the energy spectra of photoelectrons produced in the subsequent ionization of the atom from the excited state. It is found that, for Gaussian, half-Gaussian and rectangular pulses, characterized by the same pulse area, the final populations take the same values and the spectra consist of similar patterns (see Fig. 1) having the same number of peaks and approximately the same separation between the prominent edge (Autler–Townes) peaks [1]. These facts disprove the hypothesis proposed in earlier studies with Gaussian pulse [2], that the multiple-peak pattern appears due to dynamic interference of the photoelectrons emitted with a time delay at the rising and falling sides of the pulse, since the hypothesis is not applicable to either a half-Gaussian pulse that has no rising part or a rectangular pulse whose intensity is constant.

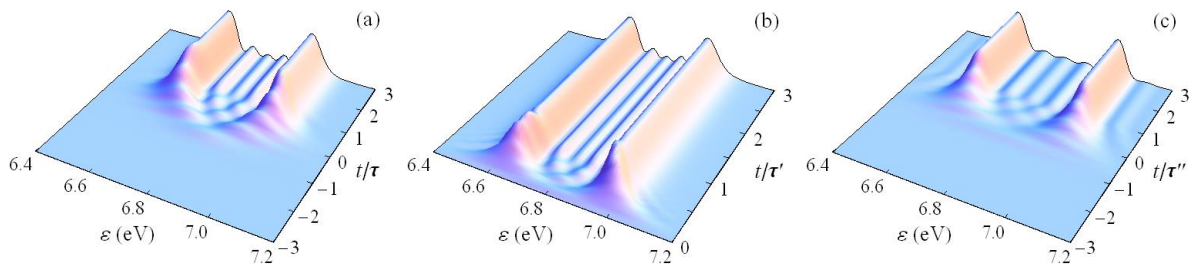


Figure 1. Time evolution of the photoelectron energy distribution (in arbitrary units) during the photoionization process of the hydrogen atom by: (a) Gaussian pulse, (b) half-Gaussian pulse and (c) rectangular pulse of carrier frequency $\omega = 0.375$ a.u. and peak intensity of 12.917 TW/cm^2 at which the atom completes five Rabi cycles during the pulse.

REFERENCES

- [1] N. S. Simonović, D. B. Popović and A. Bunjac, *Atoms* **11** (2023), 20.
 [2] P. V. Domekhin and P. V. Cederbaum, *Phys. Rev. A* **86** (2012), 063412.

Analysis of the dynamic RF projection phase in True Scalar Cs Magnetometers

Andrej B. Bunjac¹, Zoran D. Grujić¹, M. M. Čurčić¹, Theo Scholtes², Jonas Hinkel²

(1) Institute of Physics Belgrade, Pregrevica 118a, 11000 Belgrade, Serbia

(2) Leibniz Institute of Photonic Technology, Albert-Einstein-Straße 9, 07745 Jena, Germany

Contact: Andrej B. Bunjac (bunjac@ipb.ac.srs)

Abstract. A true scalar magnetometer (TSM) is one where the phase is independent of the magnetic field orientation and instead depends on the modulus only. We analyzed a magnetometer consisting of a paraffin-coated glass cell filled with CS vapor where the RF field is parallel to the light propagation direction while oscillating at Larmor frequency [1]

The magnetometer was applied in the measurement of small magnetic field components orthogonal to the main field direction. Experimental measurements of the RF projection phase show significantly different behavior in cases where the transversal field component is perpendicular to the RF field and when it is in the plane formed by the main magnetic and the RF fields. For the “in-plane” case the RF projection phase doesn’t show any perturbation on changing the intensity or field direction, while the “perpendicular” case shows significant peaks and slow relaxations under the same circumstances.

This phenomenon was initially explored through numerical simulations with a model that shows good agreement with experimental results and later backed with analytical calculations of the Bloch equation for this case in Cartesian spin components. The equations were solved analytically by moving into a rotating frame of reference and applying the Rotating Wave Approximation (RWA) and the disambiguation of the remaining solution terms by the significance of their contribution. The results show a simplified picture of the described problem but capture the qualitative behavior well. The measurements, numerical solution and the analytical approach will all be presented in a wholesome description and analysis of the described phenomenon.

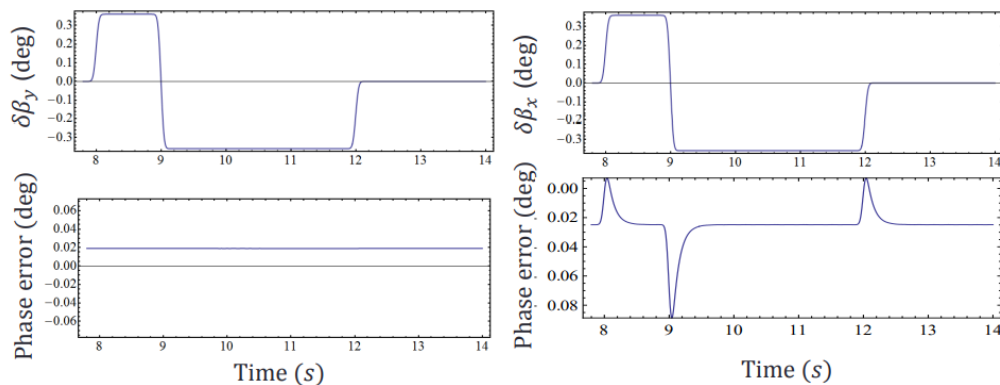


Figure 1. Two different field geometries considered for the DC transverse magnetic field scans. Left: The “in-plane” case with constant phase error, Right: The “perpendicular” case with phase error perturbations.

REFERENCES

- [1] Weis A., Bison G., Grujić Z.D. (2017) Magnetic Resonance Based Atomic Magnetometers. In: Grosz A., Haji-Sheikh M., Mukhopadhyay S. (eds) High Sensitivity Magnetometers. Smart Sensors, Measurement and Instrumentation, vol 19. Springer, Cham.

Analysis of Autler-Townes patterns in photoelectron energy spectra at resonant two-photon ionization of atom by laser pulses of different shapes

SIMONOVIĆ, Nenad (Institute of Physics Belgrade); POPOVIĆ, Duška; BUNJAC, Andrej

Using the method of time-dependent amplitudes we analyze the fingerprints of the Rabi dynamics between the ground and excited 2p states of the hydrogen atom, induced by an intense short laser pulse which resonantly couples the two states, in the energy spectra of photoelectrons produced in the subsequent ionization of the atom from the excited state. It is found that for Gaussian, half-Gaussian and rectangular pulses, characterized by the same pulse area, the spectra consist of similar patterns having the same number of peaks between the prominent edge (Autler-Townes) peaks [1]. The analysis in terms of dressed states performed within the minimal three-level model showed that the mechanism of formation of multiple-peak structures during the photoionization process is the same regardless of the pulse shape. This fact disproves the hypothesis proposed in earlier studies [2] that the multiple-peak pattern appears due to dynamic interference of the photoelectrons emitted with a time delay at the rising and falling sides of the pulse, because, in contrast to the Gaussian pulse, the pulses of other two shapes do not have one or both sides. This conclusion is in agreement with the analysis of the conditions for dynamic interference [3], where it was found that they are not always fulfilled.

References

- [1] N. S. Simonović, D. B. Popović and A. Bunjac, *Atoms* 11, 20 (2023).
- [2] P. V. Domekhin and L. S. Cederbaum, *Phys. Rev. A* 86, 063412 (2012).
- [3] M. Baghery, U. Saalman, J. M. Rost, *Phys. Rev. Lett.* 118, 143202 (2017).

A dressed states analysis of Autler-Townes patterns in the PES at resonant two-photon ionization of hydrogen by short laser pulses

Duška B. Popović¹, Andrej Bunjac¹, Nenad S. Simonović

(1) *Institute of Physics, University of Belgrade, Pregrevica 118, 11080 Belgrade, Serbia*

Contact: D. Popović (duska@ipb.ac.rs)

Abstract. Interaction of atoms with a strong laser field leads to transitions between the atomic states as well as to modification (shifting and splitting) of the atomic energy levels. We examined the Autler-Townes (AT) splitting and additional modulations (multiple-peak structure) of the resonant peak in the photoelectron energy spectra (PES) at two-photon ionization of hydrogen by intense short laser pulses, which occur via one-photon resonant $1s - > 2p$ transitions [1]. The number of peaks appearing in the pattern was found to match the number of Rabi flopping of the population between the $1s$ and $2p$ states during the pulse [2]. Analysis in terms of dressed states, which are eigenstates of the atomic Hamiltonian including the coupling with the laser field (the so-called dressed Hamiltonian), directly explains the appearance of the AT splitting of the resonant peak in the PES. Using this approach, it is shown that the mechanism of formation of multiple-peak structures during the photoionization process is the same regardless of the pulse [3].

REFERENCES

- [1] Bunjac, D.B.Popović and N.S.Simonović, *Eur.Phys.J D* **76** (2022), 249
- [2] V.Demekhin, L.S.Cederbaum, *Phys.Rev.A*, **86** (2012), 063412
- [3] N.S.Simonović, D.B.Popović and A. Bunjac, *Atoms* **11** (2023), 20

DC Transverse Magnetic Field Scan in True Scalar Cs Magnetometers

Andrej B. Bunjac¹, Zoran D. Grujić¹, M. M. Ćurčić¹, S. Topić¹, Theo Scholtes², Jonas Hinkel²

(1) Institute of Physics Belgrade, Pregrevica 118a, 11000 Belgrade, Serbia

(2) Leibniz Institute of Photonic Technology, Albert-Einstein-Straße 9, 07745 Jena, Germany

Contact: Andrej B. Bunjac (bunjac@ipb.ac.srs)

Abstract. We present a true scalar magnetometer (TSM) consisting of a paraffin-coated glass cell filled with Cs vapor with the $\vec{B}_{rf} \parallel \vec{k}$ geometry where \vec{k} is the light propagation direction for the optical pumping and \vec{B}_{rf} is a magnetic field oscillating at Larmor frequency [1]. Spin dynamics of this system are described by the Bloch equations in Cartesian spin components:

$$\frac{d\vec{S}}{dt} = \vec{S} \times \vec{\omega} - \gamma\vec{S} + \gamma_p\vec{k}.$$

The measurement of a DC magnetic field transverse to the main magnetic field in the system produced unexpected signal shapes in different transverse directions. Specifically, with the RF field in the YZ plane, the DC field in the x-direction produces unfavorable signal when modulated at sufficiently high frequencies. This difference in the dynamic RF projection phase is investigated by solving the above equation both analytically and numerically with different transverse field geometries. The theoretical calculations produce results that are in good agreement with the observed systematic effects during measurement.

We will present the measurements in both described geometries and discuss the differences between the obtained signals. We will also present the details of both calculation processes and discuss how the results compare to the measurements.

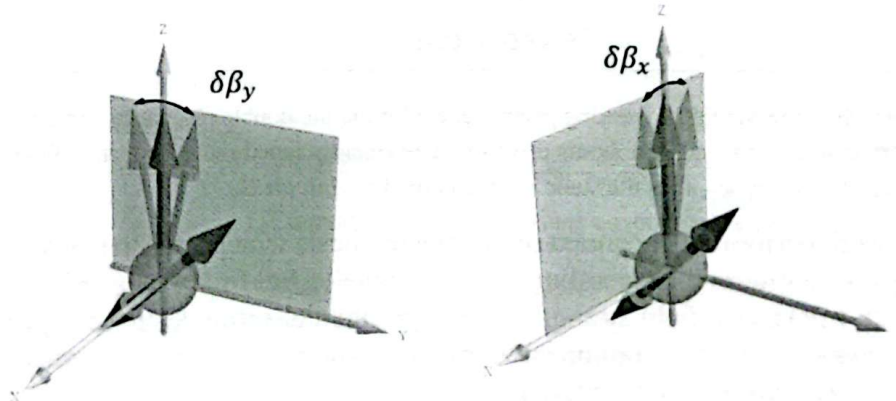


Figure 1. Two different field geometries considered for the DC transverse magnetic field scans. The additional magnetic DC field manifests as a small “rotation” of the main field in the appropriate direction.

REFERENCES

- [1] Weis A., Bison G., Grujić Z.D. (2017) Magnetic Resonance Based Atomic Magnetometers. In: Grosz A., Haji-Sheikh M., Mukhopadhyay S. (eds) High Sensitivity Magnetometers. Smart Sensors, Measurement and Instrumentation, vol 19. Springer, Cham.

All-optical Cs magnetometer based on free alignment precession

Marija M. Čurčić¹, Andrej Bunjac¹, Saša Topić¹, Jonas Hinkel², Theo Scholtes²,
Zoran. D. Grujić¹

(1) *Institute of Physics, Pregrevica 118, 11080 Belgrade, Serbia*

(2) *Leibniz Institute of Photonic Technology, Albert-Einstein-Strasse 9, 07745 Jena, Germany*

Contact: M. M. Čurčić (marijac@ipb.ac.rs)

Abstract. Since their first demonstration, in 1960s [1], optically pumped atomic-based magnetometers (OPM) [2] have been in the focus of many scientific studies. Recently, they have been of special interest due to their wide range of application, including measurements of magnetic fields in bio-medical science, environmental and geo-science.

Our focus is on the development of a compact, portable magnetometer for geophysical field measurements. We present the design and operating principle of a novel kind of OPMs, optically-pumped Cs magnetometer based on a free alignment precession (FAP). This type of magnetometer is free of some limitations of conventional OPMs, such as frequency shifts and systematic displacements. We use a paraffin-coated Cs vapor cell. Magnetometer operates at room temperature. The atomic medium is pumped with linearly polarized amplitude-modulated light at a double Larmor frequency, $2\omega_L$. This process generates spin alignment. After the optical pumping, the decay of the spin polarization can be detected in the weaker probe beam passing through the cell. The information on the magnetic field and Larmor frequency can be gathered via further signal processing.

We will discuss the influence of various parameters on the performance of our magnetometer – state of polarization of the probe and pump beam, angle between the probe and the external magnetic field, probe and pump powers and lengths. We will present our set-up and first test measurements. Finally, we will give an outlook for the further work.

REFERENCES

- [1] A. L. Bloom, *Principles of operation of the rubidium vapor magnetometer*, Appl. Opt. 1, 61 (1962).
- [2] A. Weis, G. Bison, Z. D. Grujić, *High Sensitivity Magnetometers - Magnetic Resonance Based Atomic Magnetometers*, pp 361-424 (2016).

Why do we need accurate magnetometers and how to realize them

Zoran D. Grujić¹, Andrej Bunjac¹, Saša Topić¹, Marija M. Ćurčić¹,
Jonas Hinkel², Theo Scholtes²

(1) *Institute of Physics, Pregrevica 118, 11080 Belgrade, Serbia*

(2) *Leibniz Institute of Photonic Technology, Albert-Einstein-Straße 9, 07745 Jena, Germany*

Contact: Z. Grujić (zoran.grujic@ipb.ac.rs)

Abstract. In most cases magnetometers have been developed with accent on sensitivity in order to detect very small changes of magnetic fields like brain waves, magnetic field of beating heart or variations of geomagnetic field. For such applications exist wide range of devices like fluxgates, GMR, SQUID, OPM (Optically Pumped Magnetometer), etc. [1]. Our goal is to improve accuracy or precision of OPMs based on vapors of alkali metals while retaining most of their sensitivity. Alkali metals are very well studied, their properties are measured and theoretically calculated to high precision. It is to expect that a sensor, based on, for example cesium, should be easy to deploy and understand in various schemes. It turned out this is not the case and future research is required in order to overcome heading errors of cesium based OPMs.

Accurate OPMs would have broad range of applications like precision experiments in fundamental research (like measurement of nEDM – neutron Electrical Dipole Moment), metrology, space explorations and for mapping of geomagnetic fields. The latter would benefit in archaeology, mining operations and from improved quality in tracking changes in global distribution and intensity of the Earth's magnetic field.

In my talk I will present the old nEDM experiment at PSI [2] and its improvements towards its next generation – n2EDM [3]. The last part of the talk will be dedicated to accurate magnetometry with Free Spin Precession (FSP) [4] and Free Alignment Precession (FAP) magnetometers. If time permits, prospects of a ⁴He magnetometer will be discussed.

REFERENCES

- [1] A. Grosz, M. J. Haji-Sheikh and S. C. Mukhopadhyay (eds), *High Sensitivity Magnetometers*, Springer International Publishing, Cham (2017)
- [2] C Abel, ... Z.D. Grujić, ... et. al., *Phys. Rev. Lett.* **124** (2020), 081803
- [3] NJ Ayres, ... Z.D. Grujić, ... et. al., *The European Physical Journal C* **81** (2021), 1-32
- [4] Z.D. Grujić, P.A. Koss, G. Bison, A. Weis, *The European Physical Journal D* **69** (2015), 135

Dynamic interference of photoelectrons in two-photon ionization of hydrogen by intense short laser pulses

Andrej Bunjac, Duška B. Popović and Nenad S. Simonović

Institute of Physics, University of Belgrade, Pregrevica 118, 11080 Belgrade, Serbia

Contact: Duška Popović (duska@ipb.ac.rs)

Abstract. We studied sequential two-photon ionization of hydrogen atom whose ground (1s) and excited 2p states are coupled resonantly by an intense short laser pulse. The populations of states, as well as the photoelectron energy spectrum (PES), are calculated numerically using the wave-packet propagation method. The obtained PES shows an intensity dependent splitting of the resonant peak and associated modulations. The numerical results are analyzed using a three-level model (1s, 2p, continuum) [1]. It is shown that the splitting can be attributed to the existence of two dressed states whose quasi-energies repel each other by the field-induced coupling. On the other hand the modulations can be explained by the dynamic interference of the electron wave packets emitted with the same energy, but with a time delay at the rising and falling sides of the pulse.

REFERENCES:

[1] P.V. Demekhin and L.S.Cederbaum, *Phys. Rev. A* **86** (2012) 063412

Search > Results for BUNJAC A* (Aut... > Citation Report: BUNJAC A* (Author)

MENU

Citation Report

Q BUNJAC A* (Author)

Analyze Results

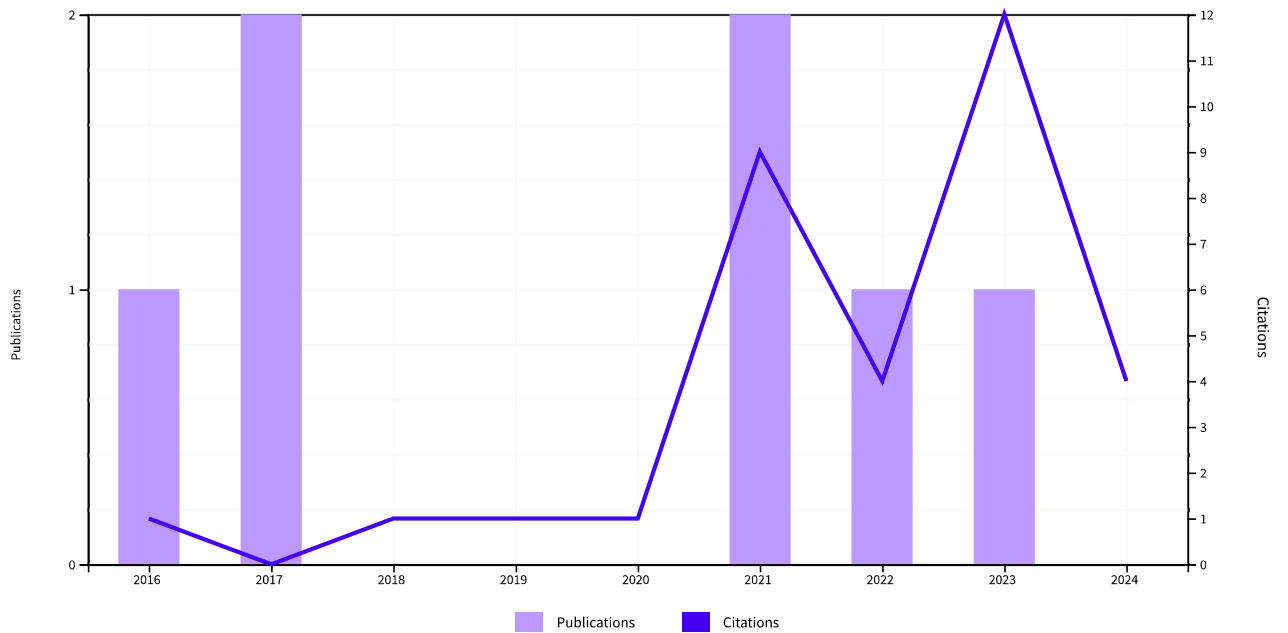
Create Alert

Export Full Report

<p>Publications</p> <p>7</p> <p>Total</p> <p>From 1996 ▾ to 2024 ▾</p>	<p>Citing Articles</p> <p>20 Analyze</p> <p>Total</p> <p>17 Analyze</p> <p>Without self-citations</p>	<p>Times Cited</p> <p>33</p> <p>Total</p> <p>29</p> <p>Without self-citations</p>	<p>4.71</p> <p>Average per item</p>	<p>4</p> <p>H-Index</p>
--	--	--	--	--------------------------------

Times Cited and Publications Over Time

DOWNLOAD



<p>7</p> <p>Publications</p> <p>Sort by: Citations: highest first ▾</p> <p>< 1 of 1 ></p>	Citations					Average per year	Total
	< Previous year		Next year >				
	2020	2021	2022	2023	2024	3.67	13
Total	1	9	4	12	4		

⊖ 1	<p>Resonant dynamic Stark shift as a tool in strong-field quantum control: calculation and application for selective multiphoton ionization of sodium</p> <p>Bunjac, A; Popovic, DB and Simonovic, NS</p> <p>Aug 14 2017 PHYSICAL CHEMISTRY CHEMICAL PHYSICS ▾ 19 (30), pp.19829-19836</p>	1	4	1	2	0	1.25	10
⊖ 2	<p>On the selective multiphoton ionization of sodium by femtosecond laser pulses: A partial-wave analysis</p> <p>Bunjac, A; Popovic, DB and Simonovic, NS</p> <p>Apr 2 2021 PHYSICS LETTERS A ▾ 394</p>	0	2	2	2	1	1.75	7
⊖ 3	<p>Analysis of the asymmetry of Autler-Townes doublets in the energy spectra of photoelectrons produced at two-photon ionization of atoms by strong laser pulses</p> <p>Bunjac, A; Popovic, DB and Simonovic, NS</p> <p>Dec 2022 EUROPEAN PHYSICAL JOURNAL D ▾ 76 (12)</p>	0	0	0	4	2	2	6
⊖ 4	<p>Manifestations of Rabi Dynamics in the Photoelectron Energy Spectra at Resonant Two-Photon Ionization of Atom by Intense Short Laser Pulses</p> <p>Simonovic, NS; Popovic, DB and Bunjac, A</p> <p>Feb 2023 ATOMS ▾ 11 (2)</p> <p>Enriched Cited References</p>	0	0	0	3	1	2	4
⊖ 5	<p>Calculations of photoelectron momentum distributions and energy spectra at strong-field multiphoton ionization of sodium</p> <p>Bunjac, A; Popovic, DB and Simonovic, NS</p> <p>Aug 2017 EUROPEAN PHYSICAL JOURNAL D ▾ 71 (8)</p>	0	2	1	1	0	0.5	4
⊖ 6	<p>Wave-packet analysis of strong-field ionization of sodium in the quasistatic regime</p> <p>Bunjac, A; Popovic, DB and Simonovic, NS</p> <p>May 24 2016 EUROPEAN PHYSICAL JOURNAL D ▾ 70 (5)</p>	0	1	0	0	0	0.22	2
	<p>Hyperfine splitting and lifetime of the positronium lowest level in a strong electric field</p>	0	0	0	0	0	0	0

7

[Milosevic, MZ; Bunjac, A; \(...\); Simonovic, NS](#)
Jan 20 2021

| [JOURNAL OF PHYSICS B-ATOMIC MOLECULAR AND OPTICAL PHYSICS](#) ▾ 54 (3)

Enriched Cited References

Citation Report Publications Table

© 2024 Clarivate
Training Portal
Product Support

Data Correction
Privacy Statement
Newsletter

Copyright Notice
Cookie Policy
Terms of Use

[Cookie Settings](#)

Follow Us



Република Србија
МИНИСТАРСТВО ПРОСВЕТЕ,
НАУКЕ И ТЕХНОЛОШКОГ РАЗВОЈА
Комисија за стицање научних звања

Број: 660-01-00001/690
21.10.2019. године
Београд

ИНСТИТУТ ЗА ФИЗИКУ			
ПРИМЉЕНО:		29. 11. 2019	
Рад. јед.	б р о ј	Арх. шифра	Прилог
0801	1873/1		

На основу члана 22. став 2. члана 70. став 4. Закона о научноистраживачкој делатности ("Службени гласник Републике Србије", број 110/05, 50/06 – исправка, 18/10 и 112/15), члана 3. ст. 1. и 3. и члана 40. Правилника о поступку, начину вредновања и квантитативном исказивању научноистраживачких резултата истраживача ("Службени гласник Републике Србије", број 24/16, 21/17 и 38/17) и захтева који је поднео

Инстѿиѿуѿ за физику у Београду

Комисија за стицање научних звања на седници одржаној 21.10.2019. године, донела је

**ОДЛУКУ
О СТИЦАЊУ НАУЧНОГ ЗВАЊА**

Др Андреј Буњац

стиче научно звање

Научни сарадник

у области природно-математичких наука - физика

О Б Р А З Л О Ж Е Њ Е

Инстѿиѿуѿ за физику у Београду

утврдио је предлог број 0801-1516/1 од 23.10.2018. године на седници Научног већа Института и поднео захтев Комисији за стицање научних звања број 1579/1 од 29.10.2018. године за доношење одлуке о испуњености услова за стицање научног звања **Научни сарадник**.

Комисија за стицање научних звања је по претходно прибављеном позитивном мишљењу Матичног научног одбора за физику на седници одржаној 21.10.2019. године разматрала захтев и утврдила да именовани испуњава услове из члана 70. став 4. Закона о научноистраживачкој делатности ("Службени гласник Републике Србије", број 110/05, 50/06 – исправка, 18/10 и 112/15), члана 3. ст. 1. и 3. и члана 40. Правилника о поступку, начину вредновања и квантитативном исказивању научноистраживачких резултата истраживача ("Службени гласник Републике Србије", број 24/16, 21/17 и 38/17) за стицање научног звања **Научни сарадник**, па је одлучила као у изреци ове одлуке.

Доношењем ове одлуке именовани стиче сва права која му на основу ње по закону припадају.

Одлуку доставити подносиоцу захтева, именованом и архиви Министарства просвете, науке и технолошког развоја у Београду.

ПРЕДСЕДНИК КОМИСИЈЕ

Ђурђица Јововић
Др Ђурђица Јововић,
научни саветник

МИНИСТАР

